TISSUE ENGINEERED BRAIDED HYBRID FIBER SCAFFOLD FOR ANTERIOR CRUCIATE LIGAMENT RECONSTRUCTION

by

NICKY TOVAR

A Dissertation submitted to the

Graduate School-New Brunswick

Rutgers, The State University of New Jersey

And

The Graduate School of Biomedical Sciences

University of Medicine and Dentistry of New Jersey

in partial fulfillment of the requirements

for the degree of

Doctor of Philosophy

Graduate Program in Biomedical Engineering

written under the direction of

Michael G. Dunn, Ph.D.

and approved by

_____

_____

_____

_____

New Brunswick, New Jersey

[January 2009]

ABSTRACT OF THE DISSERTATION

Title

By NICKY TOVAR

Dissertation Director:
Michael G. Dunn, Ph.D.

The knee joint is the largest and most complex joint in the human body. Its stability is largely dependent on the anterior cruciate ligament (ACL), a dense fibrous connective tissue that attaches the femur to the tibia. Under high tensile and torsional forces the ACL will tear and does not heal without surgical intervention. This is due to the low blood supply and ligament retraction from the synovial tissue that envelops a tear. We explored the potential of a novel ACL reconstructive device composed of a hybrid poly(desaminotyrosyl-tyrosine dodecyl dodecanedioate)(12,10) [p(DTD DD)] and type I bovine collagen fiber scaffold as an alternative to current autograft and allografts techniques. The three phase process initially tested the fabrication and characterization of p(DTD DD) fibers and compared them to poly(L-lactic acid) (PLLA), a common biomaterial. Data suggested that p(DTD DD) fibers, with their higher strength, lower stiffness, favorable degradation products and comparable cell compatibility, may be a superior alternative to PLLA fibers for development of an ACL reconstructive device. The second phase tested electron beam (E-beam) sterilized hybrid scaffolds composed of parallel 75% p(DTD DD) and 25% collagen fibers. Hybrid scaffolds were implanted for

up to 4 weeks in the ACL space of New Zealand White (NZW) rabbits. At 4 weeks there was far more cell infiltration, vascular tissue and granuloma. Inflammatory cells were concentrated on the outer part of the scaffold, which is the natural repair reaction to surgery and not the implant. The third phase used a similar scaffold in a braided configuration, a larger sheep model and a longer 12 week time point. Analysis showed an increase in the amount of cellular infiltration and vascular tissue after 12 weeks. There was a decrease in the amount of eosinophils and no change in the number of multi nucleated giant cells after 12 weeks. Cellular infiltration was apparent at the center of the scaffold, which suggests that spacing between fibers is large enough to allow cells to migrate freely throughout the scaffold. Data suggests there is a definite potential in using a braided hybrid fiber scaffold composed of p(DTD DD) and Collagen as an ACL reconstructive device.

Acknowledgement and/or Dedication

In acknowledgement of Michael G. Dunn, Ph.D. who patiently guided my growth as a scientist and a person. Thank you for your countless advice at both a professional and personal level. To my committee members Sharon Bourke, Ph.D., Charles Gatt, M.D. and Michael Jaffe, Ph.D. for your guidance and support. Also, to Joachim Kohn, Ph.D. and Sanjeeva Murthy, Ph.D. of the New Jersey Center of Biomaterials for their assistance in fiber fabrication and resources.

I would also like to acknowledge the hard-working, stellar laboratory group, past and present, at the department of orthopaedic surgery (in no particular order): Mark Ohan, Andrea Caruso, Jordan Katz, Eric Balint, Jason Saleh, Vishal Patel, Eleni Panas, Tamika Blassingame, Aaron Seto, Aaron Merriam, Ida Snyder, Barbara Perry, Mary Barrett, Eleanor and John Kehoe; I wish all much success and happiness. Also to my siblings, Jimmy, Erika and Twiggy Tovar, who assisted me in taking those necessary breaks. To my teacher, John Caprio, and fellow students, Edward Betar and Vincent Menichino, at The Woodridge Temple of Martial Arts sponsored by The Caprio Academy for Martial Arts, Incorporated; Thank you for the positive energy and words of wisdom. Lastly, to the rest of my family members, friends, and colleagues that I have met throughout my life (simply way too many to mention), Thank you.

I would like to dedicate this dissertation to my parents, Carlos and Carmen Tovar, with whose support and love this would not have been possible. Both of you were with me throughout this process and assisted me more than you will ever know or can imagine.

Table of Contents

Lists of Tables

List of Figures

1. INTRODUCTION

1.1. THE ACL

The knee joint is the largest and most complex joint in the human body, figure 1. Its stability is attributed to dense fibrous connective tissues, ligaments, that attach bone to bone and are particularly vulnerable to injury due to the large moments that can be created by forces acting on the long bones [2, 3]. Ligaments exhibit complex viscoelastic behavior in order to guide knee motion at lower applied loads while serving to restrain excessive motion at higher loads. They have few cells but a large amount of collagen fibers arranged in a hierarchal pattern that give it high tensile strength [4, 5]. The

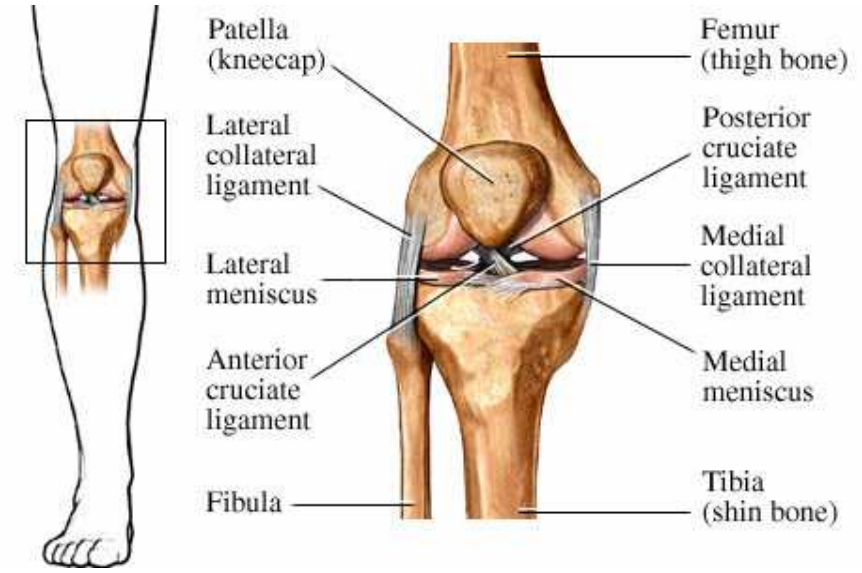

Figure 1: Anatomy of the human knee [1].

cell/extracellular matrix (ECM) interactive system uses fibroblast cells to sense changes in mechanical loads and modifies its ECM accordingly. This sophisticated system has its limitations under high tensile and torsional forces and tears occur. An anterior cruciate

ligament (ACL) tear in particular is of major concern since it plays the most crucial role in knee joint stability. It resists anterior tibial translational (primary) and rotational loads (secondary) [6, 7]. ACL tears will not heal without surgical intervention due to low blood supply and ligament retraction from the synovial tissue that envelops a tear [8-10].

1.1.1. Macroanatomy

The ACL is a vital ligament found intra-articularly in the knee and is surrounded by a synovial membrane. It attaches the femur to the tibia and is composed of two major bundles, the anteromedial bundle (AMB) and the posterolateral bundle (PLB) [7]. The femoral attachment of the ACL can be found in the posterior part of the inner surface of the lateral femoral condyle. As the ACL bundles approach the tibial attachment from the femoral attachment it takes a spiral path around the axis as its fibers fan out onto the antero-posterior surface of the tibia [7, 11-13].

1.1.2. Microanatomy

There are three zones within the ACL: (1) The proximal part which is highly cellularized with round and ovoid fibroblast, collagen type II and glycoproteins. (2) The middle part which contains a low number of fusiform and spindle-shaped fibroblasts and a high density of collagen fibers. (3) The distal part which is rich in ovoid fibroblasts and has a low density of collagen bundles [14]. It is the arrangement of the fibroblasts that determines the organization of collagen bundles [15].

The ACL has a microstructure similar to other soft connective tissues [16]. It is made up of multiple fascicles, ranging is size of 250 μm to several millimeters, and surrounded by connective tissue called the paratenon [17]. Each fascicle is enclosed in an

epitenon and is composed of 3-20 subfasciculi. The subfasciculi range in size from 100-250 μm in diameter, which are surrounded by an endotenon and are composed of collagen fibers (1-20 μm in diameter). Collagen fibers are composed of collagen fibrils that are 25-250 nm in diameter, figure 2.

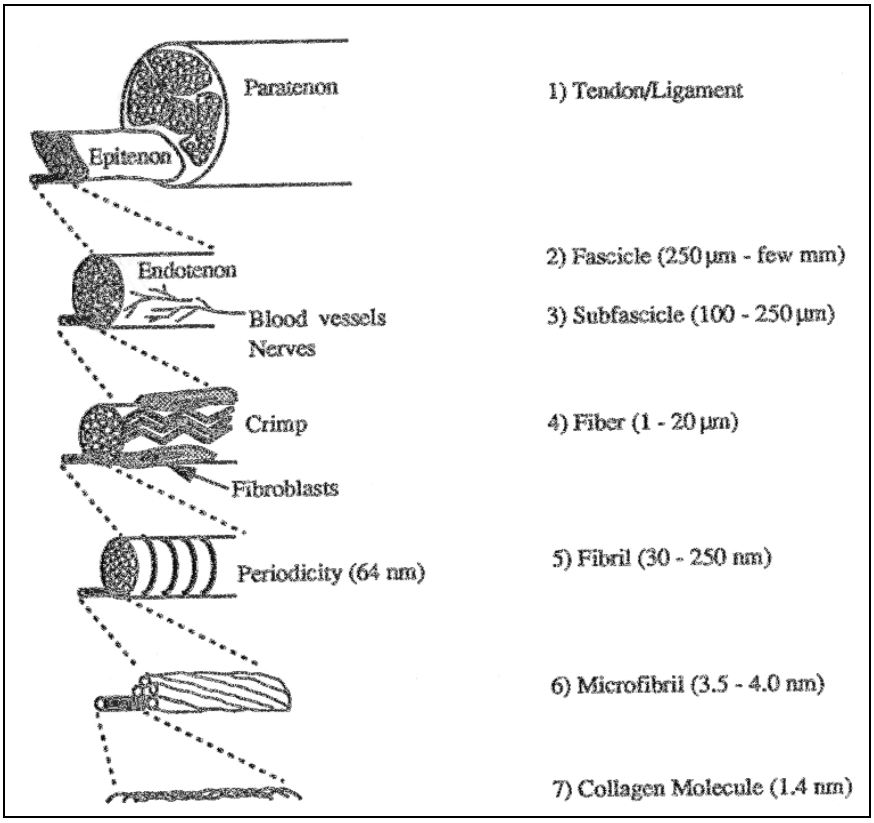

Figure 2: The hierarchical structure of the human ACL [18].

There are five different types of collagen found in the ACL. Type I collagen is the major collagen, making up roughly 70% of the dry weight [19]. They are oriented parallel to the longitudinal axis of the ligament and are responsible for the high tensile strength of the ACL [20]. Type II collagen is found in the tibial and femoral attachment sites. Type III collagen is located in the loose connective tissue that separate type I

collagen bundles. Type IV Collagen is found mainly in the proximal and distal parts of the ACL, which are more vascularized than the middle part. Type VI collagen has an orientation parallel to type III collagen and serves as a gliding component between fibrils.

The rest of the ACL matrix is composed of glycosaminoglycans, glyco-conjugates and elastic components. Glycosaminoglycans, which are highly negatively charged and possess a large number of hydroxyl groups, attract water through hydrogen bonding. Water comprises 60-80% of the total wet-weight [21]. Glyco-conjugates function to attract and combine elements in normal, healing, and growing tissues. They account for 2 μm/mg of dry tissue and include laminin, entactin, tenascin, and fibronectin [22]. Elastic components permit extreme distance changes during motion and include oxytalan, elaunin, mature elastic fibers and elastic membranes [22, 23].

1.1.3. Vascular supply

No intraligamentous blood vessels cross the attachment site of the ligament to the bone of the femur and tibia [24]. The ACL is mainly supplied blood by an artery that leaves the popliteal artery, the middle genicular artery (MGA) and some terminal branches of the medial and lateral inferior genicular arteries [14, 17, 24, 25]. A synovial sheath covers the ACL and is richly endowed with blood vessels that originate from ligamentous branches from the MGA. They penetrate in a horizontal direction and run along the ACL in a longitudinal direction parallel to collagen bundles. Only a small zone approximately 5-10 mm proximal to the tibial insertion of the ACL is avascular, but is fibrocartilaginous to support compressive loads. This low blood supply plays a role in the poor healing potential of the ACL [14]. Overall, the proximal part of the ACL is more abundant with blood vessels than the distal part.

1.1.4. Biomechanics

The motion characteristics of the knee require a full six degrees of freedom, three translational (anterior-posterior, medial-lateral and proximal-distal displacement) and three rotational (internal-external, flexion-extension, and varus-valgus rotation) [17, 19, 26]. The ACL has a load-deformation curve that consists of different regions, the toe and linear region, figure 3.

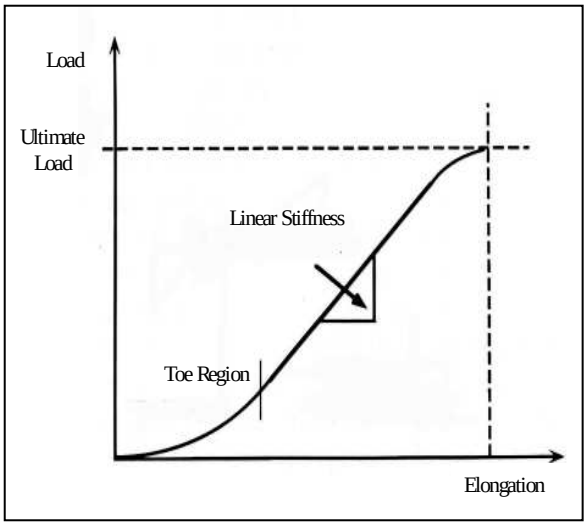

Figure 3: Typical ACL load-elongation curve for the ACL [18].

The toe region is relatively flat with a low stiffness, which is attributed to the "crimp" and "recruitment" pattern of the ligament. During tension, fibril "crimp" is straightened out by small loads and as the load increases more fibrils are "recruited" [17]. As the fibrils are subjected to higher loads, the collagen fibers are straightened out and the curve becomes linear. This region is known as the linear region. If loading continues past the yield point, the ACL will fail. The AMB tension

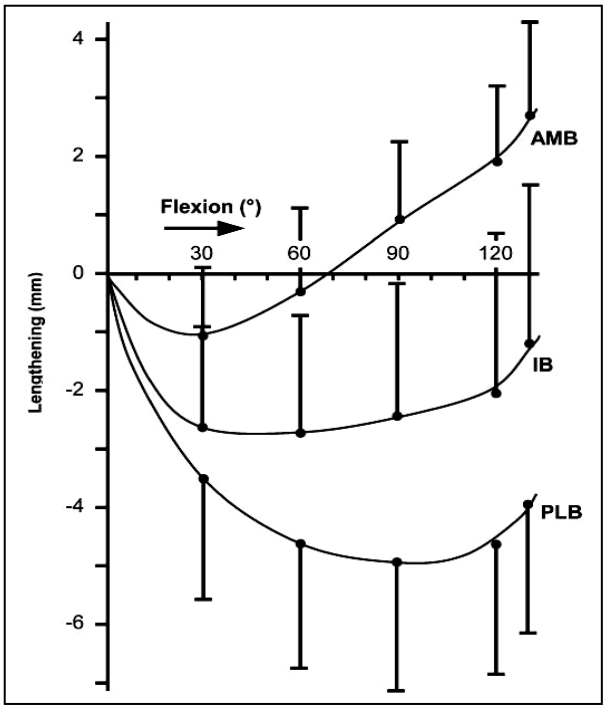

Figure 4: Mean length changes patterns. Three ACL bundles during flexion in neutral rotation. AMB anteromedial bundle, IB intermediate bundle and PLB posterolateral bundle[11].

increases in response to flexion and decreases in extension. Conversely the PLB tension increases in response to extension and decreases in flexion, figure 4.

1.1.5. ACL Treatments

Lifestyle is the most important factor to consider when reconstructing the ACL. Ideal candidates for ACL reconstructions are young athletes who wish to participate in team sports at an intermediate or professional level. Patients who decide not to reconstruct their ACL must undergo rigorous rehabilitation exercises and are strongly advised from participating in any sport that requires jumping or twisting [27]. There is also a common consensus that if left untreated an ACL injury leads to long-term complications such as meniscal injuries, failure of secondary stabilizers and the early onset of knee osteoarthritis [28]. In fact the incidence of meniscal tears in patients with unreconstructed ACL injuries is 40% at 1 year, 60% at 5 years and 80% by 10 years after initial ACL injury [29]. Though most would agree that ACL reconstruction improves knee function and decreases meniscal injuries, there is evidence that reconstruction may not decrease the onset of osteoarthritis. Follow-up studies of ACL reconstructions did not significantly delay the progression of osteoarthritis, but it is probable that they allow improved short-term function [30-32].

During the past 30 years, there has been an extensive evolution of the surgical procedures for the repair of ACL tears. Before the 1970s the ACL was excised, but that trend changed due to surgeons who believed the ACL performed an important function. After the 1970s ACL reconstructions with autografts began to take place and allografts became an option in the 1980s. An intraarticular surgery with an endoscopic single incision technique (preferred by 85% of surgeons) with either bone-patellar-bone or 4

strand hamstring autograft is currently the most common ACL reconstruction technique. However autogenous tissue for ACL reconstruction has been associated with knee pain, decreased range-of-motion and weakness [33]. It also leads to longer recovery and rehabilitation time. Allograft concerns include risk of disease transmission, bacterial infection, and the possibility of immunogenic response by the host [34, 35]. There are also concerns with altering graft mechanical properties by sterilization and storage procedures. The advantage of an allograft is decreased operative time, lower incidence of arthrofibrosis and preservation of extensor or flexor mechanisms [36-39]. Both autograft and allograft techniques have successful short-term results, but five-year follow-ups yield instability and pain [40].

Nondegradable synthetic grafts have also been of interest and were first designed as a permanent implant. As early as the 1970s, the Food and Drug Administration (FDA) approved the original Proplast (Vitek Inc, Houston, TX) which led the way for carbon based prosthetics such as the Leeds-Keio (polyethyleneterephthalate; Neoligaments Ltd, UK), Gore-Tex (polytetrafluroethylene; W. L. Gore & Associates, Flagstaff, AZ), Stryker (polyethylene terephthalatepolypropylene; Stryker, Kalamazoo, MI) prosthetics during the 1980s [41]. Mechanical properties of these prosthetics versus the human ACL can be seen in table 1. Permanent synthetic grafts do not involve the sacrifice of autogenous tissue, minimize the risk of allograft disease transmission, rehabilitation time and associated morbidity. They had satisfactory initial strength, but were prone to rupture and failure because of material degradation, foreign-body inflammation and synovitis [41-44]. A 15 year follow-up study of 855 prosthetic ligaments resulted in the failure of 40-78 % of them [45]. Permanent prosthetics are now seldom in use for ACL reconstructions [46].

The shortcomings of autografts, allografts and permanent synthetic grafts has encouraged the investigation of a tissue engineered approach to heal the ACL [41, 47-51].

	Ultimate Tensile Load (N)	Stiffness (N/mm)	Elongation at Break (%)	Young's Modulus (MPa)
Human ACL	2160 ± 157 [52]	242 ± 28 [52]	33 [53]	110 [54]
Human hamstring graft	3790–4140 [55]	776 [55]		
Human patellar-tendon graft		685 ± 86 [53]		
Gore-Tex Prosthesis	4830 [56]	322 [56]	9 [57]	
Dacron	3631 [57]	420 [57]	18.7 [57]	
Kennedy ligament augmentation device	1500 [56]	36 [56]		
Carbon fibers				2100–2350 [56]
Twisted silk matrix	2337 ± 72 [53]	354 ± 26 [53]	38.6 ± 2.4 [53]	
Parallel silk matrix	2214 [53]	1740 [53]	26.5 [53]	
Braided PLGA	907 ± 132 [49]			
Knitted PLLA–PLGA scaffold	29.4 [58]			283 [59]

Table 1: Mechanical properties of materials currently used in ACL reconstruction.

1.2. Tissue Engineering

Tissue engineering blends engineering and life sciences principles towards implanted materials in the hopes of repairing tissue through cellular growth. It is also important to mention prosthetics will not maintain the function of a native tissue for long periods of time. It is this limitation and of those previously described of allografts, autografts and permanent grafts that has sparked the interest for a new reconstructive device. An ACL reconstructive device would promote cellular growth and lead to regeneration or restoration of soft tissue. This technology has already developed

replacements for a variety of tissues, including nerve, skin, cardiac valves, myocardium, hepatic tissue, pancreas and bladder [60]. The challenge of an ACL reconstructive device is to tissue engineer a material that is biocompatible, biodegradable and has sufficient strength to withstand normal loads in the knee [47]. The problem with a biodegradable device is the possibility of toxic contaminants leaching from the implant and potential toxicity of the degradation products and subsequent metabolites [61]. These stringent requirements leave only a few natural and synthetic non-toxic, monomeric starting materials for the preparation of degradable biomaterials, table 2.

1.2.1. Poly(lactic acid)

Poly(lactic acid) [PLA] and Poly(glycolic acid) [PGA] are currently the most widely investigated, and most commonly used synthetic biodegradable polymers [61]. PLA is a chiral molecule, figure 5, which gives rise to four morphologically distinct polymers: the two stereoregular polymers, PLLA and PDLA, the racemic form PDLLA and the morphological form, meso-PLA. PLLA and PDLA are semicrystalline materials used in high mechanical strength applications, while PDLLA is always amorphous and used for drug delivery. PLLA is used more than PDLA since hydrolysis of PLLA yields L(+) lactic acid, which is a naturally occurring stereoisomer of lactic acid. But, there are clearly established disadvantages when a massive PLLA device comes in contact with bone as in the case of an ACL scaffold. As PLLA degrades the byproducts, such as lactic acid, contribute to bone resorption, local pH changes, and debris has been identified up to eight years after implantation [62-67]. PLLA can be made into a strong material by increasing its crystallinity, but highly crystalline PLLA are known to cause foreign body

Synthetic Degradable Polyesters	Current Major Research Applications
poly(glycolic acid), poly(lactic acid) and co-polymers	barrier membranes, drug delivery, guided tissue regeneration (in dental applications), orthopedic applications, stents, staples, sutures, tissue engineering
polyhydroxybutyrate (PHB), polyhydroxyvalerate (PHV), and co-polymers thereof	long-term drug delivery, orthopedic applications, stents, sutures
polycaprolactone	long-term drug delivery, orthopedic applications, staples, stents
polydioxanone	fracture fixation in non-load bearing bones, sutures, wound clip
Other Synthetic Degradable Polymers	
polyarylates and polycarbonates	soft-tissue applications
polyanhydrides	drug delivery
polycyanoacrylates	adhesives, drug delivery
poly(amino acids) and “pseudo”-poly(amino acids)	drug delivery, tissue engineering, orthopedic applications
poly(ortho ester)	drug delivery, stents
polyphosphazenes	blood contacting devices, drug delivery, skeletal reconstruction
poly(propylene fumarate)	orthopedic applications
Some Natural Resorbable Polymers	
collagen	artificial skin, coatings to improve cellular adhesion, drug delivery, guided tissue regeneration in dental applications, orthopedic applications, soft tissue augmentation, tissue engineering, scaffold for reconstruction of blood vessels, wound closure
fibrinogen and fibrin	tissue sealant
gelatin	capsule coating for oral drug delivery, hemorrhage arrester
cellulose	adhesion barrier, hemostat
various polysaccharides such as chitosan, alginate	drug delivery, encapsulation of cells, sutures, wound dressings
starch and amylose	drug delivery

Table 2: Degradable polymers and representative applications under investigation [61].

reactions [68]. The purpose is therefore to identify materials that could replace PLLA while providing similar mechanical performance and degradation properties.

1.2.2. Poly(desaminotyrosyl-tyrosine alkyl esters)

Poly(desaminotyrosyl-tyrosine alkyl esters), figure 6, were first produced by Joachim Kohn in response to the limited number of biodegradable polymers [69]. His approach incorporated amino acids into the backbone of an ester, carbonate or anhydride polymer to create materials with desirable biological and mechanical properties [70]. Poly(desaminotyrosyl-tyrosine dodecyl dodecanedioate)(12,10) [p(DTD DD)] was evaluated as a synthetic biodegradable polymer fiber scaffold for an ACL reconstructive device [71]. P(DTD DD) is a tyrosine-derived polyarylate with low crystallinity, ease of processibility, low shrinkage and some liquid crystalline characteristics. The 12 represents the number of methylene groups of the alklyl side chain in the diphenol component and 10 represent the number of methylene units of the aliphatic diacid in the diacid component. Diacids with an oxygen in the backbone are good fibroblast growth substrates, irrespective of their air-water contact angle [70]. P(DTD DD) shows complex phase behavior that could be used to obtain a broader range of properties than that obtainable from PLLA [72-74]. It also has no known toxic effects and the degradation products are completely bioresorbable [75, 76] This suggests that p(DTD DD) may be a superior biomaterial than PLLA for the construction of an ACL reconstructive device. Previous studies have shown success with PLLA scaffolds [77] and a study by Bourke *et al* showed success with a p(DTD DD) fiber scaffold device. They showed that an *in vivo* p(DTD DD) fiber scaffold was 100% intact with mechanical integrity post-implantation at 2 and 4 weeks post-implantation [71].

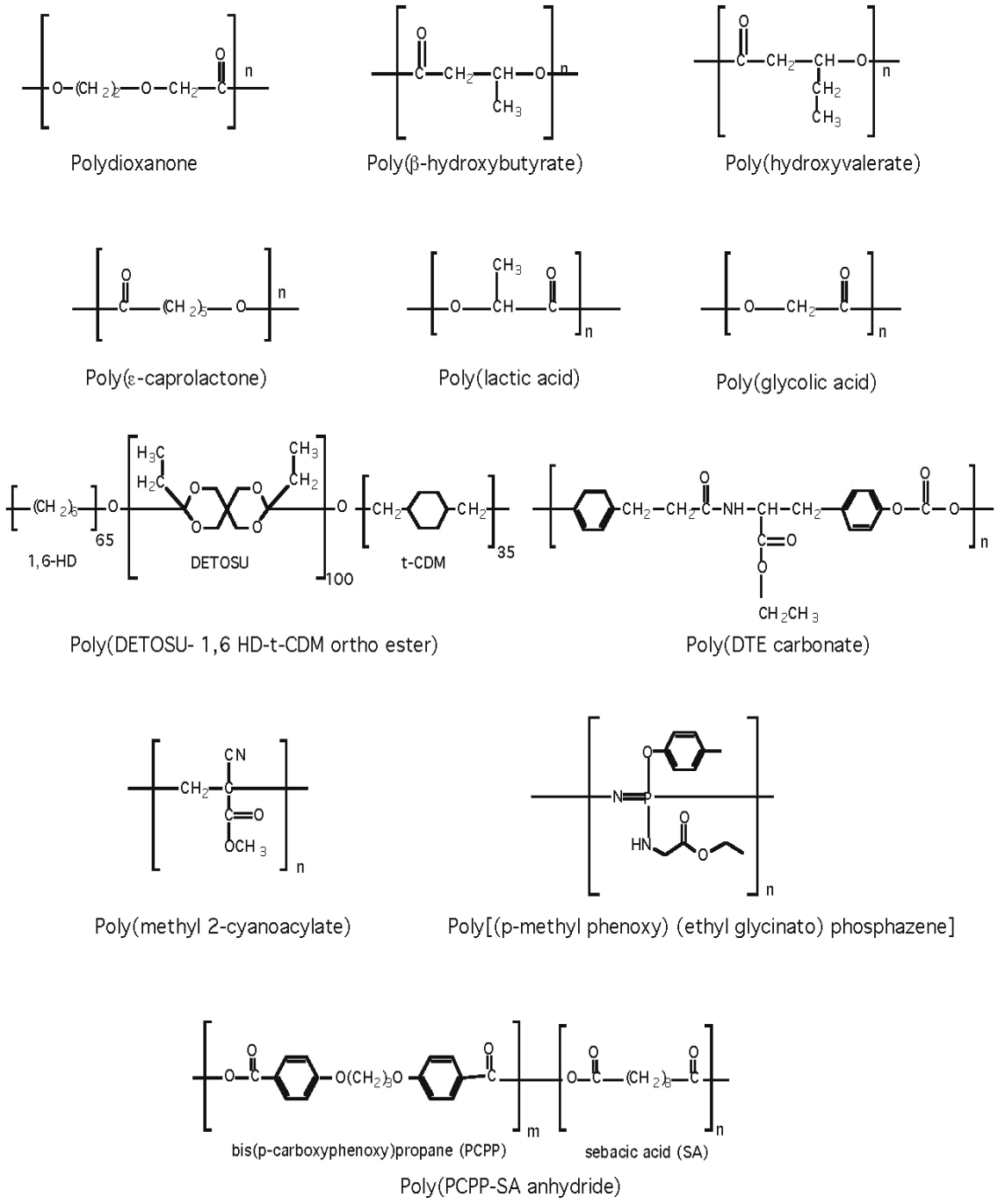

Figure 5: Chemical structures of widely investigated degradable polymers [61].

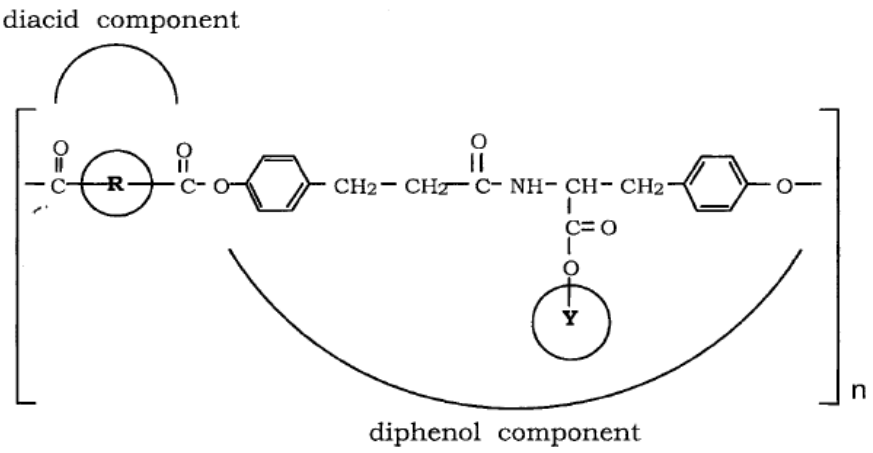

Figure 6: Chemical structure of poly(desaminotyrosyl-tyrosine alkyl esters).

1.2.3. Collagen

Natural polymers have the unique characteristic of degrading by naturally occurring enzymes. This is advantageous when it is necessary for a biomaterial to provide temporary functions, as in the case of collagen fibers in ACL reconstruction and wound coverage and healing [78, 79]. Certain chemical crosslinking methods can be used to decrease the degradation of collagen and immunogenicity while increasing strength and stiffness [80].

Collagen is the major component of connective tissues, skin, ligaments, encompassing about one-third of the total mass of proteins in the body [81]. Also, during the wound healing process collagen will bind to a wound through its natural ability to bind to fibrin, which is readily found in a wound [79]. This normal process can be disturbed by the lack of ascorbic acid and other vitamins. Collagen implants stimulate only a weak immune response, which some consider negligible. This weak response can be explained by the minute species difference found in type I collagens. Type I collagen is predominant in ligament tissue while type II and III are predominant in cartilage and

blood vessels, respectively. Besides these types of collagen, there are over 20 different types of collagen, each being dominant in a specific tissue depending on the biological and mechanical needs. The characteristic shared by these collagens is the triple helix structure. Variations are caused by the length of the helical and nonhelical sections and the number and nature of carbohydrate attachments on the triple helix [80].

1.3. Tissue Engineering Scaffolds

A tissue engineering scaffold is described as a degradable implant that is designed to act as an artificial extracellular matrix by providing space for cells to grow on and reorganize into functional tissue [59]. The mechanism behind such an implant is shown in figure 7.

In the ideal case, a tissue engineered scaffold is implanted to restore lost tissue function, maintain tissue function, or enhance existing tissue function [82]. An ACL tissue engineered fiber scaffold would allow the functional formation of neoligament tissue along the load axis and as the fibers gradually and safely degrade and lose strength, neoligament tissue bears the mechanical loads, figure 8. A few ACL reconstructive scaffold devices composed of polymer fibers have already been tested *in vivo*, table 3. Recently, interest in hybrid scaffolds has taken place and preliminary studies have proven to have a 2 fold effect. The natural collagen fiber increased fibroblast attachment and proliferation while the synthetic fiber improved scaffold strength [83].

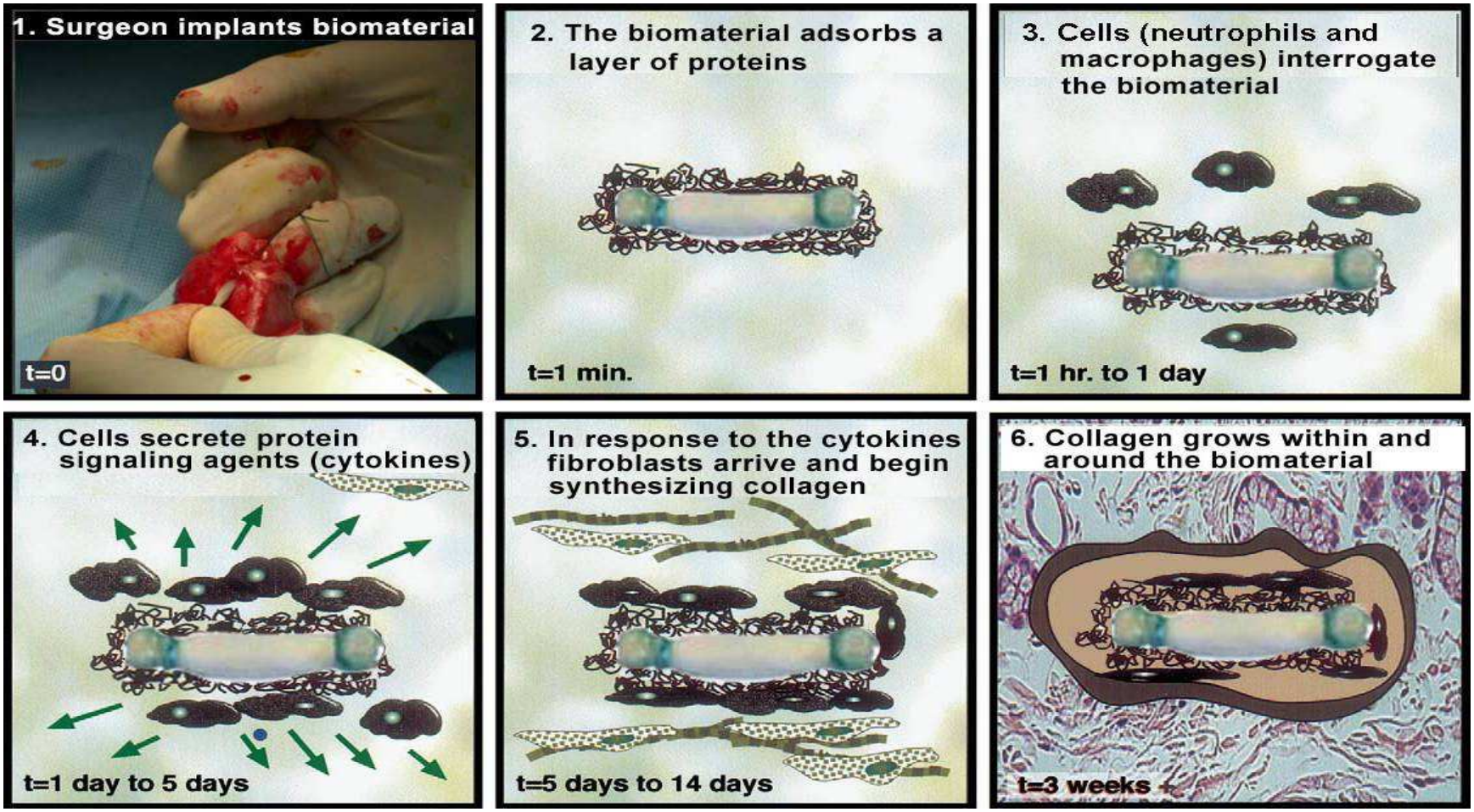

Figure 7: The reaction to an implanted synthetic material.

(1) A surgeon implants a biomaterial in a surgical site (ruptured ACL). (2) Quickly, the implant adsorbs a layer of proteins. (3) Cells (neutrophils) interrogate the biomaterial. (4) Cells send out chemical messengers (cytokines) to call in other cells. (5) Fibroblast cells arrive and begin synthesizing collagen. (6) The end stage of the reaction has the implant completely engulfed in collagen [61].

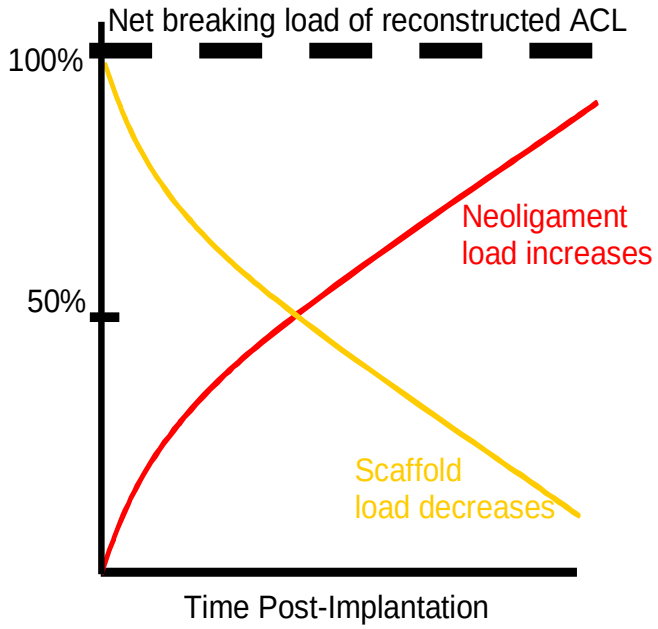

Figure 8: Transfer rate of mechanical load from scaffold to host tissue.

Processing conditions for synthetic polymer fibers allow greater control over uniformity and mechanical properties, compared to biological materials, such as collagen[89]. Dunn *et al* used crosslinked collagen fibers with some success, but it is difficult to process and has low strength [83, 90, 91]. In addition to our extensive work on collagen fibers [86, 91, 92], our laboratory examined the potential of p(DTD DD) as a biomaterial for use as an ACL reconstruction device. Three main phases were conducted.

1.4. Phase I

Phase I had two objectives (a) we compared p(DTD DD) and PLLA non-sterile and ethylene oxide (ETO) sterilized fiber strength retention and molecular weight (MW) after incubation under physiological conditions at varying time points. And (b) compared cell compatibility by quantitatively and qualitatively determining cell attachment and growth

on p(DTDD DD) and PLLA ETO sterilized fiber scaffolds. By comparing their initial strength, strength retention, MW retention, and cell compatibility, *in vitro*, we determined the potential to further develop these polymer fibers into scaffolds. From

Polymer/Structure	*In Vivo* Model /Duration	Ultimate Tensile Load (N)	Ultimate Tensile Strength (MPa)	Author/ Publication Year
Biological Polymers				
Collagen fiber, crosslinked	Rabbit/20 weeks	32	10	Dunn,1992[84]
Collagen fiber, crosslinked and braided	Goat/6 months	102		Chvapil,1993[85]
Collagen/PLA, fiber scaffold	Rabbit/4 weeks	40 ± 5	13 ± 1	Dunn,1995[86]
Collagen matrix from bone, block	Goat/1 year	474	49	Jackson,1996[87]
Synthetic polymers				
PLLA fiber, braided	Sheep/48 weeks	175 ; 295		Laitinen,1993[88]
P(DTD DD), fiber scaffold	Rabbit/4weeks	52.7 ± 5.2		Bourke, 2000[71]
P(DTE carbonate), fiber scaffold	Rabbit/8 weeks	164 ± 31		Bourke, 2004[48]
PLLA, fiber scaffold	Rabbit/3 weeks	175 ± 34		Bourke, 2004[48]
P(DTD DD) fiber scaffold	Rabbit/7 weeks	200		Tovar, 2004
PLLA/PLGA fiber, knitted	Rabbit/20 weeks	21.1		Ge, 2005 [58]
Hybrid Natural and Synthetic				
50 % PLLA/50 % Collagen, fiber scaffold	Rat/4weeks	79.54 ± 1.71	88.2 ± 3.7	Blassingame, 2005 [83]
75 % p(DTD DD)/25 % Collagen, fiber scaffold	Rat/4 weeks	115.68 ± 4.8	128.3 ± 15	Blassingame, 2005 [83]
75 % p(DTD DD)/ 25% Collagen, fiber scaffold	Rabbit/4 weeks			Tovar, 2006

Table 3: Tissue engineered ACL tested *in vivo*.

phase I it was concluded that P(DTD DD) was able to sustain fibroblast attachment and growth, has higher strength retention and a lower modulus than PLLA; all necessary parameters to consider when constructing an ACL reconstructive device. Although the biological responses of PLLA and p(DTD DD) were similar, the changes in the mechanical behavior of the two materials had different profiles after 64 weeks of incubation in a phosphate buffered solution (PBS) environment at 37 °C. These differences were attributed to the semicrystalline nature of PLLA and the small degree of crystallinity induced by mesogenic ordering in p(DTD DD). These fundamental structural and biological parameters encouraged us to proceed with the *in vivo* Phase IIa and II b safety study.

1.5. Phase II

Phase IIa was a pilot study that tested a parallel p(DTD DD) fiber scaffold for the reconstruction of the New Zealand White (NZW) rabbit for up to 7 weeks. Numerous researchers have successfully used NZW rabbits to study numerous orthopaedic applications [5, 71, 77, 86, 93-97]. It is an accepted animal model for *in vivo* ACL reconstructions due to their size, inexpensive cost, ease of histology and upkeep. The parallel scaffold consisted of 500 p(DTD DD) fibers and was sterilized by ETO. This scaffold approach focused on providing immediate joint stability postoperatively using current standard surgical anchoring techniques and acted as a degradable matrix that promoted cell attachment and neoligament formation, potentially regenerating the ACL through the body's natural ability to repair itself. This small pilot study focused on

scaffold safety, cellular compatibility, angiogenesis, and structural integrity. The scaffold's framework was purposely composed of parallel fibers to imitate the morphology of the native ACL.

The p(DTD DD) scaffold provided immediate joint stability post-surgery and within 3 days all rabbits resumed normal activity and were bearing weight on the surgical leg. Histological cross sections of the p(DTD DD) slides were analyzed and showed cellular infiltration and only a slight immune response. Mechanically, we were only able to test at the 4 week time points, in which 60% of the fibers were intact. Analysis of this study led to improvement of the strength and biological profile in Phase IIb.

Phase IIb tested the safety of a hybrid scaffold for the reconstruction of the NZW rabbit ACL up to 4 weeks. The hybrid scaffold was composed of 750 parallel fibers with a ratio of 75% p(DTD DD) and 25% collagen. In our laboratory a separate study concluded that a hybrid scaffold composed of p(DTD DD) and collagen optimized fibroblast attachment without sacrificing much of the strength[83]. The hybrid scaffold was electron beamed (Ebeam) sterilized. Histological slides of the hybrid scaffolds were graded by a medical pathologist on a low-high rank scale. There was an increase in cellular infiltration and vascular tissue between the 2 to 4 week time points. Mechanical analysis of the explant was limited due to premature failure, which was most likely due to shear forces from the bone tunnels. There was also an inflammatory response, but was most likely due to the reaction to the surgery and not the biomaterial. From this study we concluded the need for a braided framework in order to resist shear forces, a longer time point and a larger animal model.

1.6. Phase III

The lessons learned from our previous study assisted in optimizing our phase III tissue engineered ACL reconstructive device. It is once again composed of a hybrid 75% p(DTD DD) and 25% collagen fiber scaffold but in a 3 strand braided framework that evenly distributed both types of fibers throughout the scaffold [98]. Braided structures have a high compliance in axial and radial directions and low compliance in shear directions [99]. Since the primary load on the scaffold is in the axial direction a braiding structure is the best fit. A woven structure, for example has low compliance in axial and radial directions and high compliance in shear directions. The braided hybrid scaffold was also implanted in a sheep ACL instead of the smaller and hyperflexed rabbit knee joint. A rabbit model was only originally used because of its financial and physical benefits. The ACL of the sheep is not hyperflexed and has been studied extensively [100]. It has also been previously used successfully as an ACL reconstruction model [98, 101]. The sheep's ACL was excised and replaced by an Ebeam sterilized hybrid braided scaffold. At 3-6 weeks the implant was arthroscopically visualized and checked for tension, intactness and incorporation. At 12 weeks the sheep was euthanized and the implant analyzed mechanically and histologically. We chose 12 weeks since it takes approximately that long for an ACL repair to heal [102].

2. HYPOTHESIS AND OBJECTIVES

2.1. Hypothesis

A tissue engineered scaffold for ACL reconstruction would provide adequate initial strength for immediate knee joint stability, sustain cellular infiltration and degrade gradually over time to allow for neoligament formation.

- Based on preliminary studies we are developing a scaffold composed of braided p(DTD DD) and type I bovine collagen crosslinked with 1-ethyl-3-(3-dimethylaminopropyl) carbodiimide (EDC) fibers.

2.2. Objectives

The objective of this study is to determine whether:

1. P(DTD DD) and PLLA (for comparison reasons) polymers are capable of withstanding processing conditions to form fibers and its single fiber mechanical properties and degradability would not be significantly effected by sterilization,
2. Tissue engineered hybrid scaffolds composed of p(DTD DD) and Collagen fibers can sustain fibroblast attachment and proliferation and are strong enough to support the mechanical loads in the knee and
3. An ACL tissue engineered hybrid scaffold composed of p(DTD DD) and Collagen fibers would allow the functional formation of neoligament tissue along the load axis and as the fibers gradually and safely degrade and lose strength, neoligament tissue bears the mechanical loads.

2.2.1. Phase Ia: Fabrication and optimization of 1st generation fibers

P(DTD DD) and PLLA single fibers were mechanically tested after ETO sterilization in order to obtain optimal processing conditions. Processing conditions affect the mechanical properties by aligning polymer molecules along the load axis of the fiber, which are dependent on processing temperature, draw ratio, polymer MW and polymer structure.

2.2.2. Phase Ib: *In vitro* biocompatibility evaluation of 1st generation fiber scaffolds

P(DTD DD) and PLLA fiber scaffolds were ETO sterilized and tested *in vitro* using rabbit skin fibroblasts. Fibroblast attachment and proliferation were evaluated through [3-(4,5-dimethyl-thiazol-2yl)-5-(3-carboxymethoxyphenyl)-2-(4-sulfophenyl)-2H-tetrazoliym (MTS assay)] and fluorescent labeling at varying time points.

2.2.3. Phase IIa: *In vivo* ACL reconstruction using a p(DTD DD) fiber scaffold device composed of 2nd generation fibers

Using data attained from phase Ia and Ib studies we chose the optimal conditions to manufacture second generation p(DTD DD) fibers. Second generation fibers were used to construct a parallel scaffold composed of 500 p(DTD DD) and implanted in NZW rabbits. We evaluated cellular in-growth and strength.

2.2.4. Phase IIb: *In vivo* ACL reconstruction using a novel hybrid fiber scaffold device composed of 2nd generation fibers

Scaffolds constructed of hybrid 75% p(DTD DD) and 25% Collagen fibers were implanted in NZW rabbits to optimize strength and cell compatibility. Histological evaluation focused on cellular in-growth and migration. Data from this study was used to fabricate a tissue engineered fiber scaffold for a sheep study. A sheep model better resembles the human knee.

2.2.5. Phase III: *In vivo* ACL reconstruction using a braided hybrid fiber scaffold device composed of 3rd generation fiber scaffolds

Third generation p(DTD DD) fibers were used to construct a braided hybrid fiber scaffold composed of [75% p(DTD DD)]/(25% Collagen) fibers. The three strand braided scaffold was E-beam sterilized prior to implantation in a sheep model. Sheep were arthroscopically visualized at approximately 4 weeks and were then selected for immediate euthanization or left for the long-term 12 week study. We monitored sheep for joint stability, cellular infiltration and incorporation regardless of time point.

3. MATERIALS AND METHODS

3.1. Phase I: Fabrication, characterization and cell compatibility using 1st generation fibers

3.1.1. Phase Ia fabrication and characterization of fibers

P(DTD DD) was purchased from TyRx Pharma, Inc. (formerly Advanced Material Design) (Lot # AMD/SP11292001, Monmouth Junction, NJ). Medical grade PLLA (Resomer L-297, with an intrinsic viscosity of 0.9-1.1 dL/g), in pellet form, was purchased from Boehringer Ingelheim (Henley Division, Montvale, NJ). A James spinning machine (Charlotte, NC), located at the Medical Device Concept Laboratory of the New Jersey Center for Biomaterials (Newark, NJ), was used to spin p(DTD DD) and PLLA. Both polymers were dried in a vacuum oven in a nitrogen atmosphere for 2 hours at 100°C. The specific polymer was placed in a pack with a heating jack at 100°C for p(DTD DD) and 160°C for PLLA and was ramped up to 135°C and 200°C, respectively. The molten polymer was then forced through a 1 mm dye, dried at ambient temperature and spun in drums [89], figure 9 and table 4.

P(DTD DD) fibers had 2 drawing configurations; the first unit roller speed was 4. m/min and the second unit roller speed and heated shoe temperature were approximately 8.0m/min and 50°C, respectively, figure 10 and table 5. There were 2 drawing configurations for PLLA fibers; the first roller speed and heated shoe temperature were approximately 3.0 m/min and of 80°C, respectively. The second unit roller speed and heated shoe temperature were approximately 10.0 m/min and 100°C, respectively. Fiber diameters were measured at 91 ± 12 for p(DTD DD) and 84 ± 2 μm for PLLA.

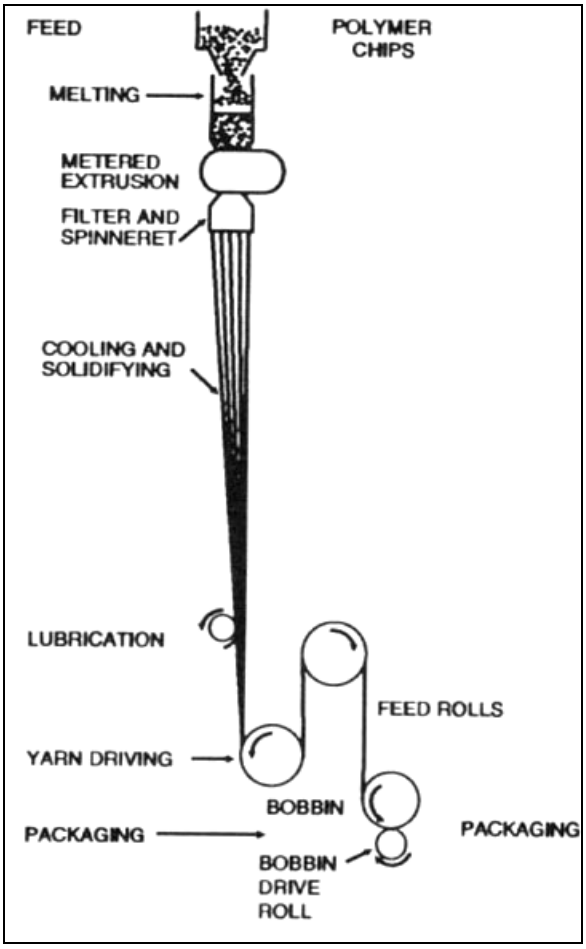

Figure 9: Schematic of the melt spinning process [89].

Polymer	Spun Fiber #	Plunger Speed (m/min)	Melt Temp. °C	Take up 1 (m/min)	Take up 2 (m/min)
P(DTD DD)	008-92-4	2.5	140	400	96
	012-01-1:	This sample was annealed from drawn sample 008-93-4, Table 5			
	008-92-3	2.5	139	350	84
	008-92-5	2.5	140	350	84
PLLA	008-87-1B	2.8	205	300	72
	008-81-1	2.8	200	280	67.2
	008-81-2	2.8	200	280	67.2

Table 4: Melt spinning stage of p(DTD DD) and PLLA.

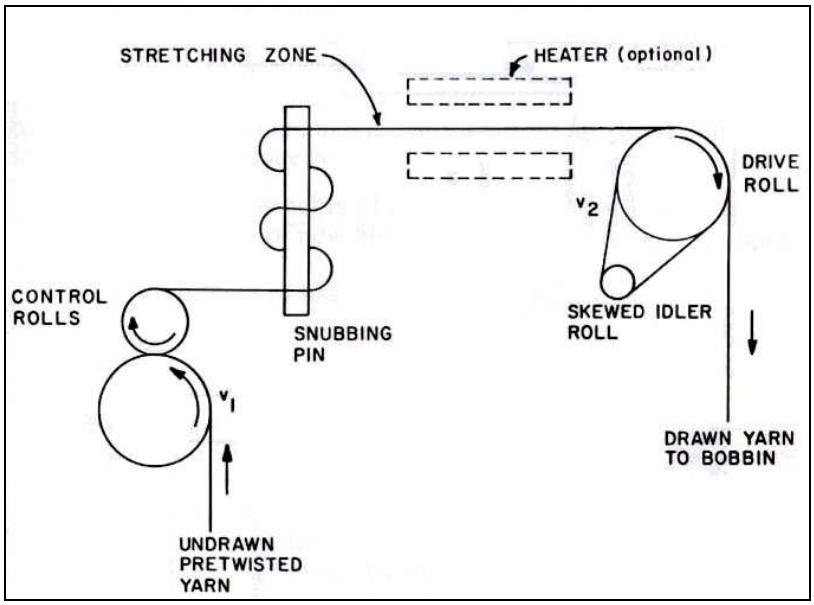

Figure 10: Schematic diagram of fiber drawing: V1< V2, drawing; V1> V2 relaxation [89].

Polymer	Drawn Fiber #	Roller 1 (m/min)	Roller 2 (m/min)	Draw ratio	Shoe Temp. °C
P(DTD DD)	008-93-4	4.00	7.00	1.75	40
	012-01-1:	2 minutes annealing time			55
	008-93-3	4.00	8.00	2.00	52
	008-93-5	4.00	8.08	2.02	50
PLLA	008-97-2	3.00	10.00	3.33	100
	008-82-1	3.08	10.11	3.28	90
	008-82-2	3.03	10.01	3.30	80

Table 5: Drawing stage of p(DTD DD) and PLLA.

3.1.2. Phase Ia fiber sterilization and incubation

An Anprolene Sterilization Tray System (Model AN72C, Andersen Products, Haw River, NC) with 5 cc ampoules of ETO (Model AN71, Andersen Products, Haw River, NC) with a weight by 84 to 97% and a molecular weight of 44.06 g/mole was used was used to sterilize p(DTD DD) and PLLA fibers. The Anprolene cycle is 12 hours for

sterilization and 2 additional hours for purging the liner bag. Sterilization took place in room temperature under a ventilator during the entire sterilization cycle to ensure that the operator was not exposed to more than the permitted level. Dosage was verified with an Exposure Indicator (Model AN85, Andersen Products, Haw River, NC). Post-sterilization aeration of the materials was performed in a vacuum chamber for 2 weeks to remove ETO residue. Sterile and non-sterile single fibers of p(DTD DD) and PLLA were incubated in PBS with a pH of 7.4 at 37 ℃ for intervals of 0, .01, 1, 2, 4, 8, 16, 24, 32 and 64 weeks.

3.1.3. Phase Ia single fiber mechanical testing and characterization

A modified version of American Society for Testing and Materials (ASTM) D3822, Standard Test Method for Tensile Properties of Single Textile Fibers, was used to mechanically load until failure single fibers. P(DTD DD) fibers (sterile n=15 and non-sterile n=15) and PLLA fibers (sterile n=15 and non-sterile n=15) were initially tested in a dry (control) environment. P(DTD DD) fibers (sterile n=15 and non-sterile n=15) and PLLA fibers (sterile n=15 and non-sterile n=15) incubated from 0.01 to 64 weeks were also tested in a wet (environmental chamber filled with distilled water at 37 °C) environment. Fiber diameters were measured using a laser micrometer (Z-mike model 1202B, Dayton, OH) prior to testing. Fibers had a 50 mm gauge length and were elongated mechanically at a displacement rate of 30 mm/min until failure using a MTS model 658.25 (MTS Systems Corporation, Eden Prairie, MN). Test environments were dry (control) and wet (distilled water environmental chamber at 37 ℃).

A differential scanning calorimetry (DSC) machine (Universal V2.6D TA Instruments) was used to measure the melting temperature (T_m) and crystallization

temperature (T_c) for p(DTD DD) fibers (sterile n=6 and non-sterile n=6) and PLLA (sterile n=6 and non-sterile n=6) fibers. A Gel permeation chromatography (GPC) machine (1100 series, Hewlett Packard, CA) in tetrahydrofuran (THF) calibrated with polystyrene standards was used to determine MW of p(DTD DD) single fibers (sterile n=6 and non-sterile n=6) and PLLA single fibers (sterile n=6 and non-sterile n=6). This chromatographic system consists of a Waters model 410 pump, a Waters model 410 refractive index detector, and a PerkinElmer model 410 computerized data station equipped with Millenium software (Waters). Two GPC columns (pore size 10^5 and 10^3 Å, 30 cm in length) were operated in series at a flow rate of 1 ml/min in THF.

3.1.4. Phase Ib scaffold preparation and cell seeding

P(DTD DD) scaffolds (sterile, N=3) and PLLA scaffolds (sterile, N=3) consisting of 50 parallel fibers were used to test for cell compatibility through *in vitro* fibroblast attachment and growth. This scaled-down scaffold restricts material use, time of preparation and is approximately 1/100 the size for an ACL reconstructive device in a human model. Scaffolds were tied at ends with cotton gauze thread to maintain uniformity. The total length of the scaffold was 1.5 cm with 1 cm length between threads. All scaffolds were ETO sterilized and aerated for 2 weeks post-sterilization. Twenty four hours prior to cell seeding sterilized p(DTD DD) and PLLA scaffolds were soaked in Dulbecco's Modified Eagle Medium (DMEM; Sigma St. Louis, MO), supplemented with 10% fetal bovine serum, 1% glutamine, 1% Hepes buffer solution, 2% antibiotic/antimycotic, and 0.4% gentamicin (complete media).

Full dermis skin samples were harvested from the hinder part of a NZW rabbit using general anesthesia and sterile surgical procedures per Institutional Animal Care and

Use Committee (IACUC) approved procedures. Samples were placed in betadine scrub for 10 minutes and transferred via cold Hanks Buffered Saline Solution (HBSS; Sigma, St. Louis, MO). To isolate fibroblast cells samples were then placed in 6-well tissue culture plates (Becton Dickinson, Franklin Lakes, NJ) with 8 ml of contained sterile filtered dispase solution (HBSS (w/o Mg^{2+} & Ca^{2+}), dispase powder (Invitrogen, Grand Island, NY, 35 units/ml)) for 16 hours at 4 °C. Dispase activity was then stopped with Iscove's Modified Dulbecco's Medium (Hyclone, Logan, UT) and the tissues were minced with a sharp blade and placed into 250 ml Tissue Culture Flask (Becton Dickinson, Franklin Lakes, NJ) along with 200 units/ml of collagenase (Sigma, St. Louis, MO) and complete media. Flasks were incubated at 37 °C in a 5% CO_2 incubator and used within the second passage. ETO Sterilized p(DTD DD) and PLLA scaffolds were placed in untreated 24-well tissue culture plates (Becton Dickinson, Franklin Lakes, NJ). Seeding was performed by pipetting a concentrated cell suspension of 1.0×10^5 cells/20 µl of complete media, further supplemented with 50 µg/ml of L-ascorbic acid, along the length of the scaffold. To prevent disruption of cells from the scaffold during the initial seeding, cells were allowed to attach for 4 hours prior to applying complete media. Complete media with ascorbic acid was then added to bring the total volume to approximately 1 ml. Medium was changed every other day.

3.1.5. Phase Ib scaffold cell compatibility measurement

In order to quantitatively analyze *in vitro* cell attachment and growth, [3-(4,5-dimethyl-thiazol-2yl)-5-(3-carboxymethoxyphenyl)-2-(4-sulfophenyl)-2H-tetrazoliym (MTS assay)](Cell Titer 96, Promega, Madison, WI) was used. MTS assay is a colorimetric method in which metabolically active cells react with MTS tetrazolium

compound and convert it into formazan dye. This dye is absorbed at 490 nm and when compared to a standard curve is directly proportional to the number of viable cells. MTS tetrazolium compound was added to all plates and incubated for 3 hours to allow for equilibration of the dye before absorbencies were read by an Emax Precision Microplate Reader using SOFTmax Plate Reader 1993 software (Molecular Devices Corp., Sunnyvale, CA). Cellular attachment and growth were determined 4 hours after seeding (initial attachment) and at 4, 8 and 16 days of post-incubation *in vitro*.

3.1.6. Phase Ib fluorescent labeling

Fluorescent labeling is a qualitative method for analyzing the cells on the scaffolds. Viable cells were labeled with PKH26-GL (Sigma, St. Louis, MO), a red fluorescent lipophylic dye that emits at a wavelength of 567 nm. The manufacturer's suggested protocol was followed. PKH26-GL stains the membrane of viable cells and is distributed amongst cells when mitosis occurs. Sterile p(DTD DD) and PLLA fiber scaffolds were placed in 24-well tissue culture plates and seeded with labeled cells by pipetting a concentrated cell suspension of 1.0×10^5 cells/20 μl along the length of the scaffold. The scaffolds were incubated in tissue culture plates for 4 hours to allow cell attachment. Complete media was added to bring the total volume to approximately 1 ml. Labeled cells were visualized using a Nikon Eclipse TE300 inverted fluorescent microscope (Micro Optics, Cedar Knolls, NJ) with imaging software (IPLabs Image Analysis, Fairfax, VA).

3.1.7. Phase I statistical analysis

Table data and graphs are presented in the form of mean ± standard deviation. Comparison among control, sterile and non-sterile groups was performed using a one-

way analysis of variance (ANOVA) ($p<0.05$) to determine significant differences. Comparison between the 2 polymer types were performed with an unpaired Student's t-test (mean) ($p<0.05$) to determine significant differences.

3.2. Phase II *in vivo* pilot study using 2nd generation fibers

3.2.1. Phase IIa polymer source and processing

P(DTD DD) was purchased from TyRx Pharma, Inc. (formerly Advanced Material Design) (Lot # AMD/SP11292001, Monmouth Junction, NJ). P(DTD DD) fibers were manufactured using a James plunger fed micromelt spinner (Charlotte, NC) with a single 1 mm diameter die, located at the Medical Device Concept Laboratory of the New Jersey Center for Biomaterials (Newark, NJ). The process was described in detail in section 3.1.1. Phase Ia fabrication and characterization of fibers. It requires p(DTD DD) to dry in a vacuum oven for 24 hours at 120 °C under flowing N_2. The polymer is then placed in the barrel gradually heated from 100 °C to 140 °C. The molten polymer, forced through the die, solidifies under ambient temperature under a take up speed of 96 m/min. The fibers were then drawn by 2 drums. The first drum speed was 4 m/min and the second drum speed was 8 m/min at 50 °C.

3.2.2. Phase IIa scaffold fabrication and sterilization

Tissue engineered scaffolds were fabricated from 500 parallel p(DTD DD) fibers. The ends were tied with 4-0 Prolene suture (Ethicon, Somerville, NJ) using a constrictor knot with a length of 4 inches. The ends of the scaffold were glued with Polyurethane (Elmer's Products, Inc., Columbus, OH) to prevent sutures from slipping and to further hold the scaffold together. The sutures will also apply tension to the scaffold once it is

implanted in the ACL space. The fiber scaffold was pulled through bone tunnels drilled in the femoral condyle and tibial plateau and held in place by polyethylene buttons, figure 11.

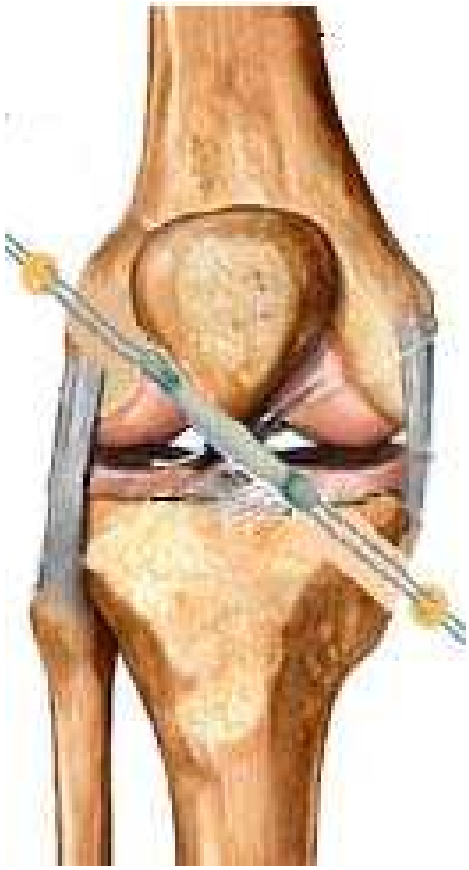

Figure 11: Knee with fiber scaffold implant and buttons.

The diameters of the entire fiber scaffolds were measured at 3.2 mm using 3.2 mm gauge block. Fiber scaffolds had a functional length of 20 mm. All fiber scaffold samples were placed in Sterilization Pouches (Fisherbrand, Pittsburgh, PA) and ETO sterilized. Post-sterilization samples were aerated for 2 weeks in a vacuum. Prior to implantation samples were hydrated in Saline Solution (Phoenix Scientific, St. Joseph, MO).

3.2.3. Phase IIa single fiber and scaffold mechanical testing

Single non-sterile P(DTD DD) fibers (n=6) were mechanically tested as described previously, section 3.1.3. Phase Ia single fiber mechanical testing and characterization, using a MTS Model 658.25 (Mechanical Testing Systems, Eden Prairie, MN) in a wet environment (distilled water environmental chamber at 37 °C). Fibers had a 50 mm gauge length and were elongated mechanically at a strain rate of 30 mm/min until failure. Fiber diameters were measured using a laser micrometer (Z-mike model 1202B, Dayton, OH) prior to testing.

Fiber scaffolds composed of 500 p(DTD DD) fibers were mechanically tested *in vitro* using an Instron Model 4204 (Instron Corp., Canton, MA) at an elongation of 60%/min. Single fiber diameters were measured using a laser micrometer (Z-mike model 1202B, Dayton, OH) in order to calculate the scaffold's total cross-sectional area. Scaffolds (n=6) had a functional length of 20 mm and were tested while gripping the ends of the scaffold. Gripping the scaffold ends applies tension directly to the hybrid scaffold and are referred as our actual hybrid scaffold values, figure 14. Prior to testing hybrid scaffolds were immersed in saline solution (IVX Animal Health, St. Joseph, MO) at room temperature for 30 minutes.

The explanted femur-scaffold-tibia-complex (FSTC) were soaked in saline solution and mechanically tested under tension until failure at a strain rate of 60%/min using an Instron Model 4204 (Instron Corp., Canton, MA). K-wires were used to secure the femur and tibia to the Instron crossheads at angle approximately 45°, aligning the ligament with the direction of the applied load. The contralateral femur-ACL-tibia complex (FATC) was also tested under similar conditions.

3.2.4. Phase IIa pre-surgical care

Surgery was performed on 3 NZW rabbits following an IACUC approved protocol. They were weighed and anesthetized by intramuscular injection of 7:5 ketamine (Fort Dodge Animal Health, Fort Dodge, IA):xylazine (Phoenix Pharmaceutical, St. Joseph, MO) solution (0.6 ml/kg body weight). The left hind limb was shaved and scrubbed with betadine for sterility. Anesthesia was maintained by inhalation of oxygen mixed with 1% halothane.

3.2.5. Phase IIa animal surgery

The knee joint was exposed via a midline skin incision and a lateral parapatellar arthrotomy, using electrocautery as needed, and the patella was dislocated. The ACL was removed by a sharp dissection at the tibial and femoral attachment sites. A 3.2 mm diameter tunnel was created via K-wires and a 3M mini-driver through the lateral femoral condyle and the tibia (exiting at the anatomic ACL attachment sites). 30 minutes prior to implantation the parallel scaffolds were hydrated in saline solution (IVX Animal Health, St. Joseph, MO) and then placed in the joint through the bone tunnels. The suture ends were secured to a polyethylene button (UMDNJ, New Brunswick, NJ) on the periosteum under initial tension of approximately 5 N. The patella was reduced, and the joint was closed with 4-0 vicryl (Ethicon, Somerville, NJ). The skin was closed with 4-0 monocryl (Ethicon, Somerville, NJ) using subcuticular stitch.

3.2.6. Phase IIa post-surgical care

NZW rabbits were returned to individual cages post-surgery with unrestricted activity and given food and water *ad libitum*. Buprenorphine (Bedford Laboratories, Bedford, OH) was given for a minimum of 2 days. After 2 days, analgesics were

administered only if the animal showed signs of pain or distress. Baytril (Bayer Healthcare, Shawnee Mission, KS) was administered only if the animal showed signs of infection. Animals were euthanized at 4, 6 and 7 weeks post-implantation by general anesthesia with ketamine/xylazine cocktail followed by an intracardial injection of the euthanasia solution Fatal Plus (Vortech Pharmaceuticals, Dearborn, MI). The FSTC and the contralateral FATC were harvested for mechanical analysis.

3.2.7. Phase IIb qualitative analysis

After mechanical testing scaffolds were stored in formalin and sent for histological analysis. Samples were sent to AML labs Inc.(Rosedale, MD) and embedded in paraffin for hematoxylin (H)- and eosin (E) staining. This staining method uses hematoxylin dye, which colors basophilic structures with blue-purple hue, and alcohol-based acidic eosin Y dye, which colors eosinophilic structures bright pink. Cross-sections were composed from neoligament midsubstance approximately 1 mm apart.

3.2.8. Phase IIb *In vivo* ACL reconstruction using a novel hybrid fiber scaffold device composed of 2nd generation fibers

3.2.9. Phase IIb p(DTD DD) fiber processing

2nd generation p(DTD DD) fibers were used and were processed as described in section 3.2.1. Polymer source and processing.

3.2.10. Phase IIb collagen fiber processing

Type I bovine dermal collagen dispersion was bought from Nitta Casings (Somerville, NJ). Fibers were processed at the Orthopaedic Research Laboratory (RWJMS-UMDNJ, New Brunswick, NJ), as seen in figure 12 [92]:

1) Lyophilized collagen was grated using a hard cheese grater

2) It was then grounded into a powder using a Wiley Mill (Thomas Scientific, Swedesboro, NJ)
3) Powder was then swollen in acid (pH 2.4) and mixed with a Jumbo Stirrer (Fisher Scientific, Pittsburgh, PA) at low speed.
4) The resultant 1% (w/v) collagen dispersion was filtered with a 149 μm Spectra/Mesh (Rancho Dominguez, CA) and then centrifuged at 2400 rpm at 20 °C for 20 minutes in 5 ml syringes.
5) A syringe pump (Sage Instruments, Boston, MA) was then used to extrude the dispersion through tubing (internal diameter of 0.58 mm) into fiber formation buffer (135 mM NaCl, 30 mM N-tris(hydroxymethyl)methyl-2-aminoethane sulfonic acid (TES), and 30mM sodiumphosphate dibasic heptahydrate) at 37 °C, pH 7.4.
6) After 24 hours fibers were rinsed with isopropanol, then with distilled water and then left overnight to hang dry at room temperature.

3.2.11. Phase IIb collagen crosslinking

Collagen fibers were crosslinked after being immersed for 24 hours in a room temperature bath of EDC (Sigma Chemical Co., St. Louis, MO) in 90% acetone. Fibers were then successively rinsed in 90% acetone for 24 hours and 50% acetone for 4 hours. They were then rinsed in 0.1 M Na_2HPO_4 for 2 hours to hydrolyze any residual EDC or remaining O-acylisourea groups [103, 104]. After these initial rinses, the fibers were finally rinsed extensively in DI water and then dried isometrically under ambient conditions.

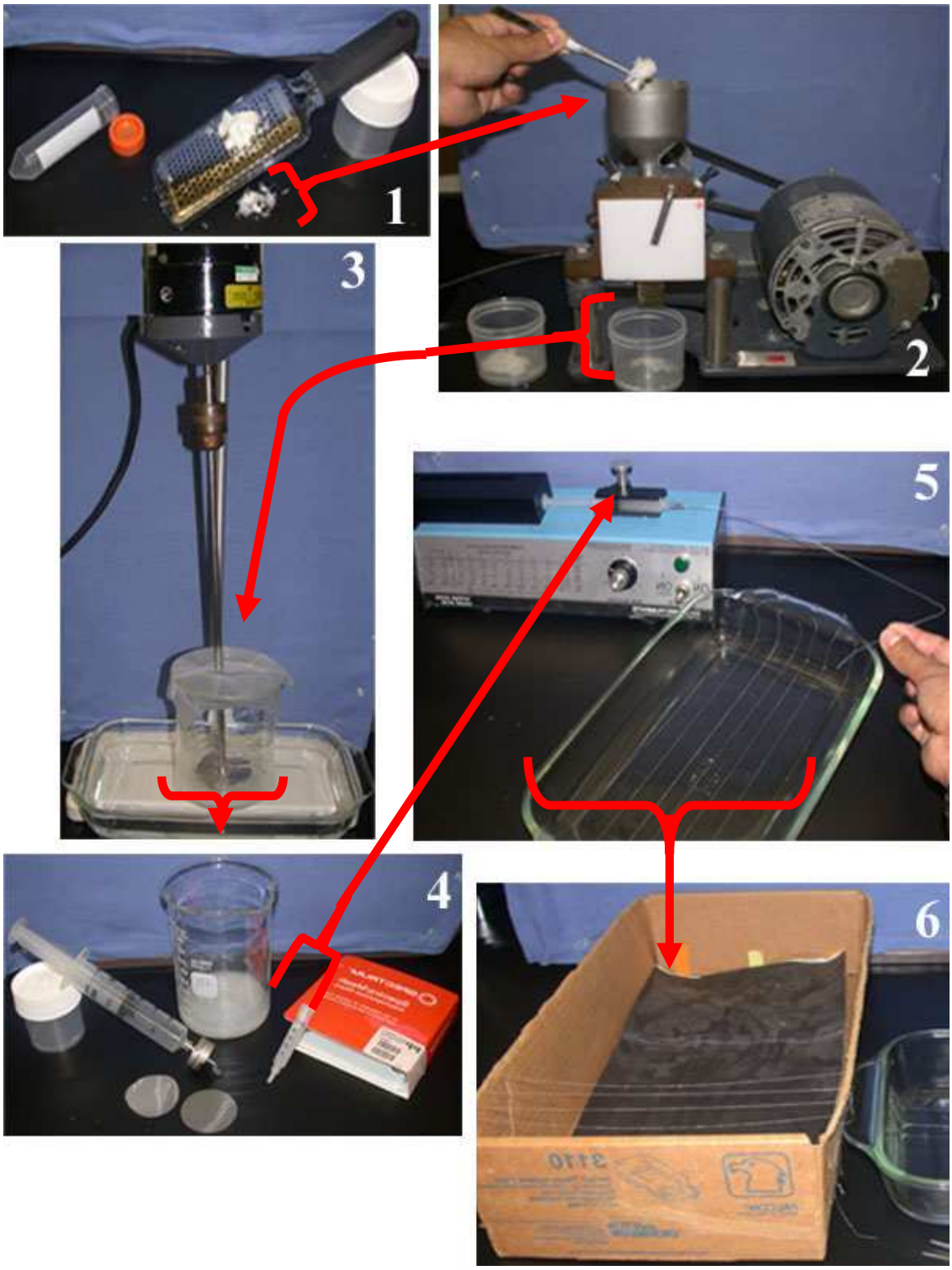

Figure 12: Schematic of the collagen fiber manufacturing process.

3.2.12. Phase IIb scaffold preparation and Ebeam sterilization

Hybrid scaffolds were composed of 750 parallel fibers at a ratio of 75% p(DTD DD)/25% collagen and had a functional length of 20 mm. The ends were secured with 4-0 Prolene suture (Ethicon, Somerville, NJ) using a constrictor knot and then immersed in Medical Device Urethane Adhesive (M-06FL, Loctite, Rocky Hill, CT) and allowed to cure for at least 24 hours. The suture was long enough to allow anchoring to polyethylene buttons (approximately 4 inches).

All hybrid scaffold samples were placed in Sterilization Pouches (Fisher brand, Pittsburgh, PA) and Ebeam (E-beam, Incorporated, Cranbury, NJ) sterilized at a dosage of 2.5 MRad. Ebeam fires a concentrated highly charged stream of electrons, which disrupts deoxyribonucleic acid (DNA) chains of microorganisms thus inhibiting reproduction [105, 106]. It has been used industrially for sterilizing medical products for over 30 years.

3.2.13. Phase IIb animal surgery

Surgery was performed on eight NZW rabbits following an IACUC approved protocol and as described in section 3.2.4-3.2.6. Previously a 3.2 mm diameter was created, but with the added collagen and p(DTD DD) a 3.5 mm diameter tunnel was made. NZW Rabbits were euthanized at 2 and 4 weeks post-implantation as previously described. The femur-hybrid scaffold-tibia complex (FHTC) and FATC were harvested and tested mechanically.

3.2.14. Phase IIb hybrid scaffold mechanical testing

A modified version of ASTM D3822 was used to mechanically test *in vitro* 750 p(DTD DD)(75%)/Collagen(25%) fiber scaffolds. Single fiber diameters were measured

using a laser micrometer (Z-mike model 1202B, Dayton, OH) in order to calculate the scaffold's total cross-sectional area. Hybrid scaffolds (n=5) with a functional length of

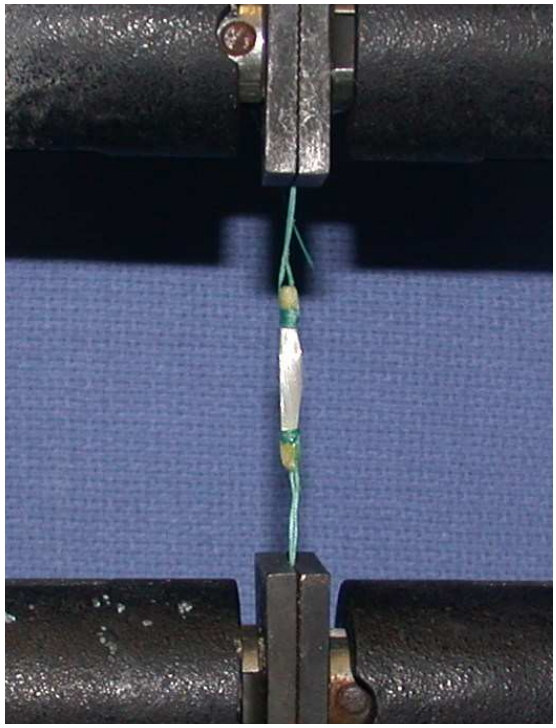

Figure 13: Mechanical testing of scaffold gripping suture ends.

20 mm were tested separately *in vitro* while gripping the suture ends and scaffold ends. Gripping the suture ends applies tension indirectly to the scaffold in a manner similar to our *in vivo* model, which anchors the scaffold using polyethylene button, figure 13. These values are referred as our initial hybrid scaffold values. Gripping the scaffold ends applies tension directly to the hybrid scaffold and is referred as our actual hybrid scaffold values, figure 14. All *in vitro* hybrid scaffolds were tested to failure using an Instron Model 5569 (Instron Corporation, Canton, MA) at a strain rate of 60%/min per. Prior to testing hybrid scaffolds were soaked in saline solution (IVX Animal Health, St. Joseph, MO) at room temperature for 30 minutes.

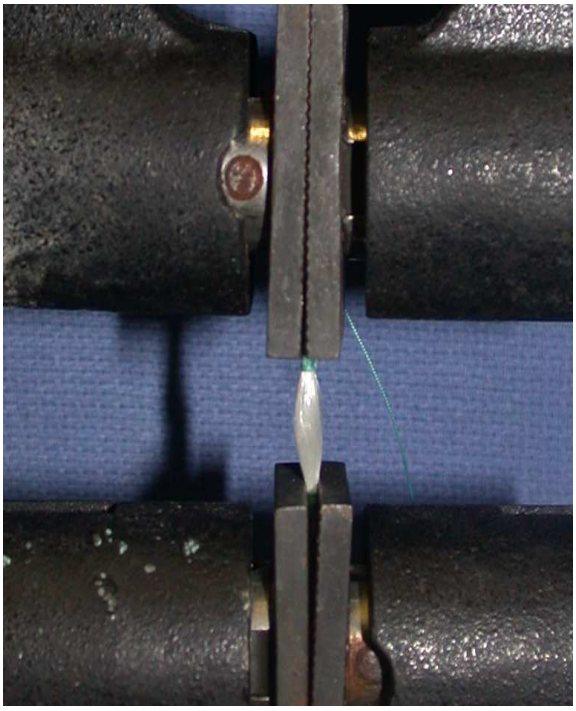

Figure 14: Mechanical testing of scaffold gripping scaffold ends.

The explanted FHTC were also soaked in saline solution and mechanically tested under tension to failure at a strain rate of 60%/min using an Instron Model 4204. K-wires were used to secure the femur and tibia to the Instron crossheads at angle approximately 45°, aligning the ligament with the direction of the applied load. The contralateral FATC was also tested under similar conditions.

3.2.15. Phase IIb qualitative analysis

After mechanical testing scaffolds were stored in formalin and sent for histological analysis. Samples were sent to AML labs Inc.(Rosedale, MD) and embedded in paraffin for hematoxylin (H)- and eosin (E) staining. Cross-sections were composed from neoligament midsubstance approximately 1 mm apart. A medical pathologist graded slides single blinded from low-1 to high-4 at 2 week intervals to prevent biased ranking. Slides were ranked based on qualitative evaluation of lymphocytes, eosinophils,

multi-nucleated giant cells (MNGC), cellular infiltration and vascular tissue and blood vessels, as outlined by van Tienen and Fox, et al [107, 108]. The average rank value was reported.

3.2.16. Phase II statistical analysis

Graphs are presented in the form of mean ± standard deviation. Comparison among 2 week and 4 week time points and their graded parameters were performed using a one-way analysis of variance (ANOVA) ($p<0.05$) to determine significant differences.

3.3. Phase III: *In vivo* ACL reconstruction using novel braided hybrid 3rd generation fiber scaffolds

3.3.1. Phase III p(DTD DD) Fiber processing and properties

P(DTD DD) was synthesized as described in the New Jersey Center for Biomaterials (Piscataway, NJ) published literature [75, 76]. It was melt-spun using an extruder manufactured by Bradford University Research Limited that used a plunger inside a heated barrel. Typical spinning conditions are given in table 6. The spinning was attempted at 135 °C as suggested in the second generation fibers. However, the polymer could only be spun above 150 °C, hence the spinning was performed at ~ 155 °C. The spun fiber was drawn at 75 °C using a heating block at draw ratio of 2. The diameter of drawn fiber, based on 15 observations using an optical microscope, was ~ 109 ± 9 μm.

P(DTD DD) fibers were sent to Georgia Institute of Technology (Atlanta, GA) for drawing. The results of these trials are summarized in table 7. The fiber could be drawn

Melt Spinning conditions	
Reservoir internal diameter	28 mm
Spinneret size	500 μm
Plunger speed	1.5 mm/min
Spinning temperature	155 °C
Take up speed	80 m/min
Die size	1.0 mm
Drawing Conditions	
Unwind speed	2 m/min
Take up speed	4 m/min
Draw ratio	2
Drawing temperature (using heating block)	75 °C

Table 6: 3rd generation P(DTD DD) spinning and drawing conditions

only 1.5X to a modulus of 1.3 GPa. The fiber was redrawn by 1.2X at 75 ºC to achieve a modulus of 2.4 GPa. In the end, we were able to achieve 2.7 GPa with further modifications to spinning and drawing conditions.

Sample		**P(DTD DD) 3rd Gen.**	**P(DTD DD) 2nd Gen.**
Powder	M_w (May)	105 (kDa)	
Drawn fiber	M_w (Oct.)	104 (kDa)	88 (kDa)
Properties	Modulus	2.7 Gpa	2.7 GPa

Table 7: Summary of the characteristics of the polymer and the fiber

3.3.2. Phase III collagen fiber fabrication

Type I bovine collagen fibers were manufactured as previously described in section 3.2.9. Phase IIb Collagen fiber processing.

3.3.3. Phase III collagen crosslinking

Collagen fibers were crosslinked using EDC in acetone was immersed in a room temperature bath of EDC (Sigma Chemical Co., St. Louis, MO) as previously described in section 3.2.10. Phase IIb collagen crosslinking.

3.3.4. Phase III scaffold fabrication and Ebeam sterilization

Three-stranded braided hybrid scaffolds had a total length of 150 mm with a total of approximately 30 loops. Each strand was composed of 500 fibers consisting of 75% p(DTD DD) and 25% type I bovine collagen fibers for a total of 1500 fibers. The ends were tied with 4-0 monocryl (Ethicon, Somerville, NJ) suture using a constrictor knot and glued with Medical Device Urethane Adhesive (M-06FL, Loctite, Rocky Hill, CT) and allowed to cure for at least 24 hours. Suture ends had 6 inches of slack to assist in anchoring. All hybrid scaffold samples were placed in Sterilization Pouches (Fisher brand, Pittsburgh, PA) and Ebeam (E-beam, Incorporated, Cranbridge, NJ) sterilized at a dosage of 2.5 MRad. The implant was inserted folded over during surgery doubling the size of the scaffold to 3000 fibers at a length of 75 mm.

3.3.5. Phase III pre-operative procedure

Five sheep were used per IACUC approved protocol procedures. 48 hours prior to surgery an area over the ribcage was shaved. Fasting from hay and grain began 24 and 20 hours prior to surgery, respectively, with water given ad-lib. A Fentanyl patch (100 μg/hr) was applied to shaved skin and secured with coban wrap 24 hours prior to surgery. On surgery day, the animal was transported to the prep area to have its neck shaved for insertion of a IV catheteter. Anesthesia was inducted with Sodium Pentothal (15-20 mg/kg) in Normasol solution in the jugular vein. The sheep was then intubated and a

Rumen tube was inserted into the rumen for draining. Anesthesia was maintained with Isoforane (1.5-3%) in O_2/N_2O (50/50). 500 mg Cefazolin was administered pre-op intravenously and then again post-op.

3.3.6. Phase III surgical procedure

General anesthesia was maintained by the surgical staff of the vivarium. A circulating hot water blanket maintained body temperature while under anesthesia. ECG, End Tidal CO_2 and SpO_2 were monitored during the procedure.

The subject was positioned on the operating table in the supine position. The operative hind limb was then prepped and draped in the usual sterile fashion. The knee joint was injected with 30 cc's of 0.25% Marcaine and Epinephrine. A lateral arthroscopy portal was created with a #11 blade and the arthroscope was introduced through the lateral portal. A diagnostic examination of the knee was performed. A medial arthroscopy portal was created with a #11 blade. A motorized shaver was introduced through the medial portal and a portion of intraarticular fat pad was resected to improve visualization. Using arthroscopic baskets and shaver, the anterior cruciate ligament was resected. Using a motorized shaver, bone was removed from the inner wall of the lateral femoral condyle creating a notchplasy. This allowed visualization in the intercondylar notch as well as visualization for anatomic placement of the ACL graft. A small incision was made over the antromedial tibial cortex. An arthroscopic drill guide was inserted into the knee joint through the medial portal and a guide wire was drilled through the antromedial tibial cortex into the knee joint at the anatomic insertion site of the ACL on the tibia. Using a cannulated reamer, a tunnel was created in the tibia over the guide wire. A guide wire was then inserted into the knee joint through the medial

arthroscopy portal and placed on the anatomic insertion site of the ACL on the femur. This guide wire was then drilled through the lateral femoral condyle of the femur and out the anterolateral upper leg. A 6 mm tunnel was drilled in the lateral femoral condyle using a cannulated reamer over the previously placed guide wire. A small incision was made on the lateral aspect of the upper leg where the guide wire exits the skin and a combination of sharp and blunt dissection was performed down to the lateral cortex of the femur where the tunnel exits the femur. Using a suture passer, the braided hybrid scaffold implant was pulled into the tibial tunnel, into the knee joint and into the femoral tunnel. This was all performed under arthroscopic guidance. Once the implant had achieved an anatomic position, the implant was secured on the femoral end by tying sutures over an extracortical polyethylene button. The implant was then tensioned against the button and secured on the tibial end with a 7 mm interference screw. Any excess material from the braided hybrid scaffold implant was cut away leaving the implant flush with the tibital surface. The knee joint was copiously irrigated. All of the wounds were copiously irrigated. The subcutaneous tissue was reapproximated with interrupted 2-0 vicryl sutures and the skin incisions were closed primarily with running subcuticular monocryl sutures. The arthroscopy portals were closed with monocryl sutures. All incisions were painted with betadine.

3.3.7. Phase III post-surgical procedure

After 24 hours and after the last antibiotic, 5 mg oral dose of Probios was administered to replace gut microflora killed by antibiotic treatment. Animals were returned to individual cages with unrestricted activity and given water and food *ad libitum*. Analgesics were given for 2 days or until no signs of pain were observed. Two

time points were assessed, a visualization time point and 12 week time point. After 3-6 weeks implantation, subjects were arthoscopically visualized. We recorded implant intactibility and made gross observations. After 12 weeks subjects were euthanized using pentobarbital infusion. The knee joint was exposed and examined grossly. The Femur-Hybrid Scaffold-Tibia Complex (FHTC) were skeletonized and harvested for mechanical and histological examination.

3.3.8. Phase III arthroscopic visualization

In an effort to decrease the number of animals while maximizing data collection we performed arthroscopic visualizations at the first time point between 3-6 weeks. Previously we sacrificed animals at this initial time point to check for intactness, incorporation and tension, all of which we can now do arthroscopically with a larger animal mode. The animals were fully anesthetized as previously mentioned and an arthroscopic camera used to visualize the braided hybrid scaffold. If we noticed scaffold rupture, then the animal would be sacrificed to minimize further pain. However, if the scaffold was intact then the animal would proceed to the full 12 week time point. 1 animal was sacrificed even if no signs of rupture are present at 4 weeks for histological analysis. 1 week after visualizations sheep were transported to the Perry Sheep Farm (Whitehouse Station, NJ) to continue rehabilitation in a normal sheep environment.

3.3.9. Phase III single fiber and braided hybrid scaffold mechanical testing

A modified version of ASTM D3822, Standard Test Method for Tensile Properties of Single Textile Fibers, was used to mechanically test single and braided hybrid fiber scaffolds. Single non-sterile P(DTD DD) fibers (n=10) were mechanically tested as described previously, section 3.1.3. Phase Ia single fiber mechanical testing and

characterization, using an Instron Model 4204. Fibers had a 50 mm gauge length and were elongated mechanically at a strain rate of 60 % min until failure. Fiber diameters were measured using a laser micrometer (Z-mike model 1202B, Dayton, OH) prior to testing.

Data from single fibers were used to calculate the total cross-sectional area of the braided hybrid scaffolds. We tested all scaffolds at a strain rate of 60% min and at three different gripping conditions: PMMA, PMMA with suture and the femur-braided scaffold-tibia complex (FBTC), figure 15. The latter was not tested until failure and used an Instron Model 4204 and the 2 former used Instron Model 5569. When testing the braided hybrid scaffold while gripping with just PMMA the entire load was placed directly onto the scaffold and is considered our actual scaffold values, figure 15. When gripping the scaffold with one end in PMMA and the other with a suture we were trying to mimic surgical anchoring which has one end held rigid with an interference screw and the other tied down to an

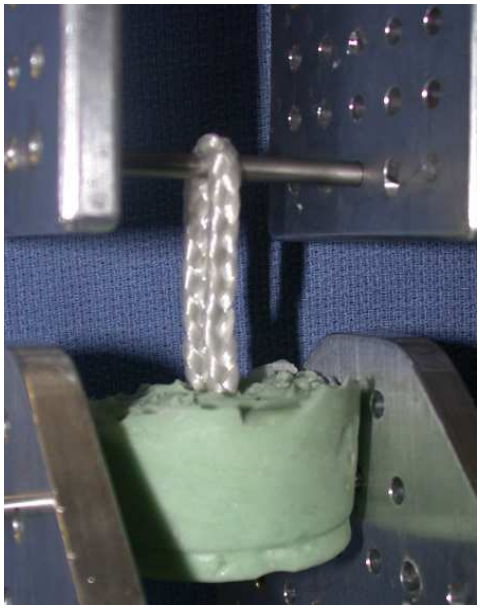

Figure 15: Mechanical testing of hybrid braided scaffold while gripping PMMA.

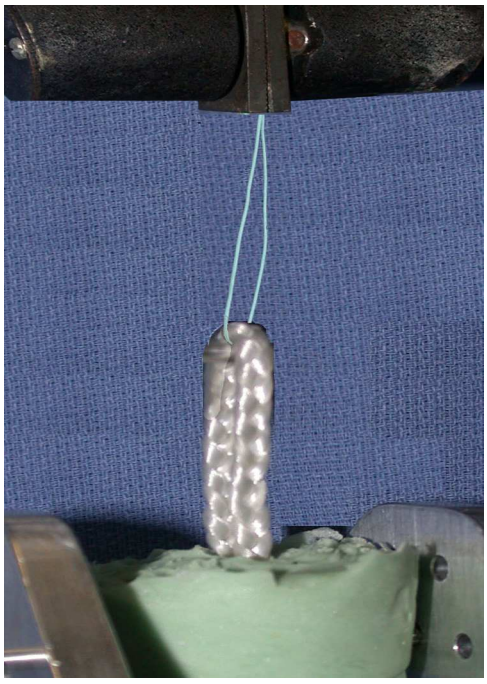

Figure 16: Mechanical testing of hybrid braided scaffold while gripping PMMA and suture ends.

endo button by suture. This type of gripping is considered our initial scaffold values and is shown in figure 16. FBTC explants, soaked in saline, were mechanically tested under tension using K-wires to secure the femur and tibia to the Instron crossheads at angle approximately 45°. This aligned the ligament to the crosshead axis. The contralateral Femur-ACL-Tibia Complex (FATC) was also tested under similar conditions and acted as the control, figure 17.

3.3.10. Phase III histological analysis of scaffolds

After mechanical testing scaffolds were stored in formalin and sent for histological analysis. Samples were examined by paraffin-embedded hematoxylin (H)- and eosin (E), Masson's trichrome and Von Kossa stained histological slides (AML labs Inc., Rosedale, MD) at neoligament midsubstance 1 mm apart and bone tunnel sections. Slides were labeled in three sections depending on their location, ACL space, Femur and Tibia. Hematoxylin (H)- and eosin (E) slides were ranked based on qualitative evaluation of lymphocytes, eosinophils, multi-nucleated giant cells (MNGC), cellular infiltration and vascular tissue and blood vessels, as explained by van Tienen and Fox, et al were ranked by a medical pathologist [107, 108]. Slides were ranked from low-1 to high-4 and the average

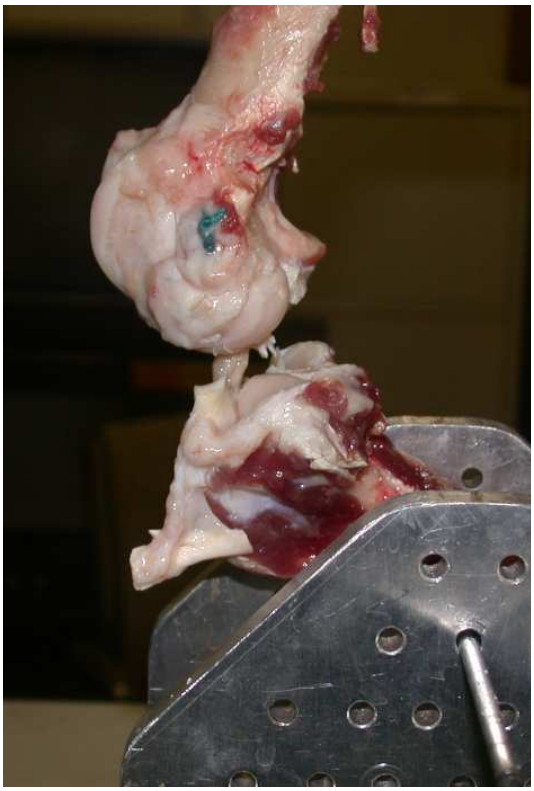

Figure 17: Mechanical testing of FBTC using K wires to align the scaffold to the

rank was reported. Von Kossa stains calcium in mineralized tissue, utilizing a silver nitrate solution followed by sodium thiosulfate; calcified bone is stained black. Masson's trichrome is a three-color staining protocol used in histology that stains collagen or bone blue.

3.3.11. Phase III statistical analysis

Table data and graphs are presented in the form of mean ± standard deviation.

4. RESULTS

4.1. Phase I studies

4.1.1. Phase Ia fiber degradation results

The mechanical properties of single fibers in dry (control) and PBS environments are summarized in table 8. P(DTD DD) and PLLA fiber batches had an average diameter of 91 ± 2 and 88 ± 3 μm, respectively. No statistically significant differences were detected in fiber diameters.

Material	Average Properties	Dry (Control)	Saline (Initial)	Saline 64 Weeks
Non-Sterile P(DTD DD)	Yield σ (MPa)	191 ± 11	144 ± 17	55 ± 24
	Yield ε (%)	9.8 ± 1.2	9.6 ± 1.4	3.6 ± 2.0
	Young E (GPa)	2.7 ± 0.2	1.8 ± 0.2	2.8 ± 0.8
	MW (kDa)	90 ± 6	85 ± 2	35 ± 2
Non-Sterile PLLA	Yield σ (MPa)	125 ± 13	95 ± 16	38 ± 21
	Yield ε (%)	3.4 ± 0.4	2.8 ± 0.6	3.0 ± 2.3
	Young E (GPa)	5.4 ± 0.2	4.8 ± 0.3	4.6 ± 0.8
	MW (kDa)	144 ± 2	145 ± 7	43 ± 15
Sterile P(DTD DD)	Yield σ (MPa)	185 ± 12	150 ± 22	37 ± 20
	Yield ε (%)	10.1 ± 1.0	10.5 ± 1.6	2.6 ± 1.2
	Young E (GPa)	2.6 ± 0.3	1.7 ± 0.1	2.7 ± 0.4
	MW (kDa)	86 ± 3	85 ± 3	35 ± 2
Sterile PLLA	Yield σ (MPa)	118 ± 9	87 ± 12	44 ± 23
	Yield ε (%)	3.2 ± 0.3	2.8 ± 0.4	1.8 ± 1.1
	Young E (GPa)	5.2 ± 0.3	4.4 ± 0.3	4.5 ± 1.2
	MW (kDa)	148 ± 6	149 ± 5	53 ± 17

Table 8: Mechanical properties of single fibers in dry and saline environments.

There were no statistically significant differences between sterile and non-sterile fibers. Mechanical testing of control sterile single fibers resulted in an average yield stress of 185 ± 12 and 118 ± 9 MPa for p(DTD DD) and PLLA, which were not significantly different from the non-sterile values of 191 ± 11 ($p=0.981$) and 125 ± 13 MPa ($p=0.828$), respectively. Yield stress values remained consistently over 100 MPa for both polymers up to 24 weeks. At 32 weeks p(DTD DD) decreased to 49%, 91 ± 9 MPa ($p=0.003$), of the initial value and PLLA decreased to 71%, 84 ± 7 MPa ($p=0.003$), of the initial value. After 64 weeks of incubation fiber strength retention decreased to 20% and 37% for the sterile p(DTD DD) and PLLA fibers and 29% and 31% for the non-sterile fibers, respectively, figures 18 and 19.

Initial moduli for control dry fibers were 2.6 ± 0.3 and 5.2 ± 0.3 GPa for p(DTD DD) and PLLA, respectively. When tested wet (at 37°C) their moduli decreased to 65%, 1.7 ± 0.1 ($p<0.05$) and 86%, 4.4 ± 0.3 ($p=0.009$) GPa of the dry value. There was a significant difference between the moduli for p(DTD DD) at the 32 and 64 week time points as it increased from 1.7 ± 0.2 to 2.7 ± 0.4 GPa ($p=0.001$).

Similar to the yield stress values, a general downward trend was observed with the MW vs. incubation time, as expected. There was a significant difference between the 32 (53 ± 3 kDa) and 64 (35 ± 2 kDa) week time points for sterile p(DTD DD), $p=0.001$, and between 24 (97 ± 15 kDa) and 64 (53 ± 17 kDa) week time points for sterile PLLA fibers, $p=0.017$. After 64 weeks p(DTD DD) and PLLA MW values decreased to 41%

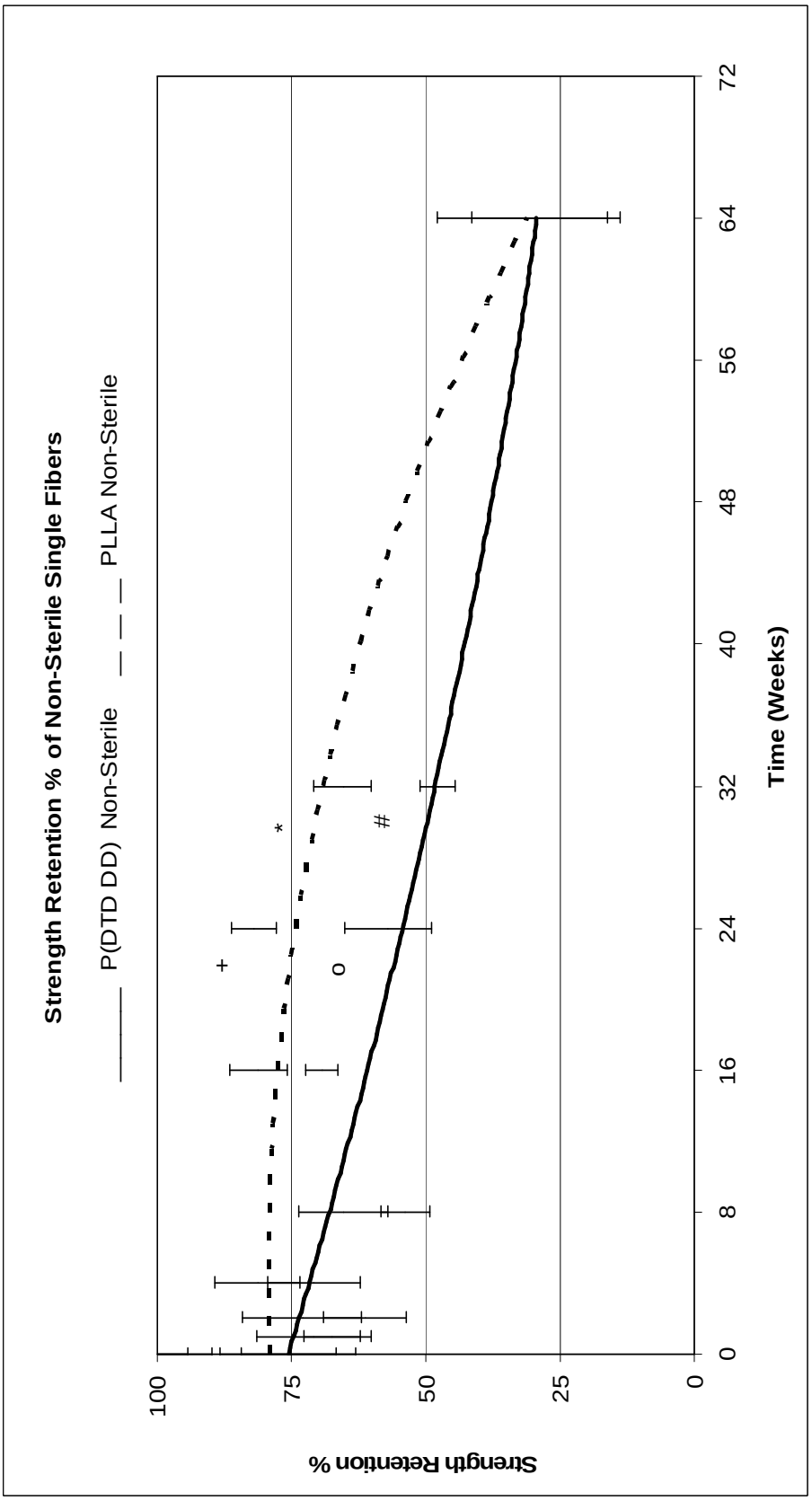

Figure 18: Strength retention Percentage trendline.

Non-sterile p(DTD DD) and PLLA single fibers after 64 weeks of incubation in PBS with a pH of 7.4 at 37°C. * indicates a significant difference, p-value < 0.05 with respect to 64 weeks. + indicates a significant difference, p-value < 0.05 with respect to 64 weeks. # indicates a significant difference, p-value < 0.05 with respect to 64 weeks. o indicates a significant difference, p-value < 0.05 with respect to 64 weeks.

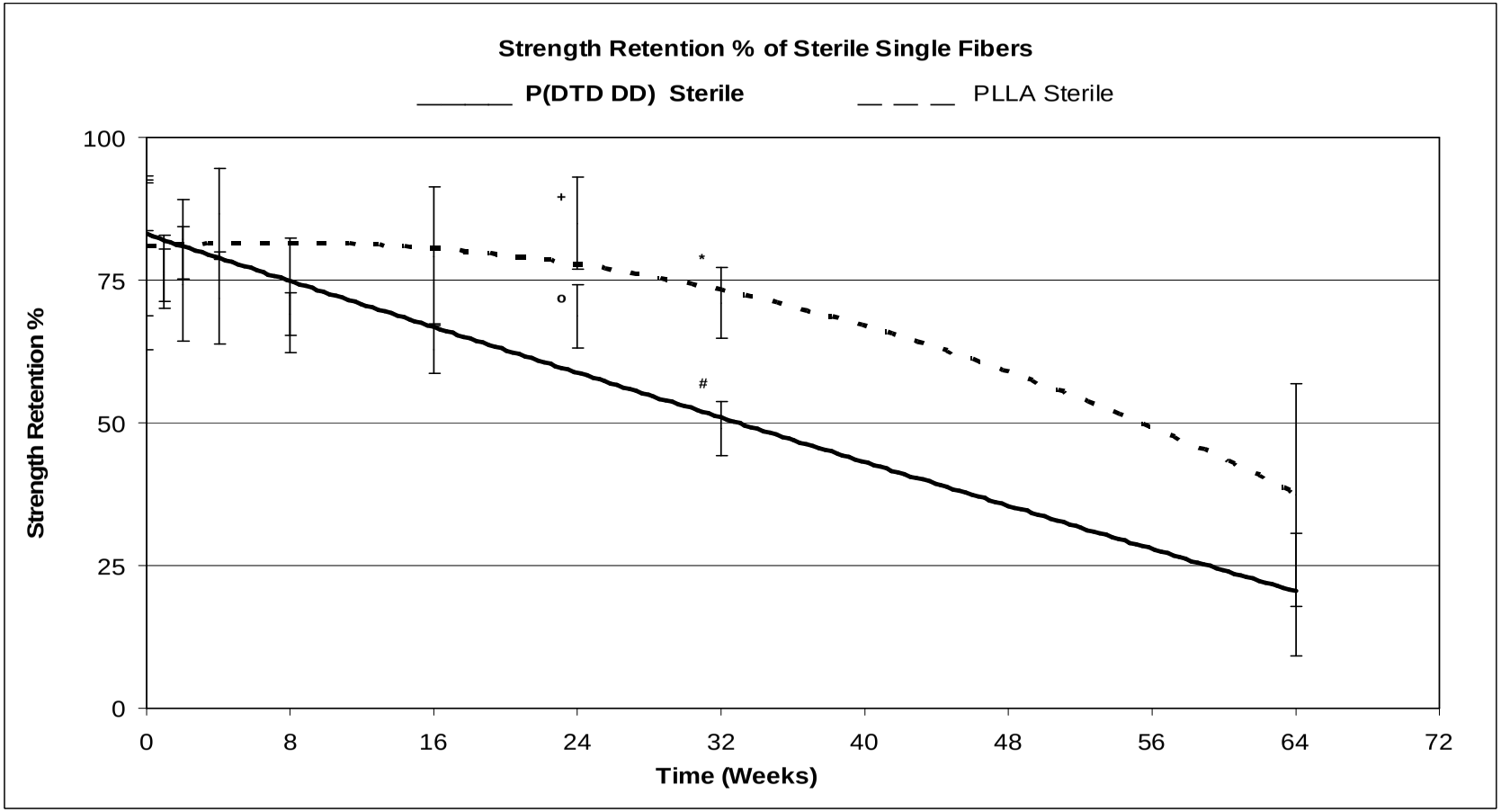

Figure 19: Strength retention percentage trendline.

P(DTD DD) and PLLA single fibers after 64 weeks of incubation in PBS with a pH of 7.4 at 37°C. * indicates a significant difference, p-value < 0.05 with respect to 64 weeks. + indicates a significant difference, p-value < 0.05 with respect to 64 weeks. # indicates a significant difference, p-value < 0.05 with respect to 64 weeks. o indicates a significant difference, p-value < 0.05 with respect to 64 weeks.

and 36% and non-sterile polymers decreased to 39% (43 ± 15 kDa) and 30% (35 ± 2 kDa) of the initial MWs, respectively, figures 20 and 21.

There was a significant decrease in T_c for sterile p(DTD DD) from 39.8 ± 0.1 to 38 ± 0.1 °C (p=0.001) between the 32 and 64 week time points. There was also a significant increase in T_m for sterile p(DTD DD) from 59.1 ± 2.6 to 63.5 ± 0.2 °C (p=0.01). This increase in T_m contrasts with the decrease in T_m observed in sterile PLLA. Figures 22 and 23 show the DSC scans of sterile p(DTD DD) and PLLA fibers at 16 weeks, respectively. The DSC of PLLA is straightforward; during heating there is a T_g at 60.3 ºC, cold crystallization at 99.5 ºC and T_m at 174.7 ºC; during cooling there was melt crystallization at 101.6 ºC and T_g at 56.7 ºC. The T_m of PLLA decreased from 174.2 ± 0.2 to 168.8 ± 3.2 °C (p=0.043) between the 32 and 64 week time point. The interpretation of DSC scan of p(DTD DD) was more complex because of the liquid crystalline characteristics that could be present in this polymer [72-74]. The main melting at 55.5 ºC was followed by secondary melting at 66.9 ºC, beyond which the polymer looses its birefringence and remnants of any order. Although p(DTD DD) passes through various types of ordering as it was heated into the isotropic state, the main endothermic peak at 55.5 ºC can be regarded as the main melting peak, T_m. Upon cooling, the polymer crystallized at 39.3ºC.

4.1.2. Phase Ib scaffold *in vitro* results

Rabbit skin fibroblasts attached and proliferated in a complete media solution on both p(DTD DD) and PLLA scaffolds after cell culture and seeding, figure 24. Initial cell attachment values with standard error of the mean after 4 hours were 500 ± 200 and 1800 ± 900 cells for p(DTD DD) and PLLA fiber scaffolds, respectively.

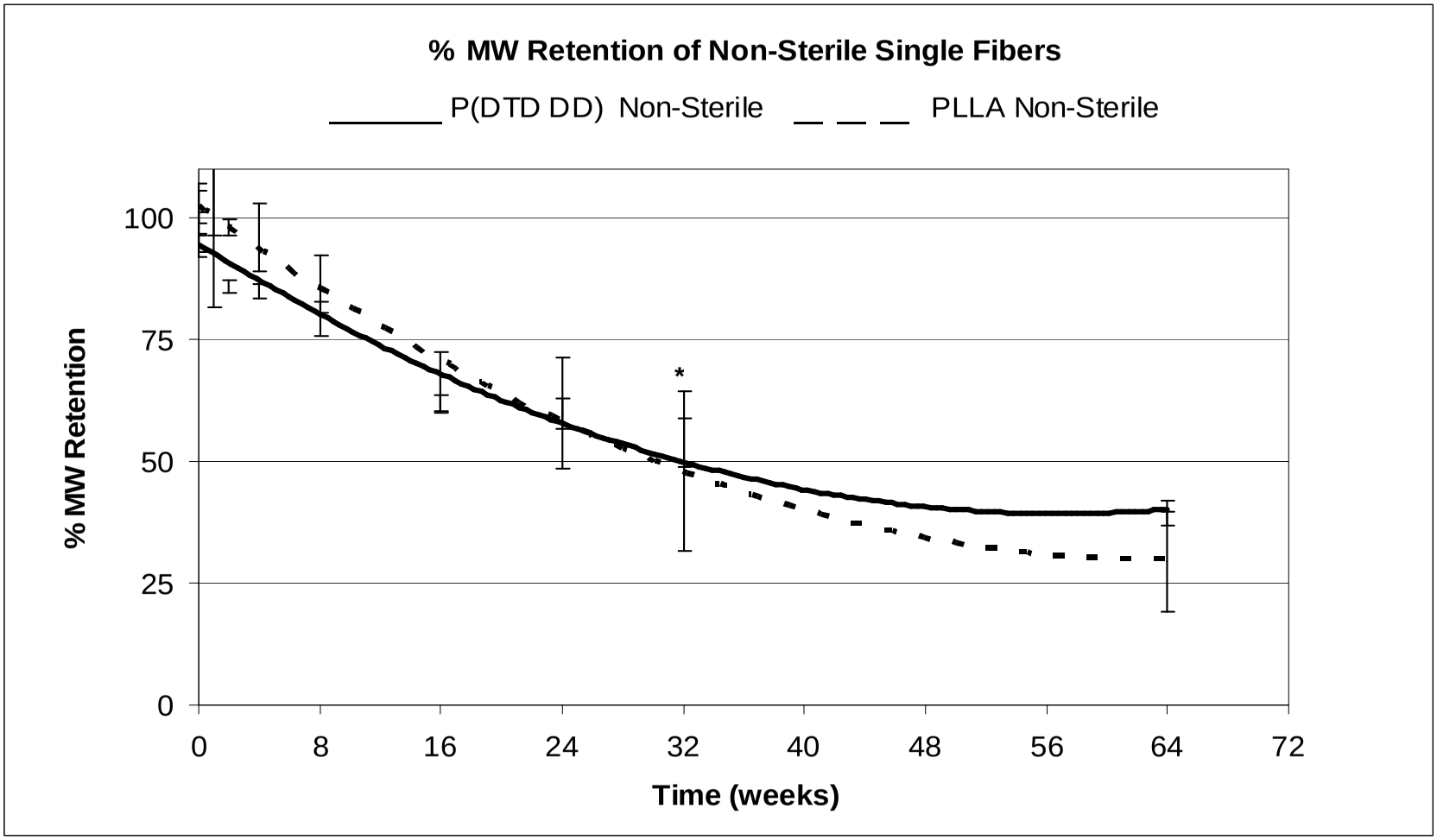

Figure 20: Percent MW retention trendline.

Non-sterile p(DTD DD) and PLLA single fibers after 64 weeks of incubation in PBS with a pH of 7.4 at 37°C. * indicates a significant difference, p-value < 0.05 with respect to 64 weeks.

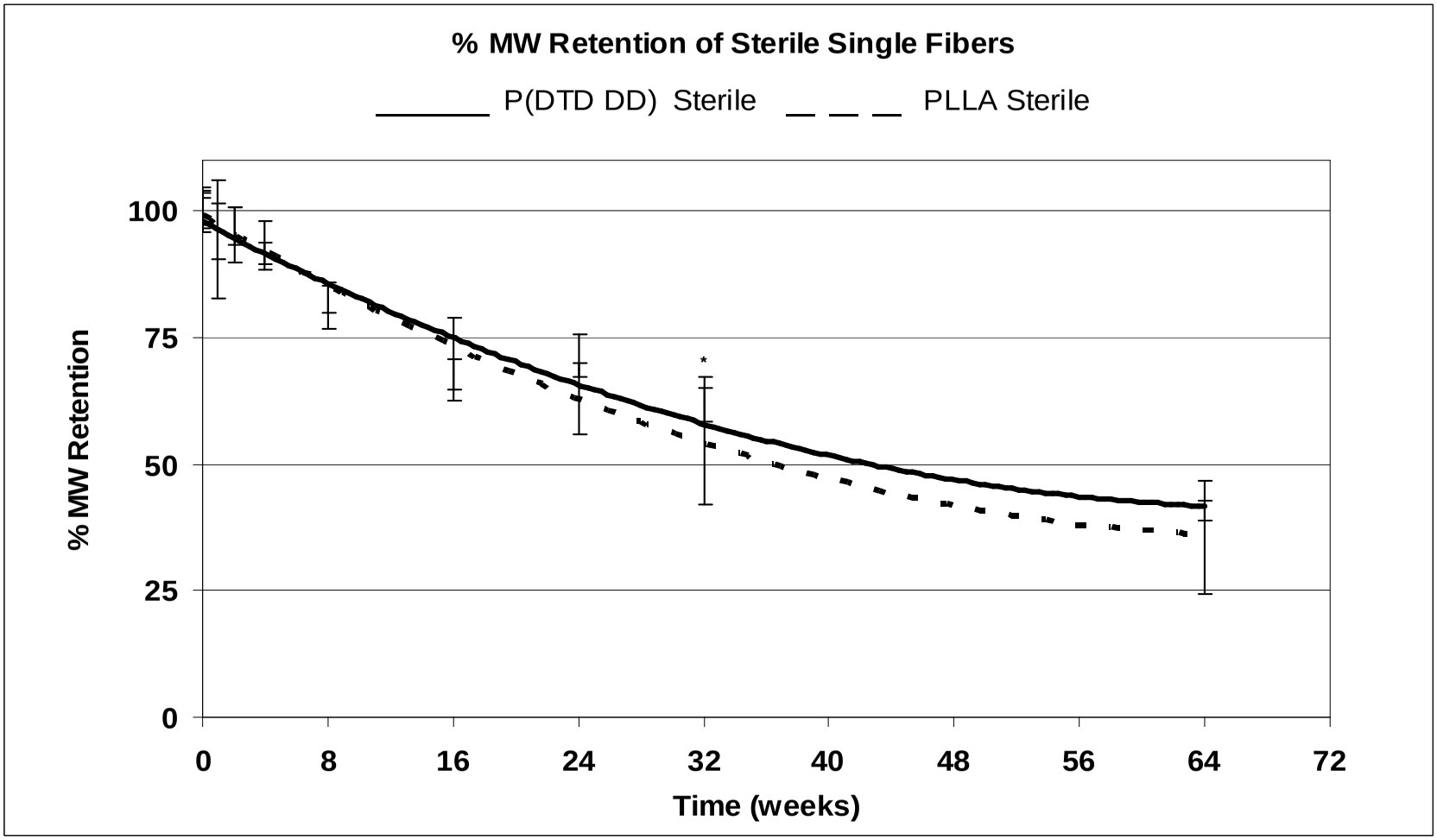

Figure 21: Percent MW retention trendline.

Sterile p(DTD DD) and PLLA single fibers after 64 weeks of incubation in PBS with a pH of 7.4 at 37°C. * indicates a significant difference, p-value < 0.05 with respect to 64 weeks.

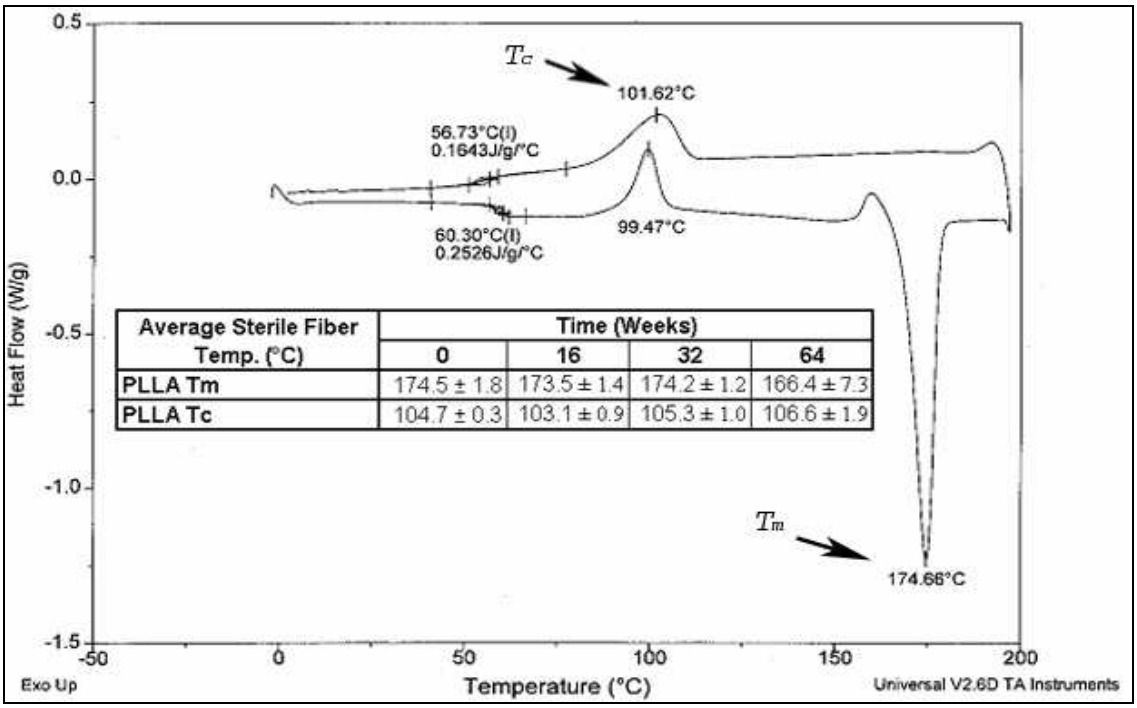

Average Sterile Fiber Temp. (°C)	Time (Weeks)			
	0	16	32	64
PLLA Tm	174.5 ± 1.8	173.5 ± 1.4	174.2 ± 1.2	166.4 ± 7.3
PLLA Tc	104.7 ± 0.3	103.1 ± 0.9	105.3 ± 1.0	106.6 ± 1.9

Figure 22: T_c and T_m values for PLLA fiber at 16 weeks, DSC.

Table of average sterile PLLA fiber T_c and T_m values up to 64 weeks.

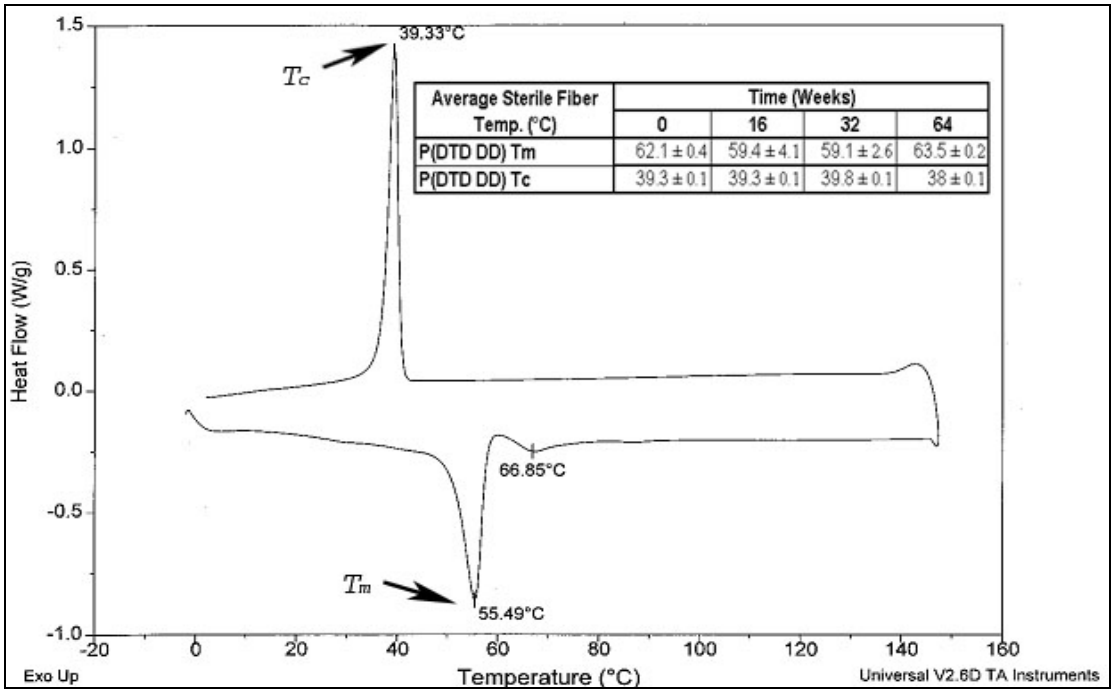

Average Sterile Fiber Temp. (°C)	Time (Weeks)			
	0	16	32	64
P(DTD DD) Tm	62.1 ± 0.4	59.4 ± 4.1	59.1 ± 2.6	63.5 ± 0.2
P(DTD DD) Tc	39.3 ± 0.1	39.3 ± 0.1	39.8 ± 0.1	38 ± 0.1

Figure 23: T_c and T_m values for p(DTD DD) fiber at 16 weeks, DSC.

Table of average sterile p(DTD DD) fiber T_c and T_m values up to 64 weeks.

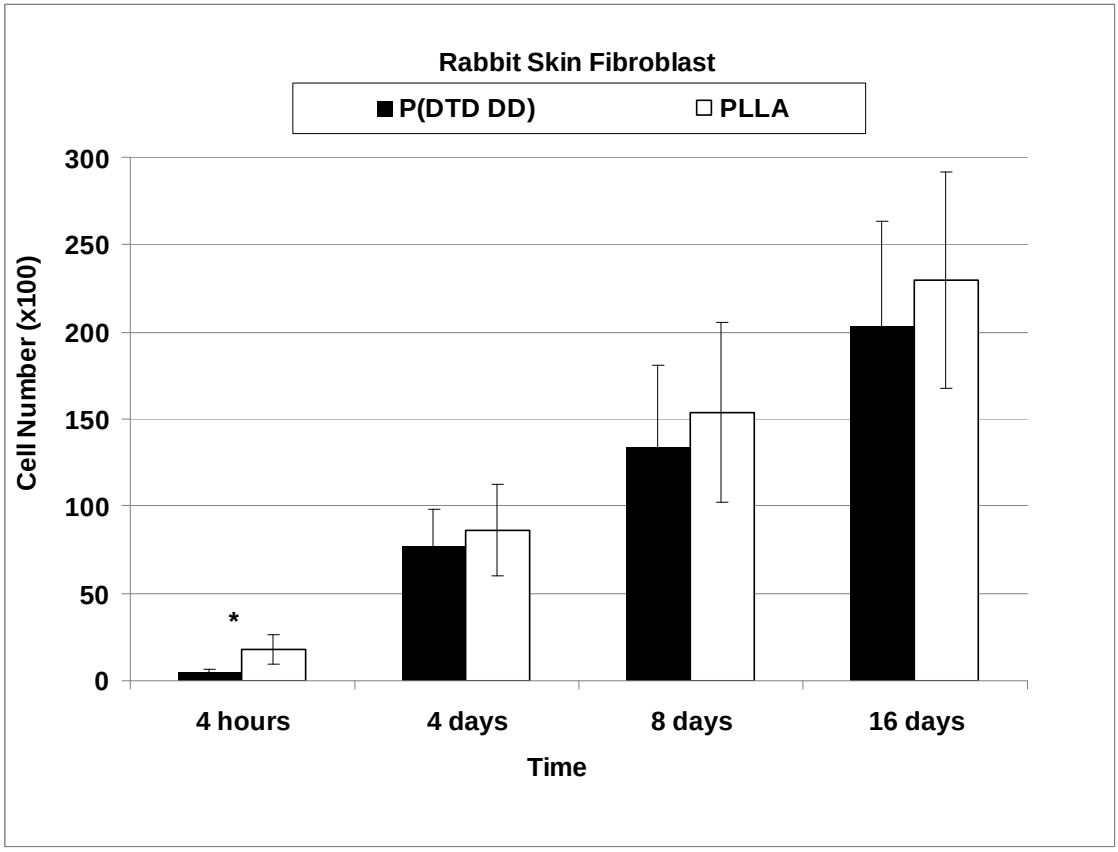

Figure 24: Fibroblast cell count.
P(DTD DD) and PLLA fiber scaffolds for 4 hours, 4, 8 and 16 days time point (Standard error of the mean). * indicates a significant difference, p-value < 0.05 with respect to 16 days.

Viable cells labeled with red fluorescent dye were seen distributed along the length of the fiber, figures 25A,B and 26A,B. After 16 days 20,300 and 23,000 cells were attached to p(DTD DD) and PLLA scaffolds, respectively. There was a 3 fold increase for both p(DTD DD) and PLLA scaffolds between the 4 and 16-day time points according to MTS Assay readings and there was a significant difference between the average values between the 4 hour and 16 day time points (p=0.021). There was no significant difference found between the number of cells populating p(DTD DD) and PLLA scaffolds after 16 days.

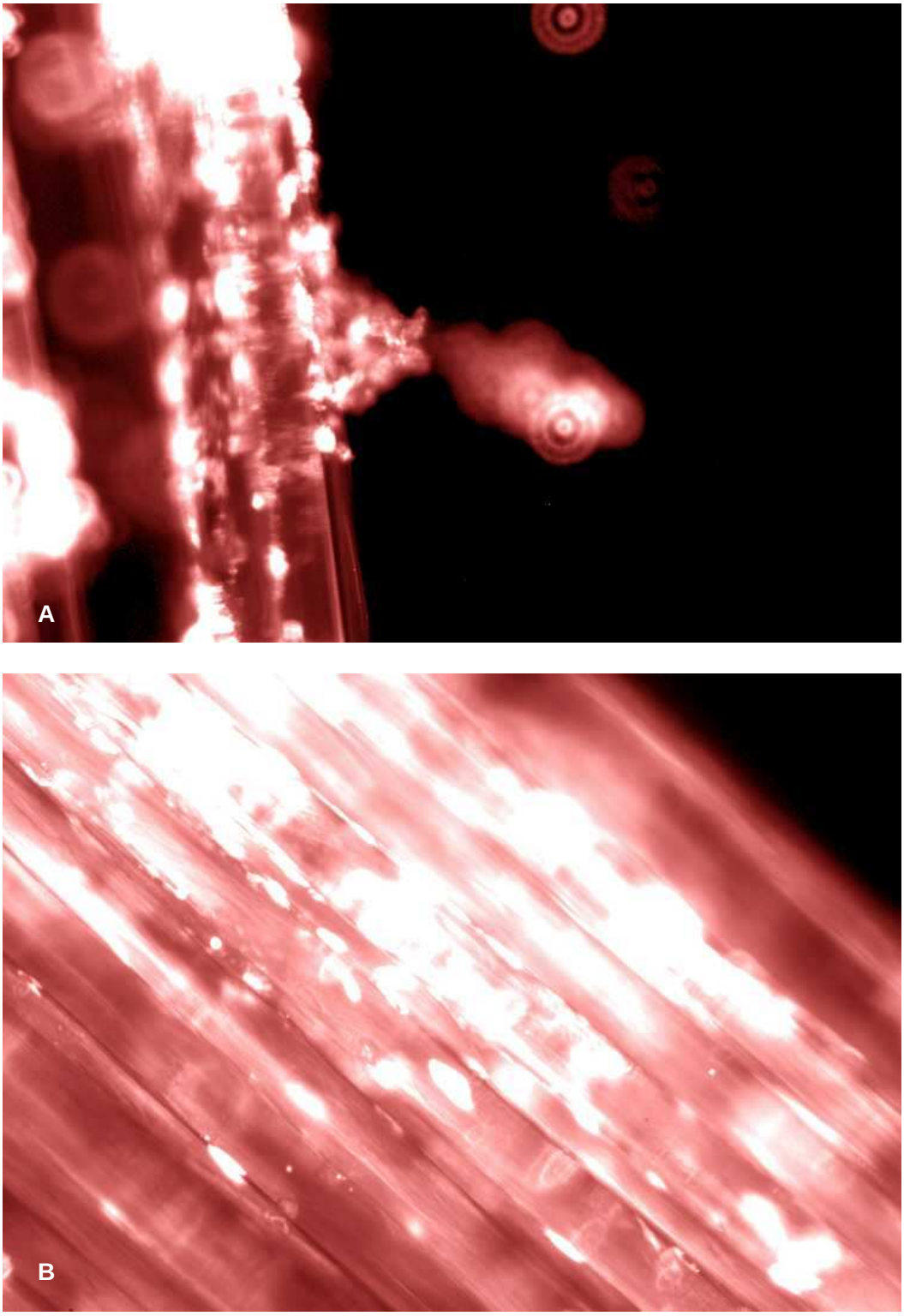

Figure 25A,B: Red Fluorescence labeled fibroblast attachment.
Sterile p(DTD DD) fiber scaffolds. (A) P(DTD DD) at 4 days (B) P(DTD DD) at 16 days. Cells were distributed along the lengths of individual fibers.

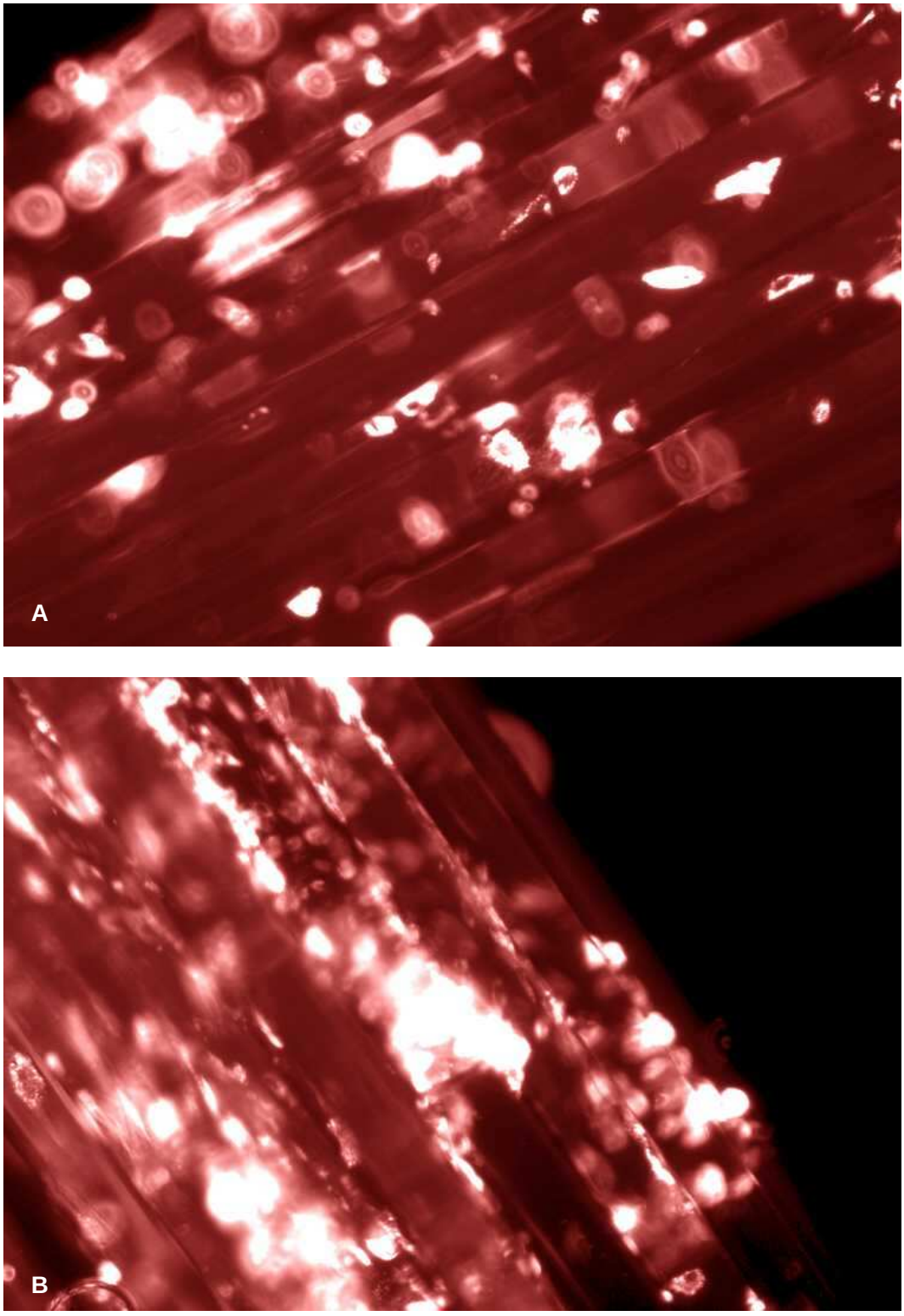

Figure 26A,B: Red Fluorescence labeled fibroblast attachment.
Sterile PLLA fiber scaffolds. (A) PLLA at 4 days (B) PLLA at 16 days time points. Cells were distributed along the lengths of individual fibers.

4.2. Phase II *in vivo* 2nd generation fibers studies

4.2.1. Phase IIa mechanical and histological results

Single p(DTD DD) fibers were mechanically tested until failure in a saline environment. P(DTD DD) fibers had an average diameter of 91 ± 2 μm. Single fiber yield stress and modulus values were measured at 94 ± 11 MPa and 1.45 ± 0.06 GPa, respectively. The FSTC had a break load of 45 N at 4 weeks post-implantation. The initial p(DTD DD) scaffolds had a break load of 208 ± 67 N. The control values, rabbit's contralateral ACL, had a load of 231 N. The *in vitro* scaffold and FSTC break loads were measured at 87 and 20 %, respectively, of the control values, figure 27. After 4 weeks, the scaffold's maximum strength decreased to 23% of the control value and upon gross observation was approximately 60% intact with no signs of arthritis or excess fluid in the knee. At the 6 week time point the FSTC was totally torn midsubstance and the rabbit knee showed no signs of arthritis or excess fluid. At week 7 the scaffold was once again totally torn midsubstance, showed no signs of excess fluid, but arthritic formation was observed. For both the 6 and 7 week time points fibers were still intact despite the fiber scaffold had completely ruptured. The modulus of the *in vitro* scaffold was measured at 635 ± 289 MPa, while the 4 week FSTC and rabbit initial ACL had a modulus of 530 and 126 MPa, respectively. FSTC at 6 and 7 weeks were not mechanically tested due to premature rupture.

Histological analysis of the explants revealed fibroblast attachment and ingrowth, reaching the center of the implants, figure 28A. There were no visible signs of inflammatory cells regardless of time points, figure 28B.

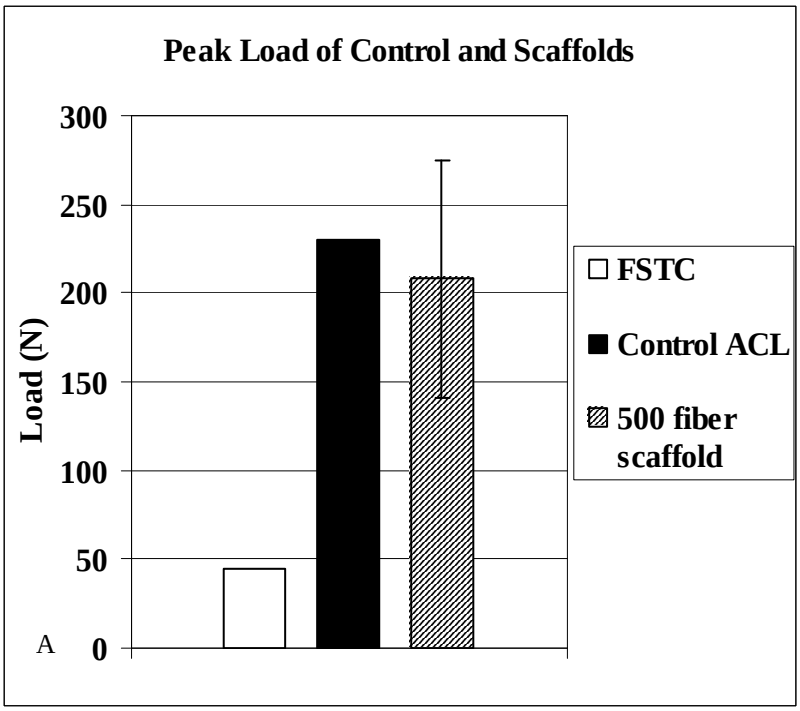

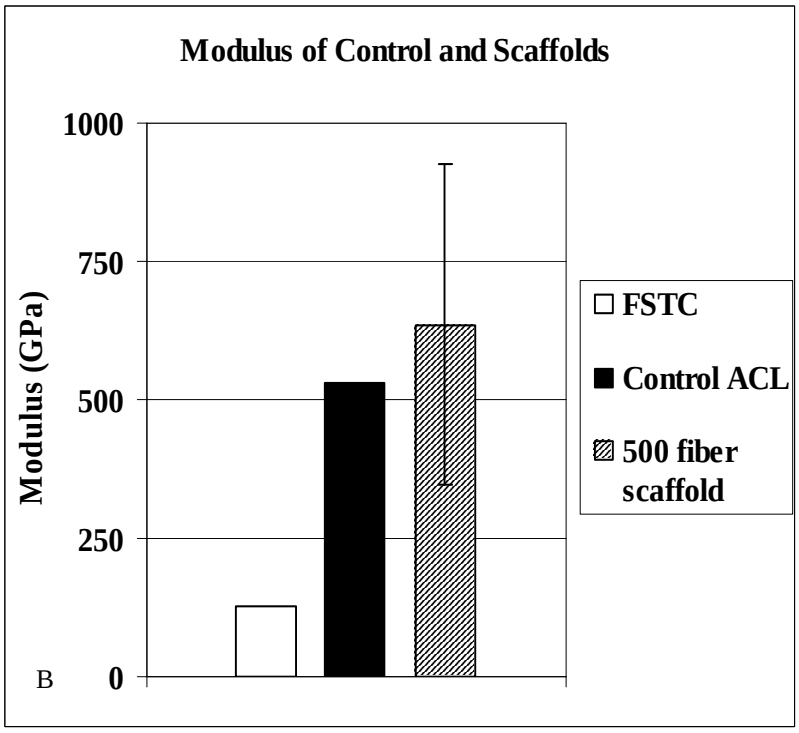

Figure 27A,B: Peak load.
(A) and Modulus (B) of the FSTC at 4 weeks explanation, Control ACL and 500 fibers scaffold.

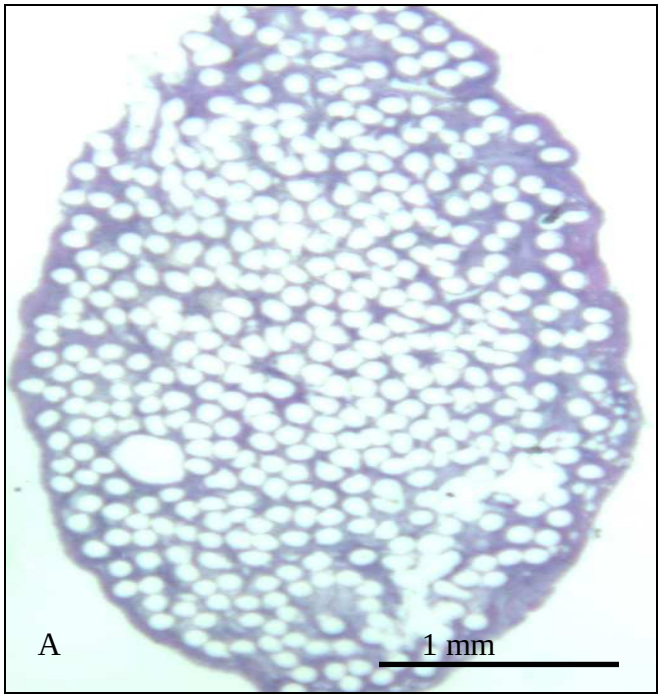

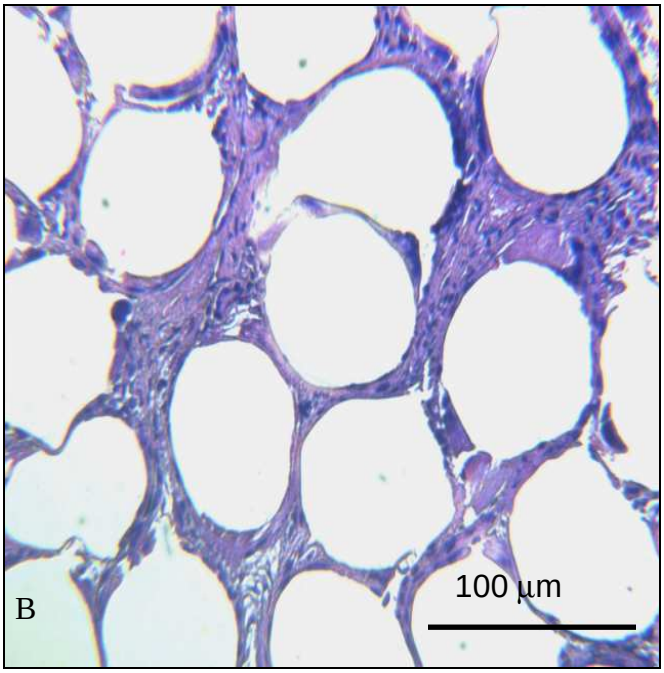

Figure 28A,B: Histological slides.
Cross sectional fiber scaffold explants after hematoxylin (H)- and eosin (E) staining and imbedding in paraffin at neoligament midssubstance. 6 week time point at 20x exposure (A) and 200x exposures (B).

4.2.2. Phase IIb mechanical and histological results

Collagen fibers had an average diameter of 61 ± 3 μm, respectively. Mechanical analysis of the initial hybrid scaffold resulted in a break load of 87 ± 9 N and modulus of 294 ± 41 MPa. Actual hybrid scaffold mechanical analysis resulted in a break load of 314 ± 65 N and a modulus of 747 ± 126 MPa. FHTC were explanted at 2 week and 4 week time points. At 2 weeks it was grossly observed that 2 of the hybrid scaffolds were approximately 90% intact, 1 was approximately 25% intact and 1 was approximately 33% intact. The 90% intact hybrid scaffolds (n=2) were used in the FHTC and mechanically elongated until failure and had a break load and modulus of 39 ± 14 N and 48 ± 5 MPa, respectively. The 25% and 33% intact scaffolds failed during preparation and are not reported. The rabbit's contralateral FATC break load and modulus were 206 ± 83 N and 2892 ± 1082 MPa, respectively. No mechanical data were attained at 4 weeks. At 4 weeks 2 of the hybrid scaffolds were approximately 33 and 15% intact while the remaining 2 were totally ruptured at the tibial bone tunnel site.

Histological analysis of the explants revealed cellular and vascular infiltration at 2 (n=4) and 4 (n=4) week time points with an increased infiltration at 4 weeks. Based on our qualitative grading scale we see an upward trend for cellular infiltration, presence of vascular tissue and blood vessels, lymphocytes, eosinophils and multi-nucleated giant cells (MNGC) from the 2 week time point to the 4 week time point, Figure 29.

Figure 30A,B shows a cross sectional view of the scaffold at the 2 and 4 week time point, the opaque circles at the outer regions are the collagen fibers and the clear circles, concentrated in the center, are the ghosts p(DTD DD) fibers. The periphery of the scaffolds at both time points shows a much larger concentration of cells, particularly

around the regions of the collagen fibers, figures 30A,B and 31A,B. The 2 week scaffold did show signs of fibrin, the early stage of collagen. A greater degree of cell infiltration was

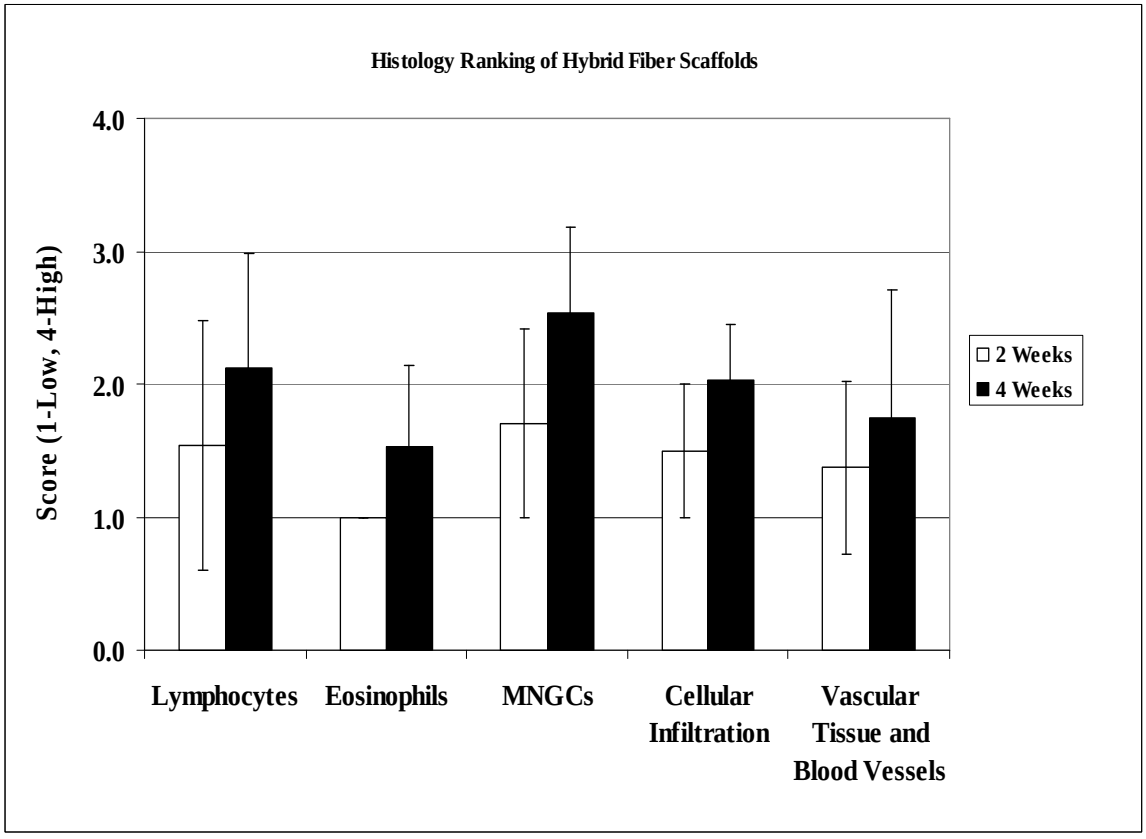

Figure 29: Average grading of hybrid scaffold.
Based on cross sections mid-substance using hematoxylin (H)- and eosin (E) stained slides. Parameters measured were lymphocytes, eosinophils, MNGC, cellular infiltration and vascular tissue and blood vessels.

also found at the center of the 4 week scaffold. Inflammation was also more evident at the 4 week time point than at 2 weeks with a higher presence of macrophages, MNGC's, lymphocytes, as well as foreign body granuloma, figure 31A,B.

Vascular tissue and blood vessels are clearly more evident at the 4 week time point with the presence of red blood cells surrounded by an endothelium, figure 32A,B.

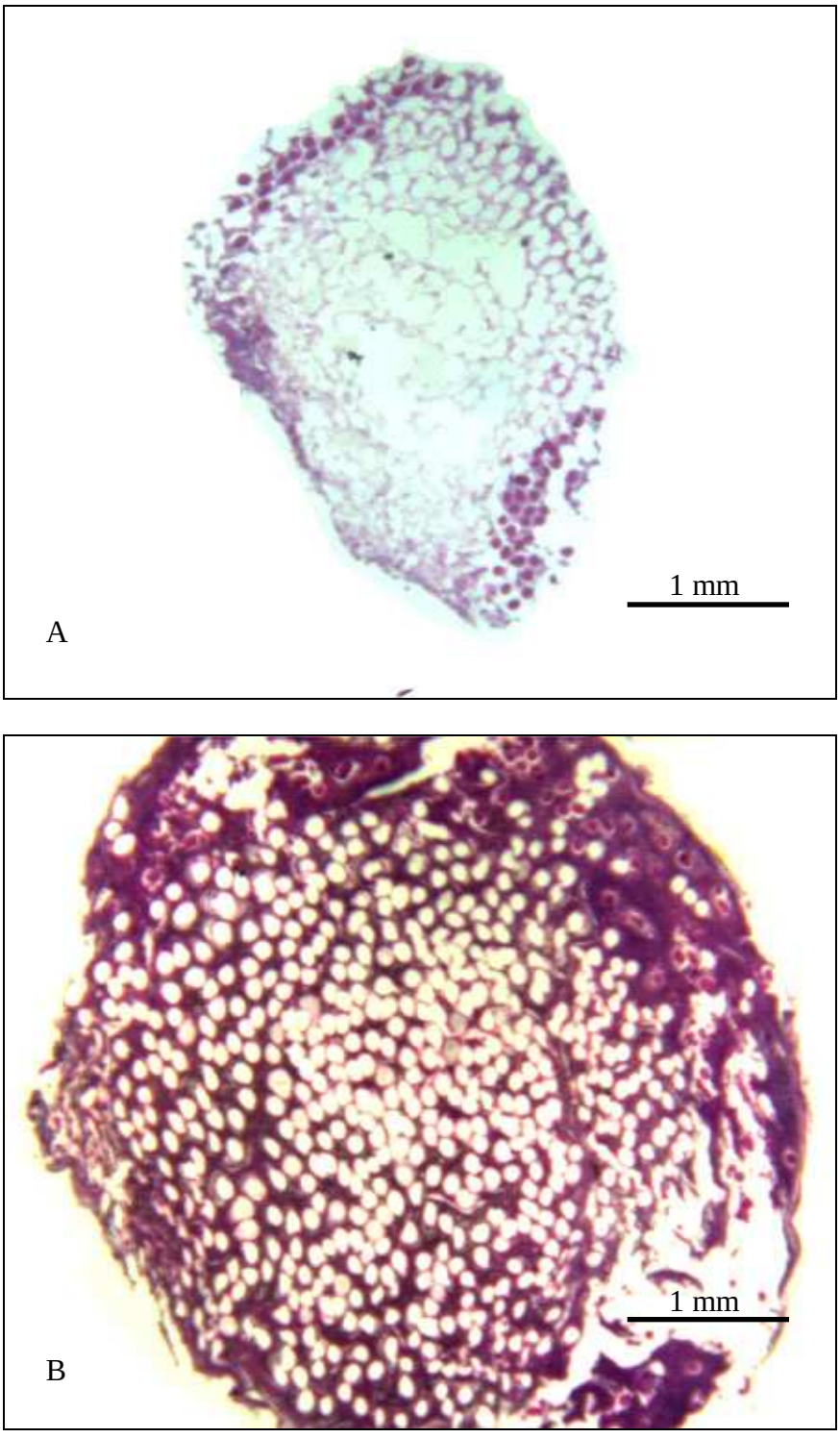

Figure 30A,B: Cellular infiltration of hybrid scaffolds.
(A) 2 weeks and (B) 4 weeks post-implantation at 20x exposure. Cellular infiltration was concentrated in the periphery of the scaffold with more developed collagen at the 4 week time point. P(DTD DD) fibers can be distinguished by their clear circular shape and collagen was seen as circular opaque shapes.

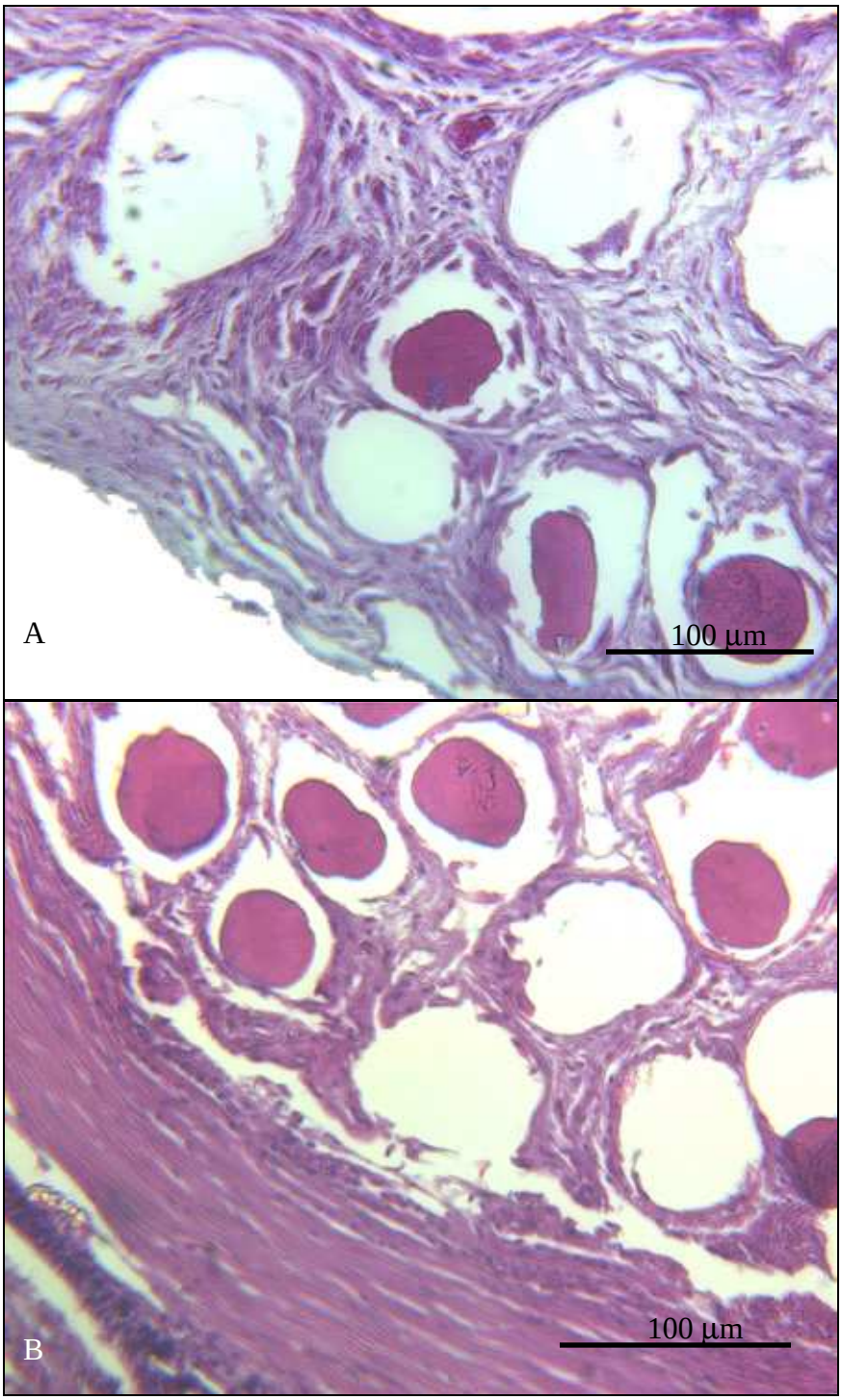

Figure 31A, B: Granuloma, fibroblasts, collagen and fibrin formation.
(A) 2 week and (B) 4 week time points on the outer cross section of hybrid scaffold mid-substance. At 4 weeks there also seems to be a more pronounced inflammatory reaction and cellular encapsulation than at 2 weeks. P(DTD DD) fibers can be distinguished by their clear circular shape and collagen was seen as circular opaque shapes.

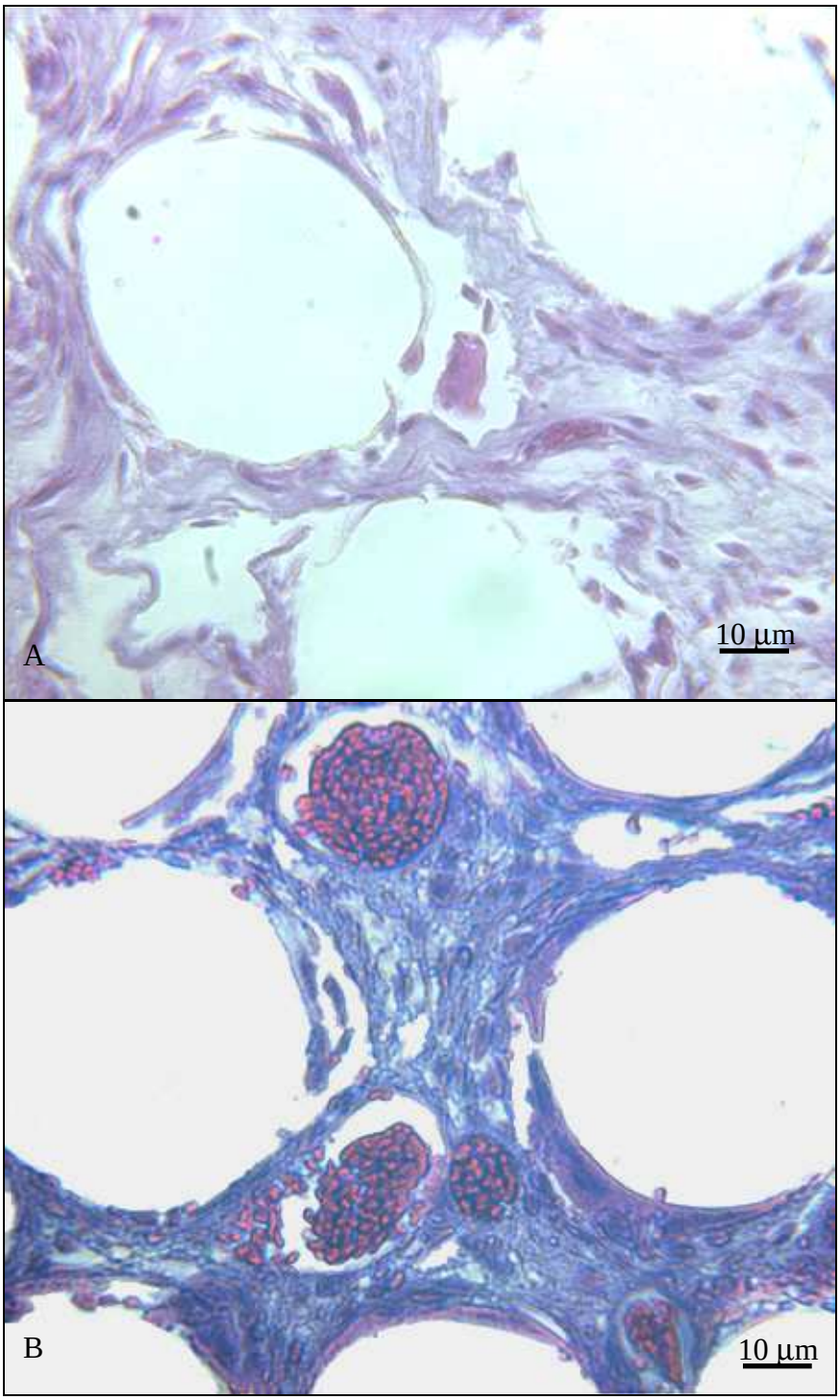

Figure 32A,B: Vascular tissue and blood vessels analysis
(A) 2 weeks and (B) 4 weeks post-implantation at 400x exposure. At 4 weeks red blood cells, surrounded by an epithelial wall, are more visible than at 2 weeks. Cellular infiltration was also far more developed. P(DTD DD) fibers are seen as clear circular shapes.

4.3. Phase III *in vivo* 3rd generation fibers mechanical and histological results

P(DTD DD) and collagen fibers had an average diameter of 66 ± 2 and 63 μm, respectively. Mechanical analysis of the actual braided hybrid scaffolds resulted in a break load of 934 ± 160 N and modulus of 353 ± 80 MPa. Initial braided hybrid scaffold mechanical analysis resulted in a break load of 313 ± 11 N and a modulus of 150 ± 8 MPa. Visualizations at 3-6 week time points showed that all scaffolds were intact, showed no major signs of inflammation and were under tension. FBTC were explanted for testing at 12 weeks and had a modulus of 7 ± 4 MPa, figure 33. The sheep's contralateral FATC break load and modulus were 1219 ± 376 N and 31 ± 12 MPa, respectively.

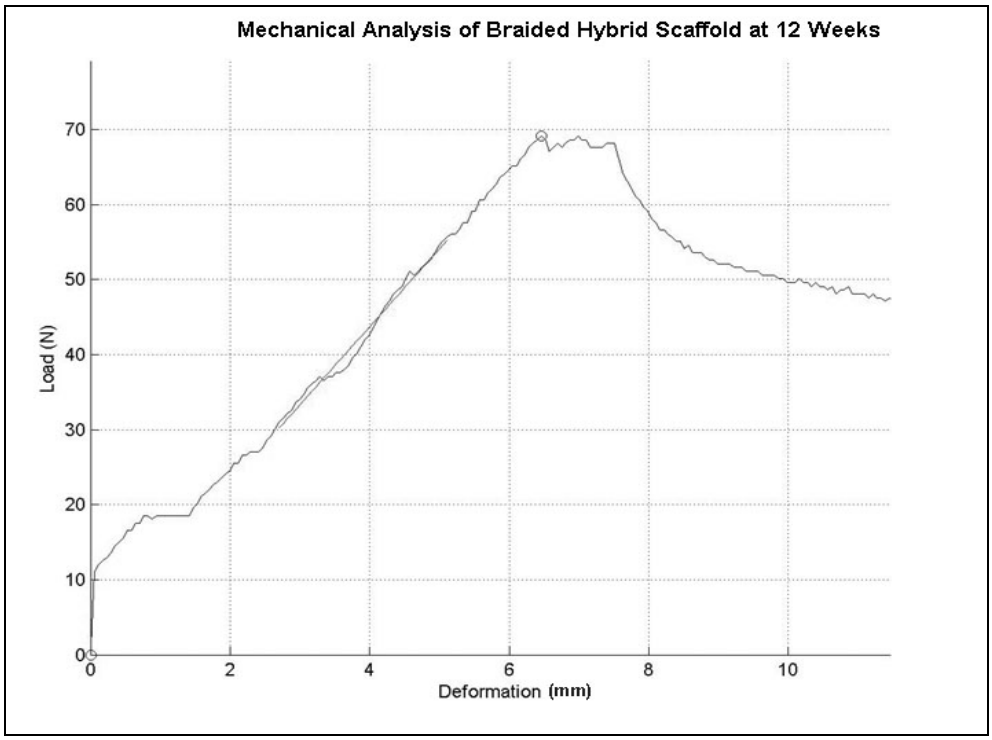

Figure 33: In vivo 12 week mechanical analysis.

Arthroscopic visualization was performed at 3-6 week time points, figure 34A,B. All braided hybrid scaffolds were found to be intact. There was a decrease in the amount of tension applied to the scaffold. A synovial sheath was noted on the braided fiber scaffold as well as tissue infiltration and encapsulation. There were also some signs of fiber fraying around the femoral tunnel with most of the scaffold intact.

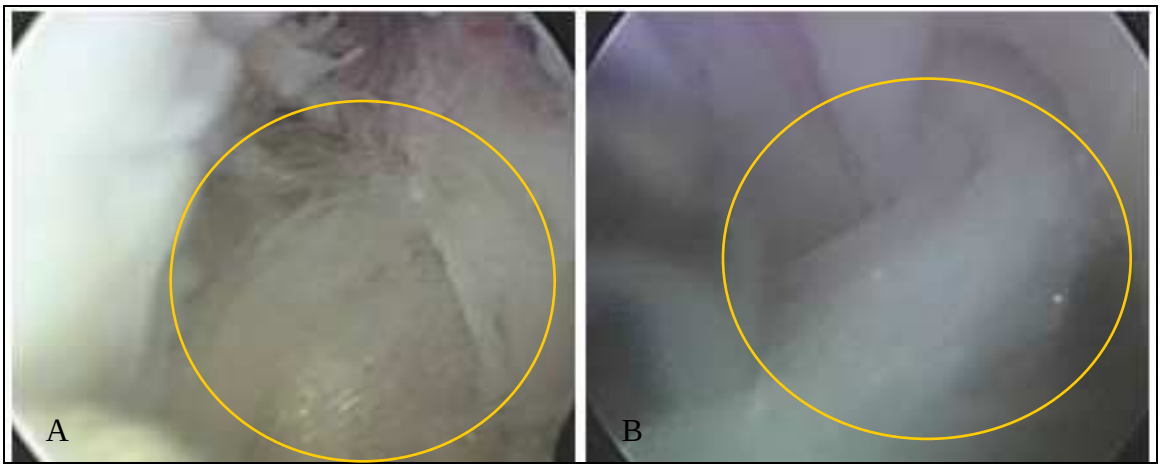

Figure 34A,B: Arthoscopic view of braided hybrid fiber scaffold.
A) 4 week and B) 6 week time points.

All sheep were euthanized at the 12 week time point. Gross obersvations of the implant revealed a large amount of tissue infiltration and encapsulation, figure 35A,B. This was verified with our qualitative histological analysis, which revealed cellular and vascular infiltration at both the 4 week and 12 week time points with an increased trend of infiltration at 12 weeks, figure 36. There was also an increase in lymphocytes, decrease in eosinophile, and no change in MNGCs.

At 12 weeks each scaffold was cut into three sections, ACL space, femur and tibia, and ranked for cellular infiltration and an inflammation response. Ranking showed an increased trend for cellular infiltration and vascular tissue and blood vessels for the

ACL space sections versus the bone tunnel sections. Inflammatory marker, eosinophils, remained low while MNGC's were more pronounced in the femur sections, figure 37.

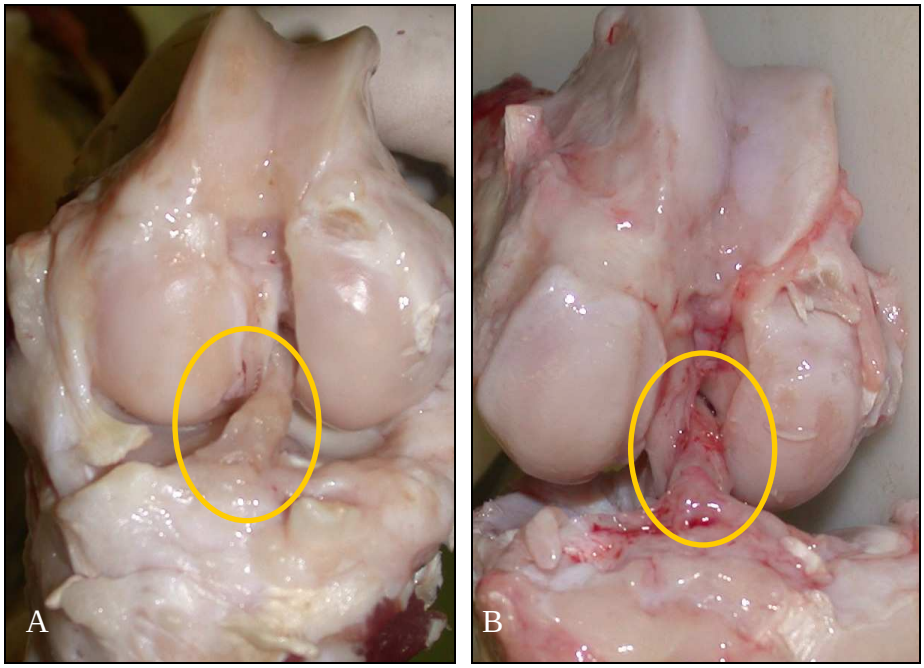

Figure 35A,B: Gross observations of braided hybrid scaffolds at 12 week time point.

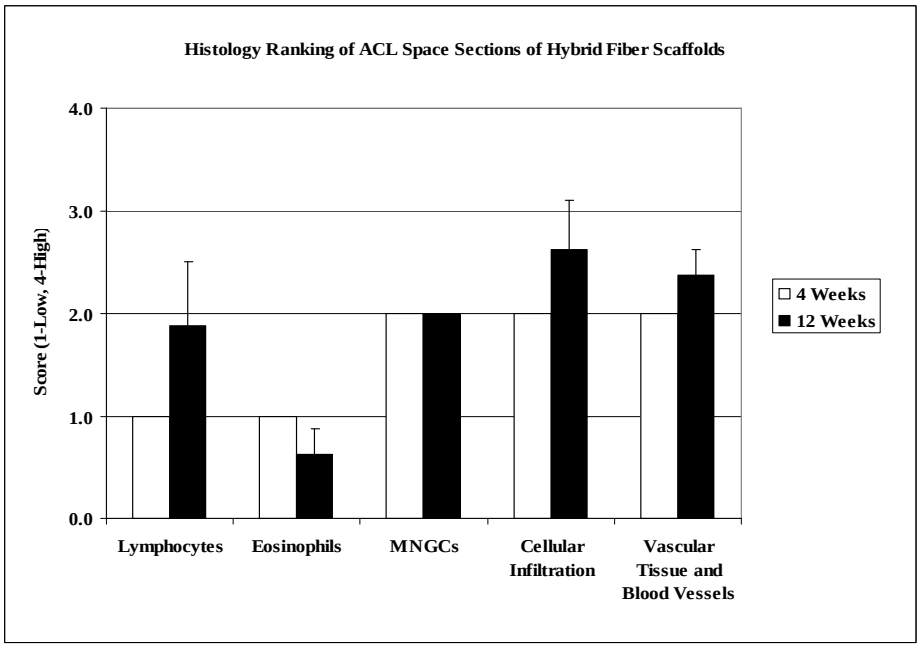

Figure 36: Average grading of braided hybrid scaffold mid-substance. Parameters measured were lymphocytes, eosinophils, MNGC, cellular infiltration and vascular tissue and blood vessels.

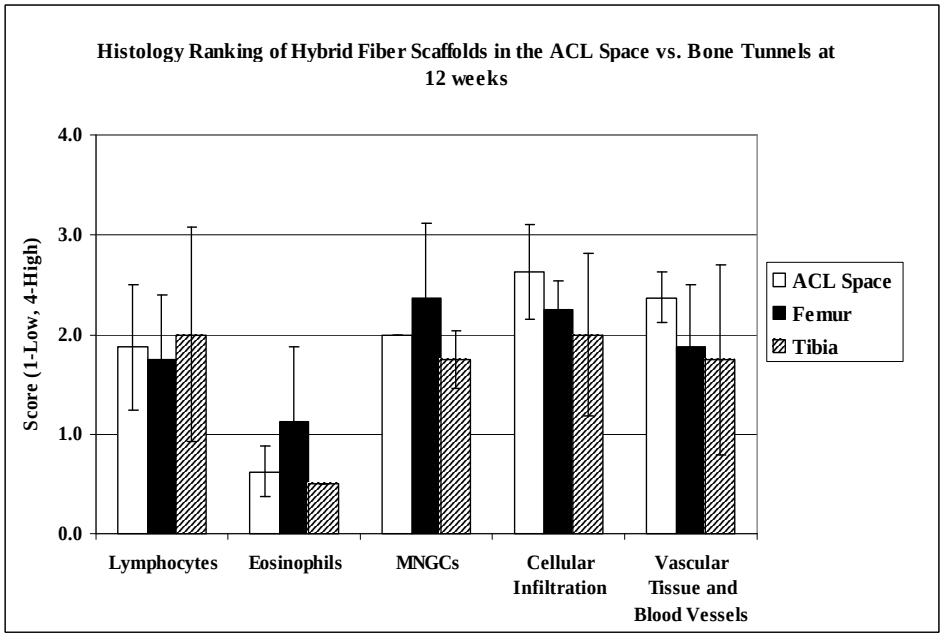

Figure 37: Average grading of braided hybrid scaffold in ACL space sections. Parameters measured were lymphocytes, eosinophils, MNGC, cellular infiltration and vascular tissue and blood vessels.

The periphery of the scaffolds at both time points shows a much larger concentration of cells with a greater amount seen in the 12 week time point. There was also a more pronounced cellular infiltration around the 12 week scaffold in the periphery as well as surrounding the collagen fibers, figure 38A,B. A greater degree of cell infiltration was also found at the center of the scaffold at 12 weeks. There was no change observed in the amount of MNGCs, while eosinophils seemed to decrease. Lymphocytes showed a small increase. Inflammation was also more evident at the 4 week time point than at 2 weeks with a higher presence of macrophages, MNGC's, lymphocytes, as well as foreign body granuloma, figure 39A,B.

Vascular tissue and blood vessels are clearly more evident at the 12 week time point with the presence of red blood cells surrounded by an endothelium, figure 40A,B. Gross observation showed that the bone was imbedded in the braided hybrid fiber

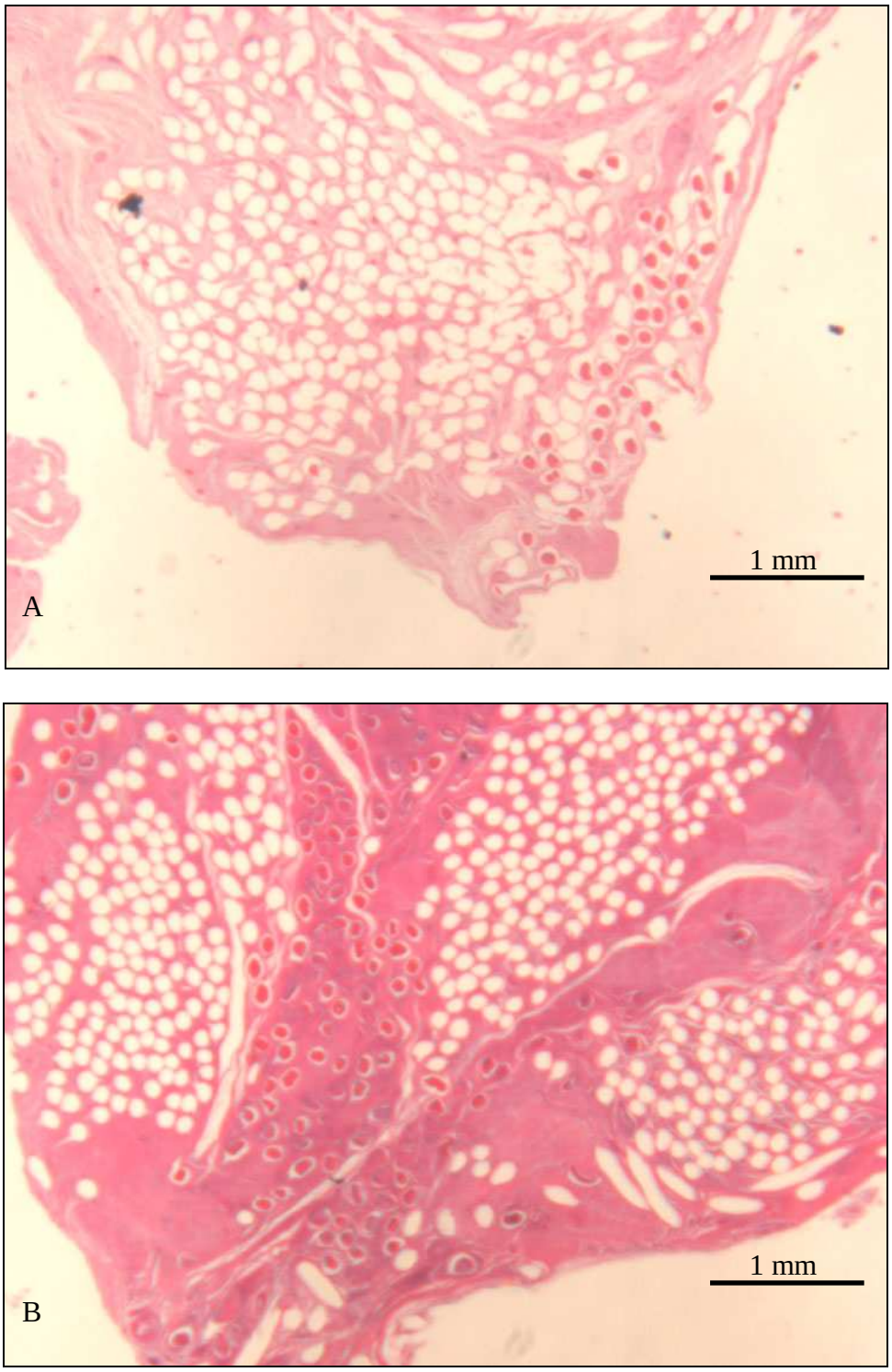

Figure 38A,B: Cellular infiltration of braided hybrid scaffold ACL space sections (A) 4 weeks and (B) 12 weeks post-implantation at 20x exposure after hematoxylin (H)- and eosin (E) staining. Cellular infiltration was concentrated in the periphery of the scaffold at the 12 weeks. P(DTD DD) fibers can be distinguished by their clear circular shape and collagen was seen as circular opaque shapes.

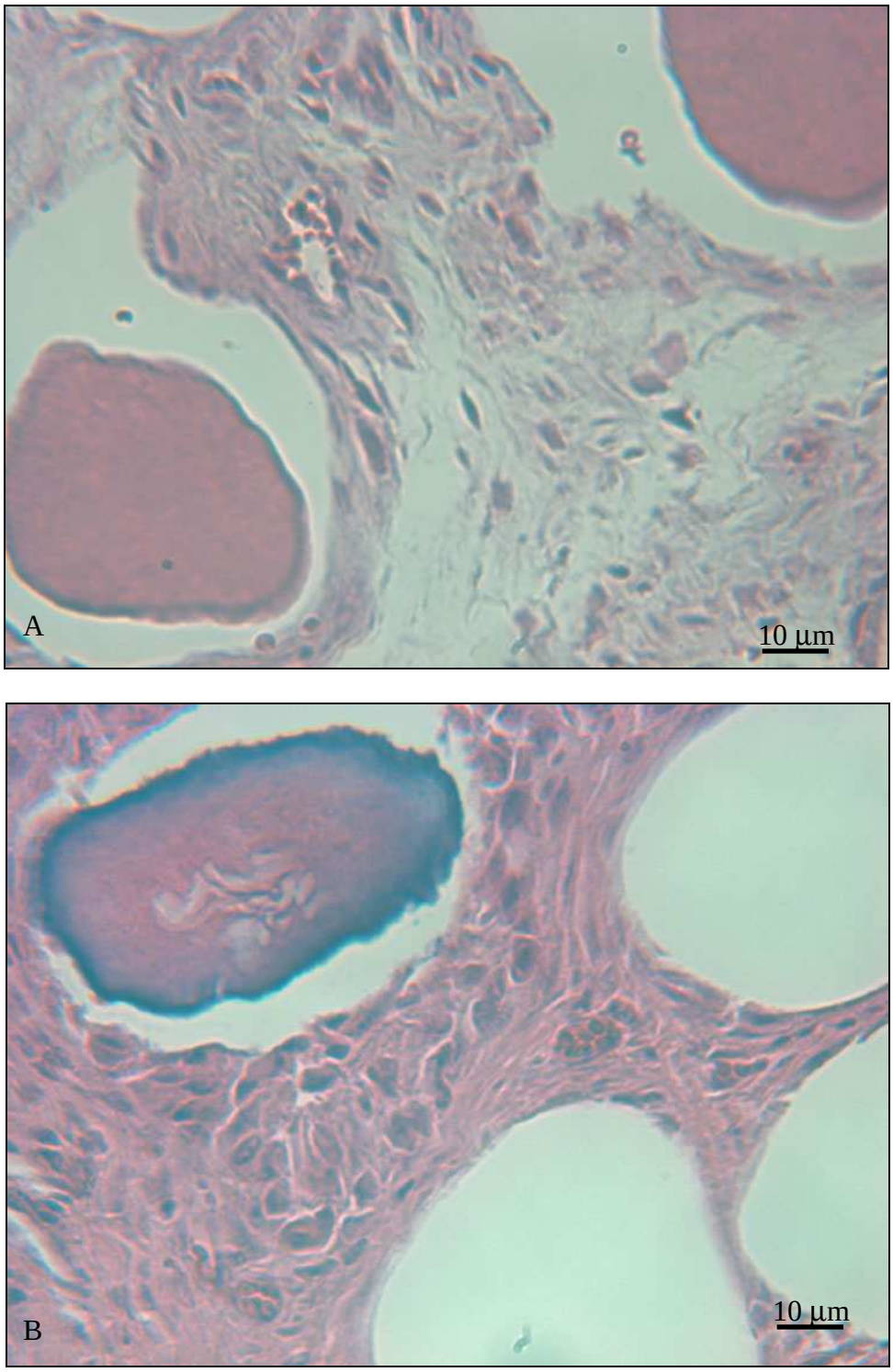

Figure 39A, B: Granuloma, fibroblasts, collagen and fibrin formation.
(A) 4 week and (B) 12 week time points hybrid scaffold in the ACL Space section at 400x exposure and after hematoxylin (H)- and eosin (E) staining. P(DTD DD) fibers can be distinguished by their clear circular shape and collagen was seen as circular opaque shapes.

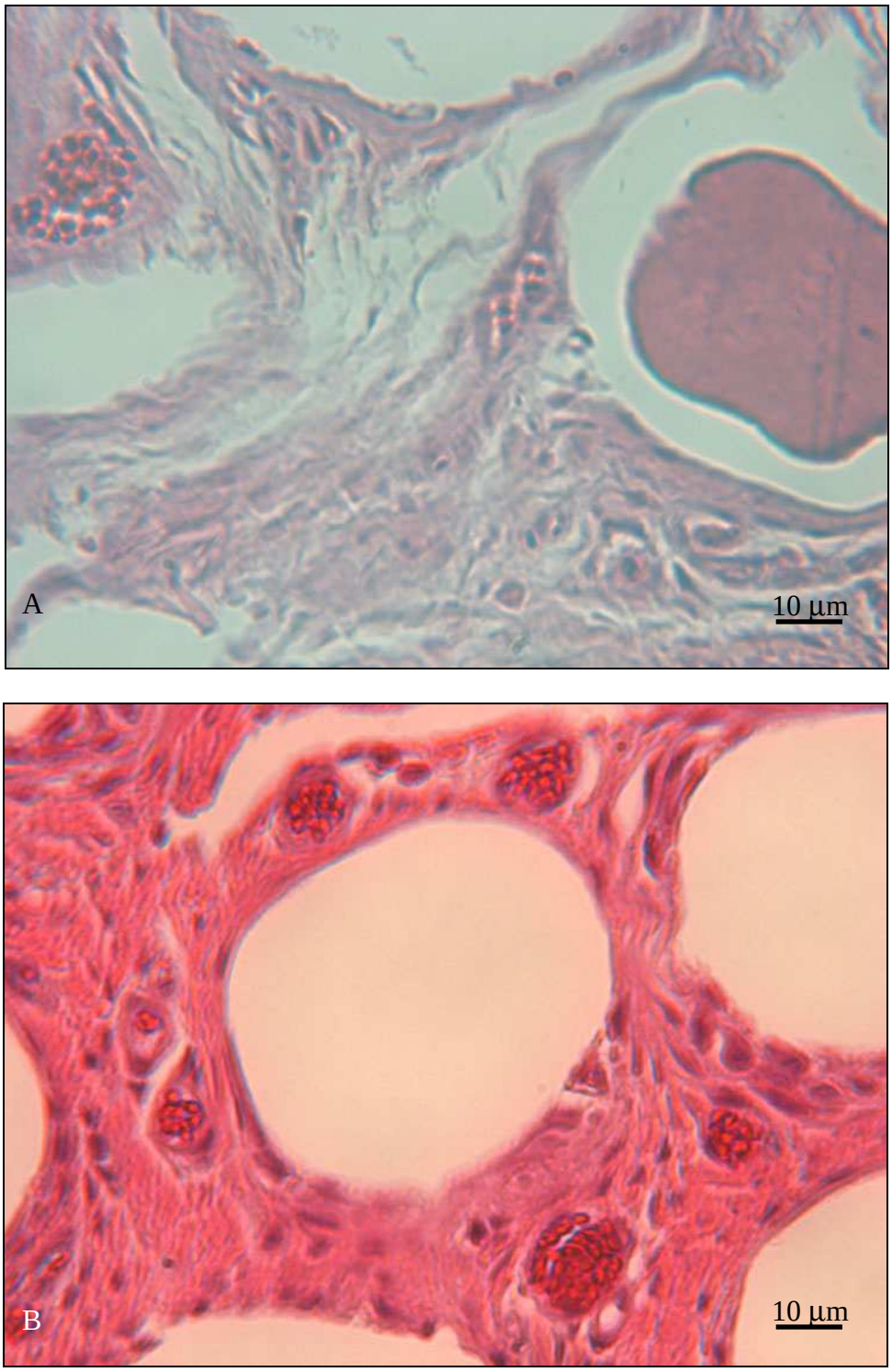

Figure 40A,B: Vascular tissue and blood vessels analysis of the ACL sectioned. (A) 4 weeks and (B) 12 weeks at 400x exposure and after hematoxylin (H)- and eosin (E) staining. P(DTD DD) fibers can be distinguished by their clear circular shape and collagen was seen as circular opaque shapes.

scaffold at 12 weeks. Bone growth was also observed at the periphery and within the braided hybrid scaffold fiber. Figure 41 shows bone growth in the periphery of the scaffold in the ACL space near the bone tunnel after hematoxylin (H)- and eosin (E) staining. Figures 42A,B shows bone growth within the scaffold in the femoral bone tunnel after Masson's Trichrome and Von Kossa's staining. Figures 43A,B shows bone growth within the scaffold in the tibial bone tunnel after Masson's Trichrome and Von Kossa's staining. It should also be noted when the implant was sent for histological slide preparation the bone surrounding the implant was also sent since there was a considerable amount of bone-growth within the scaffold.

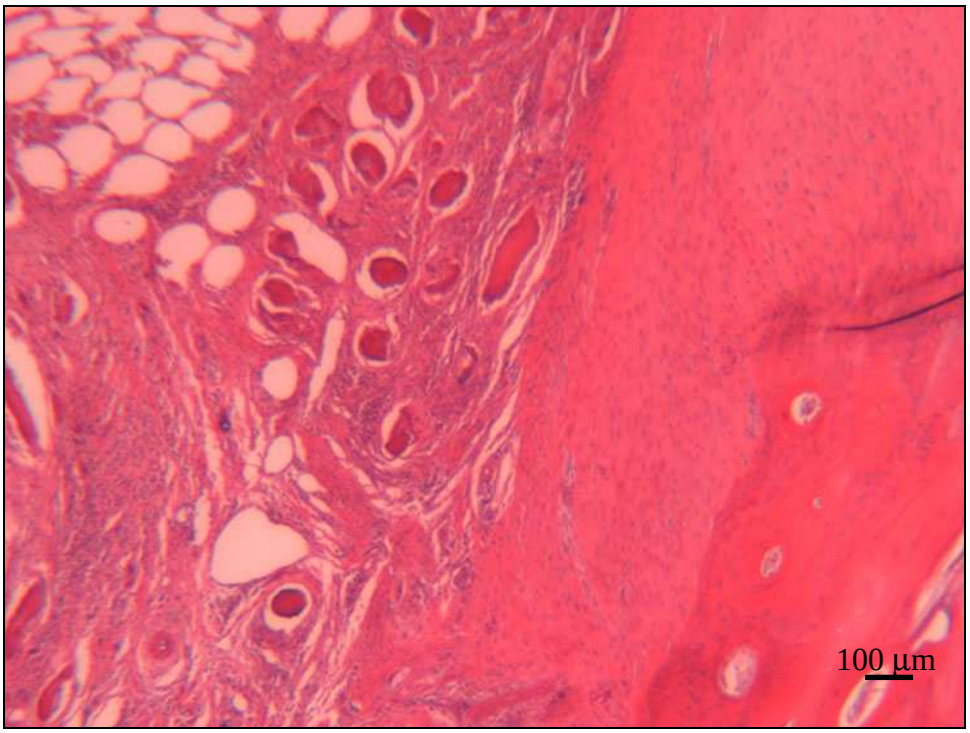

Figure 41: Histological analysis of bone growth at 12 weeks
at 40x exposure and after hematoxylin (H)- and eosin (E) staining. P(DTD DD) fibers can be distinguished by their clear circular shape and collagen was seen as circular opaque shapes.

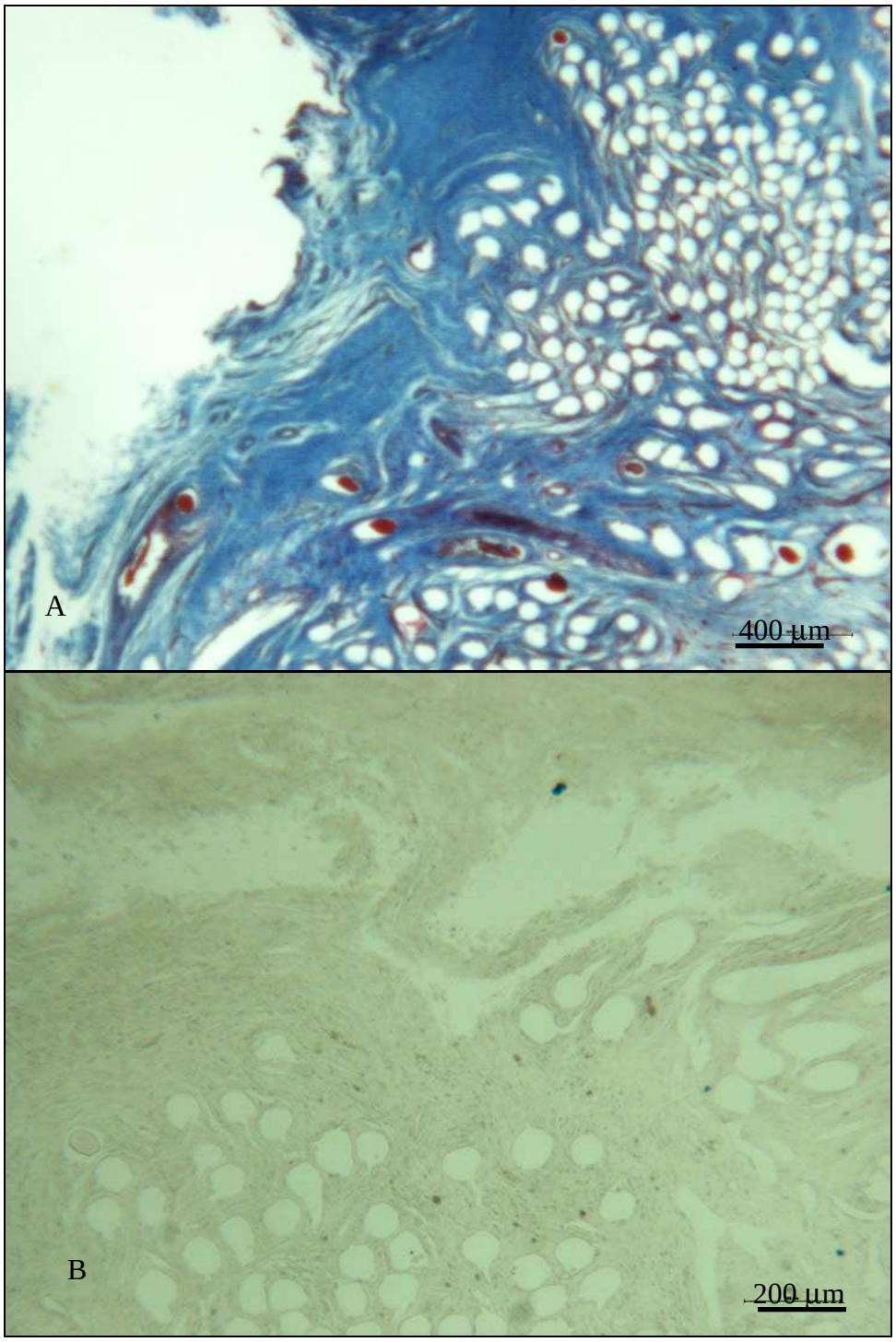

Figure 42A,B: Histological analysis of bone growth at 4 weeks
(A) after Masson's Trichrome staining at 20x exposure and (B) after Von Kossa's staining at 40x exposure. P(DTD DD) fibers can be distinguished by their clear circular shape and collagen was seen as circular opaque shapes.

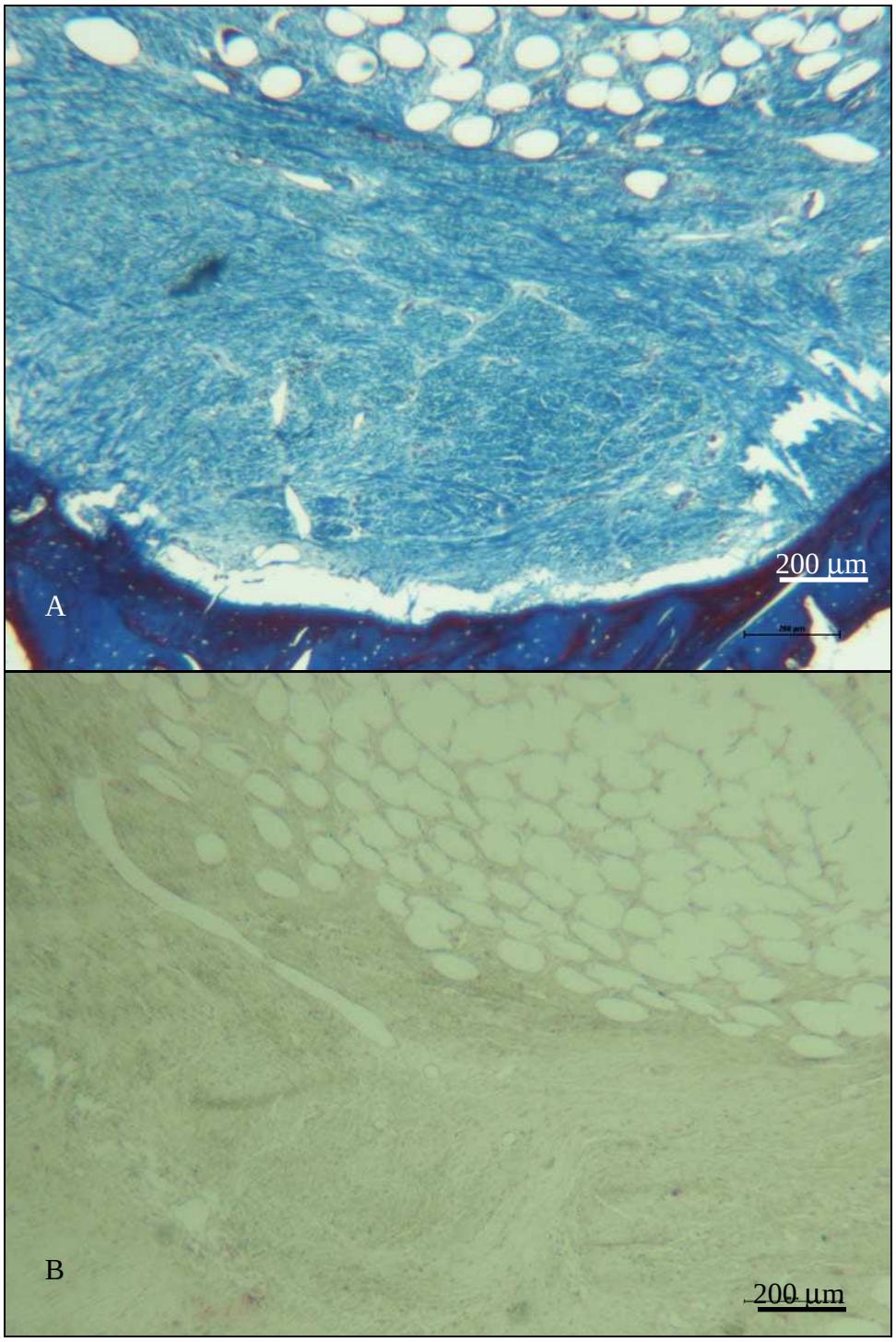

Figure 43A,B: Histological analysis of bone growth at 12 weeks
(A) after Masson's Trichrome staining at 20x exposure and (B) after Von Kossa's staining at 40x exposure. P(DTD DD) fibers can be distinguished by their clear circular shape and collagen was seen as circular opaque shapes.

5. DISCUSSION

5.1. Phase I

The purpose of this study was to evaluate the performance of p(DTD DD) fibers as a material for a ACL reconstruction scaffold. P(DTD DD) fibers were compared to PLLA fibers since PLLA is a well-studied resorbable polymer with a history of use in FDA-approved devices. Our objectives were to determine if p(DTD DD) (a) was capable of withstanding processing conditions to form fibers and it's mechanical properties and degradability was not affected by sterilization, (b) fibers can sustain fibroblast attachment and growth *in vitro* (c) fibers have yield loads within the range required to construct a tissue engineered scaffold to withstand forces typically seen on a human ACL.

Fibers were fabricated from raw polymers by a melt spinning process. Ideal processing would result in a fiber of sufficient strength and cell compatibility to support ACL reconstruction. Fiber strength depends on the alignment of polymer chains along the load axis, conditions achieved by varying processing temperature, draw ratio, MW of polymer, structure, and crystallinity. Assuming fibers follow the two-parameter Weibull distribution, we calculated the number of fibers needed to sustain loads typically seen on a rabbit [100] and human [52] ACL. Numerous researchers have successfully used a rabbit model to study numerous orthopaedic applications [71, 77, 86, 93, 94, 96, 97]. This calculation was attained by using Chi's load strain formula for a bundle, based on Coleman's survival function for a single filament to a bundle [109, 110]:

$$P(\varepsilon) = AE_f \varepsilon N_o \exp\left[-L\left(\frac{\varepsilon}{\varepsilon_o}\right)^m\right]$$

Where $P(\varepsilon)$ is the tensile load, A is the cross-sectional area of a single fiber, E_f is Young's modulus for a single fiber, N_o is the fiber count, ε is the applied strain, L is the fiber length. The Weibull shape parameter m and scale parameter ε_o were measured to be 1.45 and 2.25, respectively, with the following equations as shown by Chi [109]:

$$\varepsilon_{\max} = \varepsilon_o \left(\frac{1}{Lm} \right)^{1/m}$$

$$m = \frac{1}{\ln\left(\frac{\varepsilon_{\max} S_o}{P_{\max}} \right)}$$

Mechanical data was attained from a 500 p(DTD DD) fiber scaffold, figure 44, as described in section 3.2.3. Phase IIa single fiber and scaffold mechanical testing.

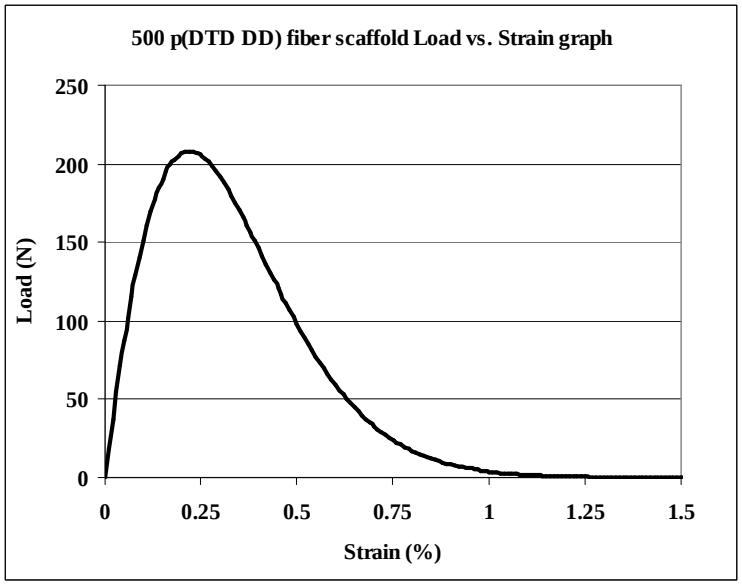

Figure 44: Load versus strain graph of 500 parallel fiber scaffold composed of p(DTD DD).

Inserting the Weibull parameters back into Chi's load strain equation it was calculated that p(DTD DD) fiber scaffolds composed of 750 fibers (cross-sectional area of 4.5 mm^2)

would potentially sustain loads of a rabbit ACL, 360 ± 20 N [100]. For a human ACL with a breaking load of 2160 ± 157 N [52], a scaffold composed of 5000 fibers (cross-sectional area of 29.7 mm^2) would potentially suffice.

The strength retention and MW of non-sterile and ETO sterilized fibers were evaluated through 64 weeks of incubation in PBS with a pH of 7.4 at 37 °C. It was found that ETO sterilization did not significantly affect p(DTD DD) or PLLA fiber mechanical properties and MW. Strength retention decreased to 20 and 37% and MW decreased to 41 and 36% for ETO sterilized p(DTD DD) and PLLA fibers, respectively. P(DTD DD) yield stress values remained significantly higher (p=0.01) up to the 8 week time point in which yield stress values were 49% higher than PLLA, 128 ± 7 MPa versus 86 ± 12 MPa. The decrease in T_c of p(DTD DD) between the 32 and 64 week time points was consistent with the observed decrease in yield strength, and could be attributed to the decrease in the molecular weight due to degradation. Lower T_c and the increased T_m could both be indicative of the mesogenic ordering of the polymer chains that contributes to the higher modulus at 32-64 week time points. No such ordering was observed in PLLA as indicated by decrease in T_m. While the decrease in T_m could be attributed to decrease in crystalline order (decrease in size or increase in the number of defects) in PLLA, the increase in T_m suggests aging-induced reordering of the mesogenic chains in p(DTD DD). This was consistent with the observed increase in the modulus of p(DTD DD) fibers at the 64 week time point despite a decrease in molecular weight associated with degradation, table 8.

Values at the 64 week time point were used to predict the time in which the strength retention and MW would reach 0%. At 86 and 99 weeks strength retention

would reach 0% and 127 and 124 weeks MW retention would reach 0% for p(DTD DD) and PLLA, respectively. The MW of the materials decreased over time due to degradation of the backbone chain, caused by the polymer's hydrophilic sensitivity, which decreased the strength of the polymer. This was ideal since our goal was to have the material resorb, allowing the neoligament tissue to take on the axial load gradually over time. A graphical analysis of strength retention versus MW curve confirmed that the result was linear, figure 45.

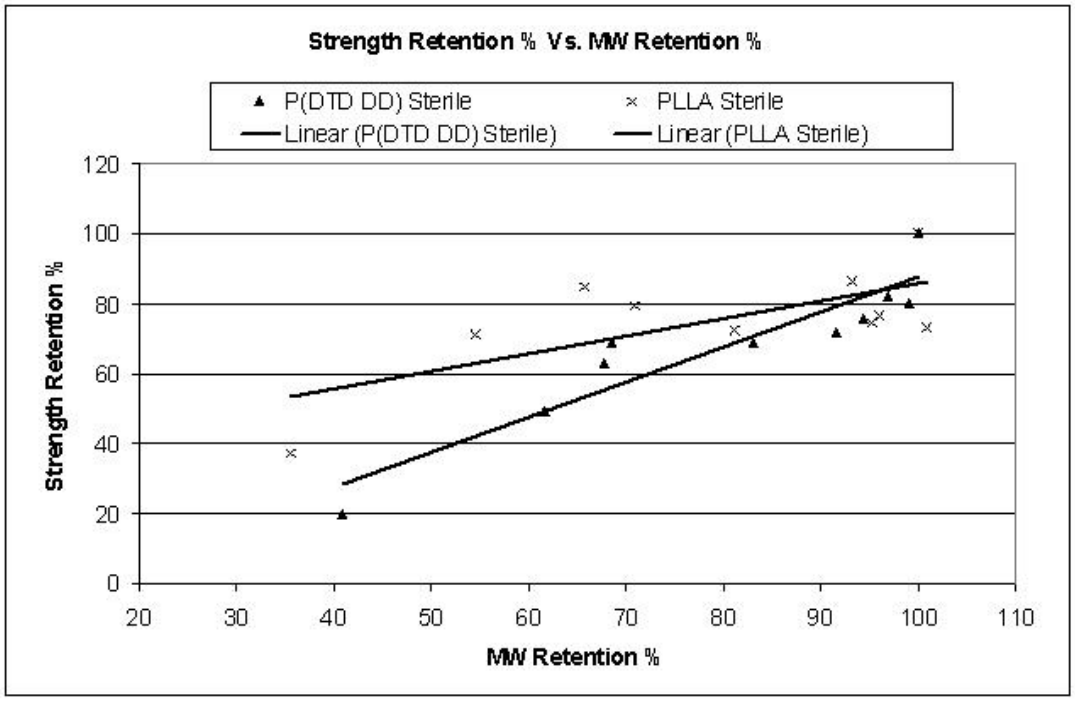

Figure 45: Sterile p(DTD DD) and PLLA fiber linear trendlines.
Percent strength retention versus percent molecular weight with linear trendlines after 64 weeks of incubation PBS with a pH of 7.4 at 37°C.

The moduli of the ACL's anteromedial bundle (AMB) and posterolateral bundle (PMB) have been measured at 283 ± 114 and 155 ± 120 MPa, respectively [111]. If the modulus of the implant exceeds that of the neoligament, in-growth tissue stress shielding would occur and the load-deprived neoligament tissue may not mature. It was therefore

important that the moduli be low enough to allow for normal neoligament remodeling but strong enough to protect the scaffold from high loads in the early postoperative period. P(DTD DD) was stronger than PLLA and has a significantly lower modulus at both the initial (1.69 ± 0.10 vs. 4.43 ± 0.3, p=0.001) and 64 week time points (2.68 ± 0.4 vs. 4.46 ± 1.2, p=0.005).

An ACL reconstruction device has to maintain a population of fibroblasts to achieve deposition of new extracellular matrix. We evaluated cell compatibility of a sterile scaffold in complete media by determining cell attachment and growth, which are affected by surface characteristics and geometry [112, 113]. Results confirmed cell compatibility, by the attachment and proliferation of fibroblasts on both types of scaffold. At 4 hours, cell attachment was low for both p(DTD DD) and PLLA and showed an increased trend up to 16 with no significant difference in the cell attachment between the two polymers. In contrast when comparing our 16 day time point to the 14 day time point of a collagen scaffold by Caruso *et al*, collagen had approximately three times the population of fibroblasts, but lacked the strength of the synthetic polymers [78].

5.2. Phase IIa

From phase Ia and Ib we optimized first generation fibers to sustain mechanical and biological functionality. Once these parameters were attained the focus changed to Phase IIa: a pilot *in vivo* ACL reconstruction using a p(DTD DD) scaffold from second generation fibers. This study gave us insight to the limitations of fibroblast attachment compared to collagen fibers [83].

Mechanical and histological evaluation on this pilot study of ACL implanted scaffolds indicated mixed results. It was evident p(DTD DD) was a cell compatible material in the rabbit knee up to 7 weeks, but the scaffold had ruptured even though individual fibers showed mechanical integrity when subjected to tension. Mechanically, we were only able to test at the 4 week time point in which 60% of the fibers were intact. It was difficult to conclude whether scaffold fibers failed due to fatigue or an abrupt rupture due to the rabbit jumping. There were no signs of a major immune response in the explants and fibroblasts were concentrated around the fibers in the scaffold. This was seen throughout the 4, 6, and 7 week time points. To rectify these issues the focus for Phase IIb was to maximize fibroblast attachment while maintaining mechanical function through a hybrid synthetic/natural fiber scaffold. Dunn *et al* previously tried a hybrid PLA fiber scaffold with a collagen matrix to some success [86]. Blassingame *et al* continued this hybrid design comparing p(DTD DD) and PLLA with varying ratios of ultraviolet (UV) crosslinked collagen fibers in an *in vitro* model [83]. This study calculated the scaffold's optimal ratio (figures 46 and 47A,B) between synthetic and natural fibers using 2nd generation p(DTD DD) fibers processed as described in section 3.2.1. Phase IIa polymer source and processing. Scaffolds were prepared and seeded as described in section 3.1.4. Phase Ib scaffold preparation and cell seeding and 3.1.5. Phase Ib scaffold cell compatibility measurement, respectively. With this in mind the phase IIb consisted of a much larger 750 parallel fiber scaffold composed of 75% p(DTD DD) and 25% Collagen

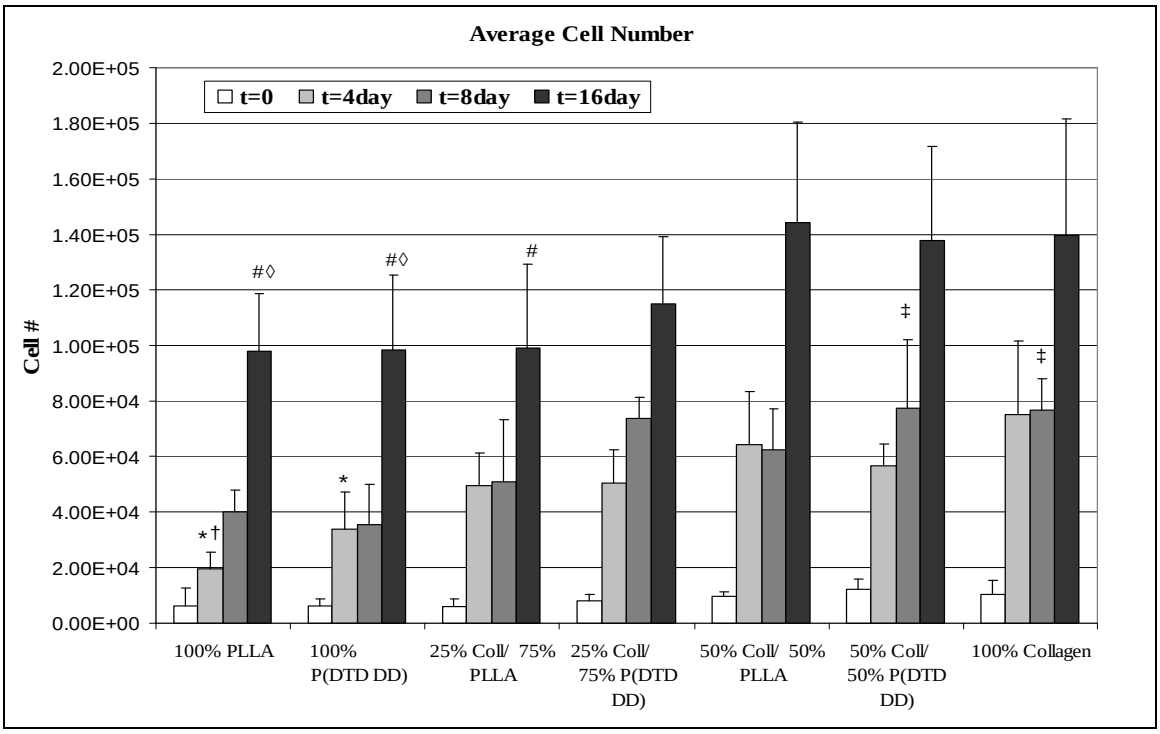

Figure 46: Average cell number per *in vitro* seeded scaffold with varying ratios. There was no significant difference between the average numbers of cells that initially attached to each scaffold. * indicates a significant difference with respect to 100% Collagen at day 4. † indicates a significant difference with respect to 50%Collagen/50% PLLA at day 4. ‡ indicates a significant difference with respect to 100% P(DTD DD) at day 8. # indicates a significant difference with respect to 50%Collagen/50% PLLA at day 16. ◊ indicates a significant difference with respect to 100% Collagen at day 16. Significant differences have a $p<0.05$ [83].

5.3. Phase IIb

We previously tested p(DTD DD) single fibers and scaffolds *in vitro* as a potential biomaterial for the reconstruction of the ACL. It was concluded that p(DTD DD) was able to sustain fibroblast attachment and growth, has higher initial strength than PLLA and lower modulus, both of which are necessary parameters to support the initial loads found in the knee and the ACL, while preventing stress shielding. These fundamental differences as well as favorable degradation products of p(DTD DD) encouraged us to proceed to this *in vivo* safety study.

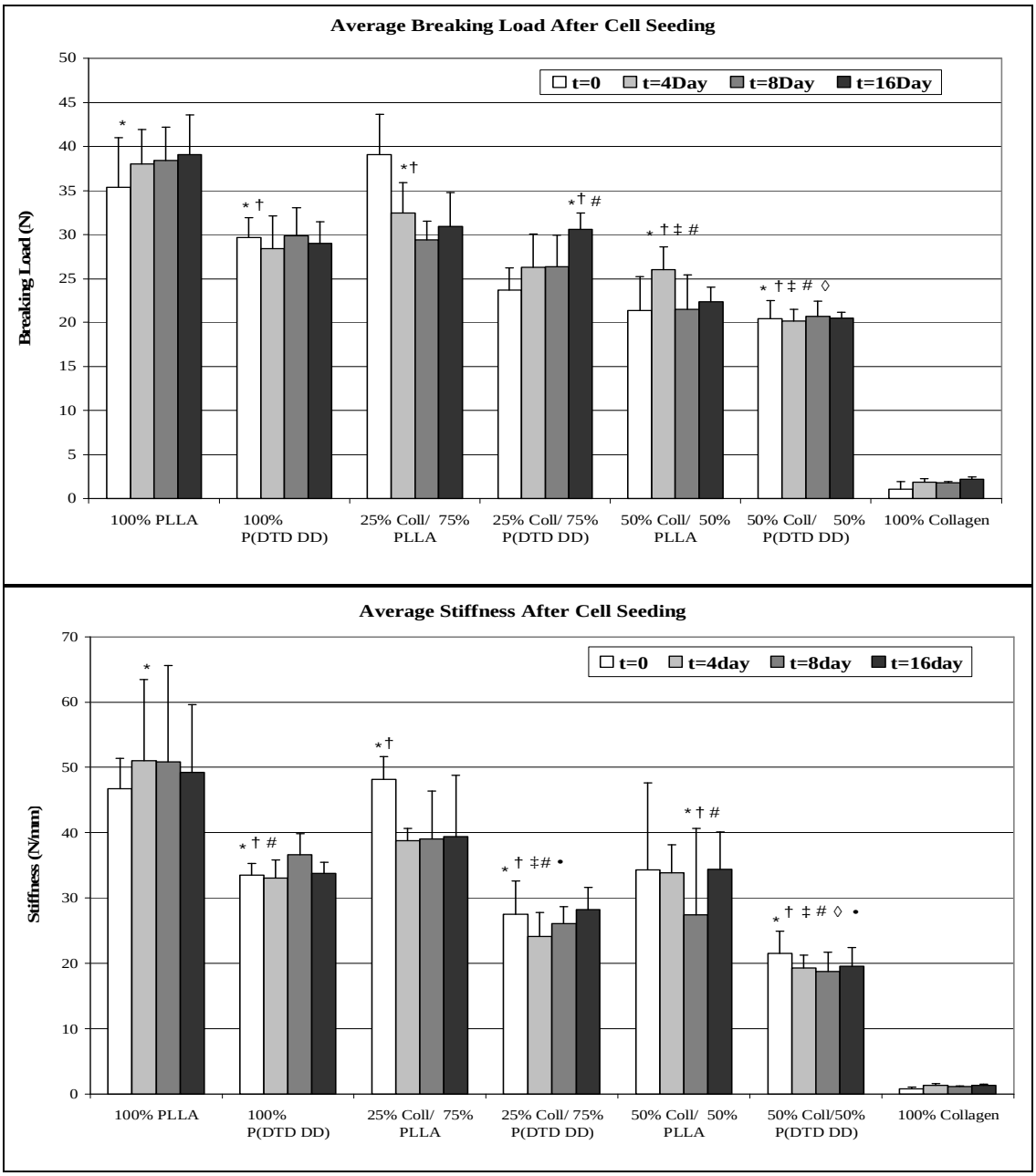

Figure 47A,B: Breaking load and stiffness of *in vitro* seeded scaffolds with varying ratios. Within each group there was an insignificant difference in the structural properties over each time period, yet differences were found when cross-referencing; (A) Average Breaking Load; (B) Average Stiffness; * indicates a significant difference with respect to 100% Collagen, † indicates a significant difference with respect to 100% PLLA, ‡ indicates a significant difference with respect to 100% P(DTD DD), # indicates a significant difference with respect to 25%Collagen/75%PLLA;), ◊ indicates a significant difference with respect to 25%Collagen/75% P(DTD DD), • indicates a significant differencewith respect to 50%Collagen/50% PLLA. Significant differences have a $p<0.05$ [83].

We tested *in vivo* a novel hybrid p(DTD DD) and Collagen fiber scaffold that was sterilized by Ebeam and monitored parameters such as safety, strength retention, cellular in-growth, inflammation and tissue remodeling as a function of time post-implantation. Ebeam sterilization is a reliable, cost-effective method used to sterilize most degradable polymeric devices that would not survive sterilization via steam, dry heat or irradiation. We previously used ethylene oxide sterilization but opted to used Ebeam due to its high electron penetration, dose uniformity, increased speed of sterilization and lack of aeration post-sterilization [114, 115]. Besides testing for the biological safety of our hybrid scaffold we also examined the safety of the surgical technique. We used current surgical anchoring and implantation techniques that potentially allows immediate joint stabilization post-operatively. Anchoring the implant and post-operative joint stabilization are both necessary considerations when using an animal model that does not receive any form of leg restraint. This safety study gave us insight to both the surgical and biological safety measures that should be considered before moving to a larger animal model, i.e. sheep.

Within 5 hours post-operatively all NZW rabbits were fully awake, responsive and sternal, a clear sign of immediate joint stability. There were no signs of swelling post-operatively or species specific signs of pain. After 2 days of the required analgesics, per an IACUC approved protocol, all NZW rabbits resumed normal activity and were bearing weight on their surgical leg. Analgesics or antibiotics were no longer necessary after this time. Only 1 NZW rabbit was noted as having signs of arthritis when euthanized at 4 weeks.

The hybrid scaffold was composed of 750 parallel fibers at a ratio of 75% p(DTD DD) with 25% collagen in the periphery. Fibers were aligned parallel in the scaffold to imitate the morphology of the native NZW rabbit's ACL. Mechanical analysis of the 2 week FHTC samples showed a 55% and 84% decrease in strength and modulus, respectively, when compared to the initial hybrid scaffolds. Previous studies calculated the break load and modulus of the rabbit ACL at 360 ± 20 N and 516 ± 64 MPa, respectively, which are similar to our actual hybrid scaffolds [3]. A review of our surgical anchoring method, where most of the load was applied directly to the scaffold instead to indirectly through suture tension, was explored in later studies. The application of an interference screw as an anchor instead of a polyethylene button is a prime example. The thread within the screw would apply pressure onto the scaffold and the bone tunnels as it is screwed in.

Qualitative analysis of histological slides suggests hybrid scaffolds may encourage cellular in-growth and remodeling allowing for the formation for a neoligament as a function of time post-implantation. It was observed that at 2 weeks there was far less cell infiltration, vascular tissue and inflammation than its 4 week counterpart. Collagen was more developed at the 4 week time point and cellular in-growth was apparent even at the center of the scaffold. This migration suggests that the spacing between fibers was large enough to allow cells to migrate freely throughout the scaffold, which is essential in the formation of a neoligament. There was also more vascular tissue, including red blood cells found throughout the scaffold. Angiogenesis is an important parameter in the repair and restoration of soft tissues since it supplies necessary nutrients to surrounding cells. There were also far more inflammatory cells at

4 weeks that seemed to be concentrated on the periphery. At 4 weeks it was difficult to fully differentiate between an inflammatory response to the surgery or the scaffold implant. It was important to note that it was unusual that at 2 weeks there were far less inflammatory cells since an immediate inflammatory repair reaction would be expected due to surgery followed by a decrease over time. In our case there seems to be a delayed response or decreased reaction at 2 weeks followed by an increase at 4 weeks.

The major difference between the initial and 2 week rabbit explant can be attributed to the biomechanical function of the knee. In the healthy human knee, for example, the average ratio of the peak joint contact forces on the medial tibial plateau to that on the lateral plateau was 2.2 ± 0.9 [116]. The rabbit knee joint spends a majority of the time in a hyperflexed state. A study by Gushue et al found a prevalence of forces on the lateral plateau during normal rabbit hopping, with the average contact force ratio on the medial tibial plateau to that on the lateral plateau for hopping trials measure at 0.89 ± 0.25 [117]. This was further corroborated by Messner et al who found an increased mineral density in the lateral tibial plateau when compared to the medial plateau [118]. The small intra-articular ligaments also make surgery difficult and limits scaffold size. These knee biomechanics and size factors may have contributed to the premature failure of our scaffold and makes it difficult to truly predict how the mechanical integrity of the implant would react in a human model. It was also possible bone tunnels may have played an unexpected role. During explantation at the 2 and 4 week time points 6 out of 8 of the scaffolds were either considerably or completely torn, but individual fibers were still capable of sustaining an applied load. We speculate the bone tunnels unexpectedly applied a shear force perpendicular to the parallel fibers slowly tearing the scaffold. To

rectify this issue we researched numerous studies that have shown the potential of braided, twisted or knitted fiber scaffolds for the reconstruction of the ACL and other soft tissues [53, 77, 85, 88] . Braided structures have a high compliance in axial and radial directions and low compliance in shear directions, similar to that of the native ACL [99] and may be better suited than a parallel matrix.

5.4. Phase III

We previously tested a hybrid p(DTD DD) and Collagen parallel fibers scaffold and its safety as a potential biomaterial composite for the reconstruction of the ACL. It was concluded that after 4 weeks the hybrid scaffold had an increase in cellular infiltration and vascular tissue, both of which are biologically necessary in the repair and reconstruction of the ACL. These fundamental parameters, however; were not sufficient to address the biomechanical requirements in the NZW rabbit knee. At 4 weeks the hybrid scaffolds had ruptured and failed even though there was still mechanical integrity in individual fibers when subjected to tension. This data encouraged us to proceed to phase III, which made three significant changes: (1) Changed the parallel configuration to a three-strand braid, (2) Used a larger animal model that was more similar to the biomechanics in a human knee and (3) Modified the anchoring technique to better apply mechanical loads to the hybrid scaffold.

Using a sheep model, we tested a braided hybrid p(DTD DD) and Collagen fiber scaffold that was sterilized by Ebeam. We monitored parameters such as immediate joint stability, cellular infiltration, and inflammation for up to 12 weeks post-implantation. Previously we used a surgical anchoring with endo buttons on both the femur and tibial

ends that applied tensile load indirectly to the parallel hybrid scaffold through suture. For the sheep model we used an endo button on the femoral end and an interference screw on the tibial end. This configuration applied direct tension on the braided hybrid scaffold on the tibial end and indirect tension on the femoral end. This anchoring technique allowed for immediate joint stabilization post-operatively, which was necessary when using an animal model that would not have its leg restrained.

All sheep knee joints were stable post-operatively and were bearing some weight on their surgical leg within 36 hours. After 15 ± 4 days only minor limping was observed for all sheep. After 40 ± 10 days all sheep showed no signs of limping and resumed normal activity for the remaining days. It should be noted that sheep are social and when animal interaction was restricted for more than 48 hours post-operative the sheep no longer wanted to walk or eat. Sheep that were permitted to socialize quickly resumed normal exploratory behavior and appetite.

The braided hybrid scaffold was composed of 3000 braided fibers at a ratio of 75% p(DTD DD) with 25% collagen. Mechanical analysis of the 12 week post-operative FBTC samples showed a modulus that was 7% of the initial values. The actual braided hybrid scaffold was 3x the break load of the initial values and the modulus was more than 2x the initial values. This suggests the need for an interference screw to be used for the tibial end instead of the endo button. There was no noticeable rupture within the scaffolds at 12 weeks, but it was noted that during the arthroscopic visualizations the braided hybrid scaffolds were not as tense.

Qualitative analysis of histological slides of the cross sectioned braided hybrid scaffolds had an increase in the amount of cellular infiltration after 12 weeks post-

operatively when compared to the 4 week samples. It was observed that at 4 weeks there was far less cell infiltration, vascular tissue and lymphocytes than at 12 weeks. Cellular infiltration was apparent even at the center of the scaffold regardless of time point, which suggests that spacing between fibers was large enough to allow cells to migrate freely throughout the scaffold. This migration was essential in the production of neoligament, which acts to reconstruct the ACL. There was also more vascular tissue, including red blood cells found throughout the scaffold at 12 weeks, which was an important parameter in the repair and restoration of soft tissues. There was a decrease in the amount of eosinophils at 12 weeks and no change in the number of MNGCs in the ACL space section of the braided hybrid scaffold. When comparing the ACL space cross-section to the femoral and tibial cross-sections there was a larger amount of cellular infiltration, vascular tissue and blood vessels in the ACL space. This may be due to the bone growth within the bone tunnels which may obstruct the flow of cells. When comparing the braided hybrid scaffold in the femoral and tibial bone tunnels we found an increase of eosinophils in the femoral tunnel sections. This may be a factor of fixation and not an effect of the graft due to the floating fixation in the femoral section. The tibial fixation on the other hand used a rigid screw fixation.

6. CONCLUSION

6.1. Phase I

These data suggest that p(DTD DD) was able to sustain fibroblast attachment and growth and has higher initial strength than PLLA, which was necessary to support the mechanical requirements typically seen on a human ACL. Although the biological responses of the PLLA and p(DTD DD) are similar, the changes in the mechanical behavior of the two materials after incubation in PBS at 37 °C have different profiles. These differences are attributed to the semicrystalline nature of PLLA and the small degree of crystallinity induced by mesogenic ordering in p(DTD DD). These fundamental structural differences as well as favorable degradation products in p(DTD DD) encourage us to proceed to phase II, an *in vivo* model.

6.2. Phase II

There was in increase in cellular infiltration as a function of time. There was also an inflammatory response present surrounding the scaffold. This reaction however was most likely due to the natural repair reaction to surgery and not the implant. The unexpected premature failure of the scaffold brought to question the functional stability of a parallel scaffold. The rabbit model was also another variable to consider changing during phase III. Even though it was a decent preliminary biological model a much larger animal model was needed.

6.3. Phase III

There was in increase in cellular infiltration, vascular tissue and blood vessels as a function of time. There was a decrease in the inflammatory response present surrounding the scaffold after 12 weeks. We may consider an anchoring method with interference screws on both the femoral and tibial ends and a longer time point for future studies. At 12 weeks all braided hybrid scaffolds seemed intact and cells were able to move freely throughout the matrix. There was also a need for further mechanical data post-implantation for mechanical integrity analysis.

6.4 Phase IV

Our hypothesis stated that A tissue engineered scaffold for ACL reconstruction would a) provide adequate initial strength for immediate knee joint stability, b) sustain cellular infiltration and c) degrade gradually over time to allow for neoligament formation.

a) We have shown that only after a few days post-surgery our sheep model was capable of placing weight on surgical leg and showed no signs of limping weeks later. All braided hybrid scaffolds were intact.
b) Cellular infiltration and proliferation was apparent in our *in vitro* Phase I study. Our *in vivo* models all showed signs of cellular infiltration as well and a synovial sheath was apparent both our rabbit and sheep models, Phase II and III, respectively.
c) During Phase I we showed that strength retention and molecular weight decreased over time up to 64 weeks in a PBS environment at 37 °C. Tissue infiltration was

apparent in our Sheep model up to 12 weeks in our Phase III study with signs of vascular tissue, blood vessels, collagen and cellular infiltration throughout our scaffold and bone growth within the tibial and femoral bone tunnels.

7. APPENDIX

Average Diameter (mm) (n=15)	Time of incubation (weeks)									
Fiber Name	0	0.01	1	2	4	8	16	24	32	64
P(DTD DD) Non-Sterile	0.087	0.087	0.095	0.097	0.088	0.097	0.089	0.089	0.095	0.087
PLLA Non-Sterile	0.084	0.086	0.092	0.090	0.088	0.095	0.088	0.085	0.095	0.087
P(DTD DD) Sterile	0.087	0.088	0.092	0.086	0.089	0.091	0.091		0.097	0.089
PLLA Sterile	0.086	0.085	0.091	0.087	0.086	0.092	0.084	0.086	0.092	0.086

Average StDev Diameter (mm)	Time of incubation (weeks)									
Fiber Name	0	0.01	1	2	4	8	16	24	32	64
P(DTD DD) Non-Sterile	0.003	0.002	0.001	0.007	0.003	0.002	0.002	0.003	0.001	0.002
PLLA Non-Sterile	0.003	0.003	0.002	0.002	0.004	0.003	0.003	0.003	0.002	0.003
P(DTD DD) Sterile	0.003	0.002	0.003	0.002	0.002	0.002	0.002		0.002	0.002
PLLA Sterile	0.002	0.003	0.004	0.004	0.003	0.003	0.003	0.003	0.002	0.003

Average Yield Stress (MPa) (n=15)	Time of incubation (weeks)									
Fiber Name	0	0.01	1	2	4	8	16	24	32	64
P(DTD DD) Non-Sterile	191	144	129	117	135	102	132	109	91	55
PLLA Non-Sterile	125	95	88	91	102	81	101	102	82	38
P(DTD DD) Sterile	185	150	140	152	133	128	116	127	91	37
PLLA Sterile	118	87	90	87	102	86	94	100	84	44

Average StDev Yield Stress (MPa)	Time of incubation (weeks)									
Fiber Name	0	0.01	1	2	4	8	16	24	32	64
P(DTD DD) Non-Sterile	11	17	10	15	17	9	6	15	6	24
PLLA Non-Sterile	13	16	13	14	10	10	7	5	7	21
P(DTD DD) Sterile	12	22	9	13	15	7	8	10	9	20
PLLA Sterile	9	12	8	12	9	12	14	10	7	23

Average Break Stress (MPa) (n=15)	Time of incubation (weeks)									
Fiber Name	**0**	**0.01**	**1**	**2**	**4**	**8**	**16**	**24**	**32**	**64**
P(DTD DD) Non-Sterile	195	201	170	153	170	134	146	109	88	55
PLLA Non-Sterile	315	258	239	219	253	191	218	194	145	35
P(DTD DD) Sterile	185	205	187	197	173	156	131	127	88	37
PLLA Sterile	309	250	243	239	270	211	219	205	153	43

Average StDev Break Stress (MPa)	Time of incubation (weeks)									
Fiber Name	**0**	**0.01**	**1**	**2**	**4**	**8**	**16**	**24**	**32**	**64**
P(DTD DD) Non-Sterile	17	22	12	24	24	19	19	25	6	23
PLLA Non-Sterile	20	29	23	45	35	29	14	22	15	19
P(DTD DD) Sterile	14	23	29	27	27	24	15	10	8	20
PLLA Sterile	32	27	29	40	30	27	13	27	14	22

Average Young Modulus (GPa) (n=15)	Time of incubation (weeks)									
Fiber Name	0	0.01	1	2	4	8	16	24	32	
P(DTD DD) Non-Sterile	2.69	1.82	1.61	1.55	1.66	1.48	2.01	2.05	1.78	
PLLA Non-Sterile	5.42	4.78	4.09	4.38	4.82	4.06	5.09	5.23	4.20	
P(DTD DD) Sterile	2.61	1.69	1.69	1.86	1.94	1.74	1.88	2.35	1.67	
PLLA Sterile	5.16	4.43	4.12	4.44	4.69	4.14	5.00	5.21	4.06	

Average StDev Young Modulus (GPa)	Time of incubation (weeks)									
Fiber Name	0	0.01	1	2	4	8	16	24	32	
P(DTD DD) Non-Sterile	0.25	0.17	0.13	0.11	0.12	0.18	0.18	0.18	0.13	
PLLA Non-Sterile	0.22	0.33	0.76	0.70	0.32	0.62	0.34	0.47	0.42	
P(DTD DD) Sterile	0.27	0.14	0.28	0.13	0.23	0.13	0.17	0.20	0.24	
PLLA Sterile	0.25	0.31	0.42	0.48	0.49	0.33	0.48	0.21	0.28	

Average MW (kDa) (n=6)	Time of incubation (weeks)									
Fiber Name	0	0.01	1	2	4	8	16	24	32	64
P(DTD DD) Non-Sterile	90	85	87	77	77	72	56	54	49	35
PLLA Non-Sterile	144	145	149	141	138	124	96	87	69	43
P(DTD DD) Sterile	86	85	81	83	79	71	58	59	53	35
PLLA Sterile	148	149	142	141	138	120	105	97	81	53

Average StDev MW	Time of incubation (weeks)									
Fiber Name	0	0.01	1	2	4	8	16	24	32	64
P(DTD DD) Non-Sterile	6	2	14	1	1	3	2	3	5	2
PLLA Non-Sterile	2	7	10	2	10	8	9	16	24	15
P(DTD DD) Sterile	3	3	10	3	2	3	3	1	3	2
PLLA Sterile	6	5	8	8	7	6	12	15	19	17

Average Tm (n=6)							
Fiber Name	**0**	**1**	**2**	**4**	**16**	**32**	**64**
p(DTD DD) Non-Sterile	62.03	58.86	58.00	59.18	59.61	60.31	63.02
PLLA Non-Sterile	173.27	173.82	173.86	173.61	173.17	174.29	167.18
p(DTD DD) Sterile	62.13	59.25	62.46	59.12	59.38	59.09	63.46
PLLA Sterile	174.45	173.56	174.05	173.49	173.53	174.23	166.43
Average StDev Tm							
Fiber Name	**0**	**1**	**2**	**4**	**16**	**32**	**64**
p(DTD DD) Non-Sterile	0.15	3.61	3.10	3.96	4.07	4.16	4.07
PLLA Non-Sterile	1.58	1.79	1.83	1.98	1.63	1.09	4.77
p(DTD DD) Sterile	0.44	3.80	4.87	4.04	4.13	2.59	0.22
PLLA Sterile	1.80	2.19	1.78	1.74	1.43	1.22	7.26

Average Tc (n=6)							
Fiber Name	**0**	**1**	**2**	**4**	**16**	**32**	**64**
p(DTD DD) Non-Sterile	39.25	39.50	39.36	39.45	39.38	39.88	38.73
PLLA Non-Sterile	104.71	101.58	100.76	102.51	104.50	108.27	106.41
p(DTD DD) Sterile	39.32	39.47	39.40	39.46	39.33	39.77	37.95
PLLA Sterile	104.68	103.33	102.35	102.37	103.13	105.34	106.61
Average StDev Tc							
Fiber Name	**0**	**1**	**2**	**4**	**16**	**32**	**64**
p(DTD DD) Non-Sterile	0.05	0.07	0.03	0.07	0.07	0.19	0.88
PLLA Non-Sterile	0.44	1.75	2.66	0.56	0.89	0.88	1.03
p(DTD DD) Sterile	0.05	0.17	0.11	0.03	0.06	0.10	0.13
PLLA Sterile	0.34	0.55	0.75	0.62	0.94	0.97	1.89

8. REFERENCES

1. Ruggiero G. Anterior Knee Ligaments. In. Princeton: Nucleus Medical Art Inc.; 1999-2006.

2. Miller MD. Biomechanics. Philadelphia: W. B. Saunders; 1992.

3. Woo SL, Newton PO, MacKenna DA, Lyon RM. A comparative evaluation of the mechanical properties of the rabbit medial collateral and anterior cruciate ligaments. J Biomech 1992;25(4):377-86.

4. Danylchuk KD, Finlay JB, Krcek JP. Microstructural organization of human and bovine cruciate ligaments. Clin Orthop Relat Res 1978(131):294-8.

5. Woo SL, Gomez MA, Sites TJ, Newton PO, Orlando CA, Akeson WH. The biomechanical and morphological changes in the medial collateral ligament of the rabbit after immobilization and remobilization. J Bone Joint Surg Am 1987;69(8):1200-11.

6. Butler DL, Noyes FR, Grood ES. Ligamentous restraints to anterior-posterior drawer in the human knee. A biomechanical study. J Bone Joint Surg Am 1980;62(2):259-70.

7. Tria AJ, Jr. Ligaments of the Knee. New York: Churchill Livingstone Inc.; 1995.

8. Kohn D. Arthroscopy in acute injuries of anterior cruciate-deficient knees: fresh and old intraarticular lesions. Arthroscopy 1986;2(2):98-102.

9. Warren RF. Primary repair of the anterior cruciate ligament. Clin Orthop Relat Res 1983(172):65-70.

10. Murray MM, Martin SD, Martin TL, Spector M. Histological changes in the human anterior cruciate ligament after rupture. J Bone Joint Surg Am 2000;82-A(10):1387-97.

11. Amis AA, Dawkins GP. Functional anatomy of the anterior cruciate ligament. Fibre bundle actions related to ligament replacements and injuries. J Bone Joint Surg Br 1991;73(2):260-7.

12. Arnoczky SP. Anatomy of the anterior cruciate ligament. Clin Orthop Relat Res 1983(172):19-25.

13. Girgis FG, Marshall JL, Monajem A. The cruciate ligaments of the knee joint. Anatomical, functional and experimental analysis. Clin Orthop Relat Res 1975(106):216-31.

14. Duthon VB, Barea C, Abrassart S, Fasel JH, Fritschy D, Menetrey J. Anatomy of the anterior cruciate ligament. Knee Surg Sports Traumatol Arthrosc 2006;14(3):204-13.

15. Ralphs JR, Benjamin M. Cell and matrix organization in tendons and ligaments. Amsterdam: Gordon and Breach, Amsterdam; 1999.

16. Smith BA, Livesay GA, Woo SL. Biology and biomechanics of the anterior cruciate ligament. Clin Sports Med 1993;12(4):637-70.

17. Dienst M, Burks RT, Greis PE. Anatomy and biomechanics of the anterior cruciate ligament. Orthop Clin North Am 2002;33(4):605-20, v.

18. Yahia LH, Drouin G. Microscopical investigation of canine anterior cruciate ligament and patellar tendon: collagen fascicle morphology and architecture. J Orthop Res 1989;7(2):243-51.

19. Woo SL, Livesay GA, Runco TJ, Young EP. Structure and function of tendons and ligaments. 2nd ed. Philadelphia: Lippincott-Raven; 1997.

20. Amiel D, Billings E, Akeson WH. Ligament structure, chemisty and physiology. New York: Raven Press; 1989.

21. Ogston AG. The biological function of the glycosaminoglycans. London: Academic; 1970.

22. Strocchi R, de Pasquale V, Gubellini P, et al. The human anterior cruciate ligament: histological and ultrastructural observations. J Anat 1992;180 (Pt 3):515-9.

23. Neurath MF, Stofft E. Structure and function of matrix components in the cruciate ligaments. An immunohistochemical, electron-microscopic, and immunoelectron-microscopic study. Acta Anat (Basel) 1992;145(4):387-94.

24. Petersen W, Tillmann B. Structure and vascularization of the cruciate ligaments of the human knee joint. Anat Embryol (Berl) 1999;200(3):325-34.

25. Dodds JA, Arnoczky SP. Anatomy of the anterior cruciate ligament: a blueprint for repair and reconstruction. Arthroscopy 1994;10(2):132-9.

26. Beynnon BD, Amis AA. In vitro testing protocols for the cruciate ligaments and ligament reconstructions. Knee Surg Sports Traumatol Arthrosc 1998;6 Suppl 1:S70-6.

27. Wilson AB, Scott W. Anterior Cruciate Ligament. New York: Churchill Livingstone Inc.; 1995.

28. Beynnon BD, Johnson RJ, Abate JA, Fleming BC, Nichols CE. Treatment of anterior cruciate ligament injuries, part I. Am J Sports Med 2005;33(10):1579-602.

29. Levy AS, Meier SW. Approach to cartilage injury in the anterior cruciate ligament-deficient knee. Orthop Clin North Am 2003;34(1):149-67.

30. Fink C, Hoser C, Hackl W, Navarro RA, Benedetto KP. Long-term outcome of operative or nonoperative treatment of anterior cruciate ligament rupture--is sports activity a determining variable? Int J Sports Med 2001;22(4):304-9.

31. Gillquist J, Messner K. Anterior cruciate ligament reconstruction and the long-term incidence of gonarthrosis. Sports Med 1999;27(3):143-56.

32. Jones HP, Appleyard RC, Mahajan S, Murrell GA. Meniscal and chondral loss in the anterior cruciate ligament injured knee. Sports Med 2003;33(14):1075-89.

33. Bach BR, Jr., Tradonsky S, Bojchuk J, Levy ME, Bush-Joseph CA, Khan NH. Arthroscopically assisted anterior cruciate ligament reconstruction using patellar tendon autograft. Five- to nine-year follow-up evaluation. Am J Sports Med 1998;26(1):20-9.

34. Crawford C, Kainer M, Jernigan D, et al. Investigation of postoperative allograft-associated infections in patients who underwent musculoskeletal allograft implantation. Clin Infect Dis 2005;41(2):195-200.

35. Harner CD, Fu F. The immune response to allograft ACL reconstruction. American Journal of Knee Surgery 1993;6:45-6.

36. Barber FA. Should allografts be used for routine anterior cruciate ligament reconstructions? Arthroscopy 2003;19(4):421.

37. Harner CD, Olson E, Irrgang JJ, Silverstein S, Fu FH, Silbey M. Allograft versus autograft anterior cruciate ligament reconstruction: 3- to 5-year outcome. Clin Orthop Relat Res 1996(324):134-44.

38. Hess T, Duchow J, Roland S, Kohn D. Single-versus two-incision technique in anterior cruciate ligament replacement: influence on postoperative muscle function. Am J Sports Med 2002;30(1):27-31.

39. Victor J, Bellemans J, Witvrouw E, Govaers K, Fabry G. Graft selection in anterior cruciate ligament reconstruction--prospective analysis of patellar tendon autografts compared with allografts. Int Orthop 1997;21(2):93-7.

40. Feagin JA, Jr., Curl WW. Isolated tear of the anterior cruciate ligament: 5-year follow-up study. Am J Sports Med 1976;4(3):95-100.

41. Guidoin MF, Marois Y, Bejui J, Poddevin N, King MW, Guidoin R. Analysis of retrieved polymer fiber based replacements for the ACL. Biomaterials 2000;21(23):2461-74.

42. Bolton CW, Bruchman WC. The GORE-TEX expanded polytetrafluoroethylene prosthetic ligament. An in vitro and in vivo evaluation. Clin Orthop Relat Res 1985(196):202-13.

43. Mody BS, Howard L, Harding ML, Parmar HV, Learmonth DJ. The ABC carbon and polyester prosthetic ligament for ACL-deficient knees. Early results in 31 cases. J Bone Joint Surg Br 1993;75(5):818-21.

44. Richmond JC, Manseau CJ, Patz R, McConville O. Anterior cruciate reconstruction using a Dacron ligament prosthesis. A long-term study. Am J Sports Med 1992;20(1):24-8.

45. Frank CB, Jackson DW. The science of reconstruction of the anterior cruciate ligament. J Bone Joint Surg Am 1997;79(10):1556-76.

46. Muren O, Dahlstedt L, Brosjo E, Dahlborn M, Dalen N. Gross osteolytic tibia tunnel widening with the use of Gore-Tex anterior cruciate ligament prosthesis: a radiological, arthrometric and clinical evaluation of 17 patients 13-15 years after surgery. Acta Orthop 2005;76(2):270-4.

47. Atala A, Mooney DJ. Synthetic biodegradable polymer scaffolds. Boston: Birkhäuser; 1997.

48. Bourke SL. Preliminary development of a novel resorbable synthetic polymer fiber scaffold for anterior cruciate ligament reconstruction. Tissue Engineering 2004;10(1/2):43-52.

49. Cooper JA, Lu HH, Ko FK, Freeman JW, Laurencin CT. Fiber-based tissue-engineered scaffold for ligament replacement: design considerations and in vitro evaluation. Biomaterials 2005;26(13):1523-32.

50. Lin VS, Lee MC, O'Neal S, McKean J, Sung KL. Ligament tissue engineering using synthetic biodegradable fiber scaffolds. Tissue Eng 1999;5(5):443-52.

51. Lu HH, Cooper JA, Jr., Manuel S, et al. Anterior cruciate ligament regeneration using braided biodegradable scaffolds: in vitro optimization studies. Biomaterials 2005;26(23):4805-16.

52. Woo SL, Hollis JM, Adams DJ, Lyon RM, Takai S. Tensile properties of the human femur-anterior cruciate ligament-tibia complex. The effects of specimen age and orientation. Am J Sports Med 1991;19(3):217-25.

53. Altman GH, Horan RL, Lu HH, et al. Silk matrix for tissue engineered anterior cruciate ligaments. Biomaterials 2002;23(20):4131-41.

54. Noyes FR, Grood ES. The strength of the anterior cruciate ligament in humans and Rhesus monkeys. J Bone Joint Surg Am 1976;58(8):1074-82.

55. Rittmeister M, Noble PC, Lintner DM, Alexander JW, Conditt M, Kohl HW, 3rd. The effect of strand configuration on the tensile properties of quadrupled tendon grafts. Arthroscopy 2002;18(2):194-200.

56. Dunn MG. Anterior cruciate ligament prostheses. In: Fahey T, ed. Encyclopedia of sports medicine and science; 2004.

57. Ge Z, Yang F, Goh JC, Ramakrishna S, Lee EH. Biomaterials and scaffolds for ligament tissue engineering. J Biomed Mater Res A 2006;77(3):639-52.

58. Ge Z, Goh JC, Lee EH. The effects of bone marrow-derived mesenchymal stem cells and fascia wrap application to anterior cruciate ligament tissue engineering. Cell Transplant 2005;14(10):763-73.

59. Ge Z, Goh JC, Wang L, Tan EP, Lee EH. Characterization of knitted polymeric scaffolds for potential use in ligament tissue engineering. J Biomater Sci Polym Ed 2005;16(9):1179-92.

60. Petrigliano FA, McAllister DR, Wu BM. Tissue engineering for anterior cruciate ligament reconstruction: a review of current strategies. Arthroscopy 2006;22(4):441-51.

61. Abramson S, Kohn J, Langer R. Bioresorbable and bioerodible materials. 2nd ed. San Diego: Elsevier Inc.; 2004.

62. Choueka J, Charvet JL, Koval KJ, et al. Canine bone response to tyrosine-derived polycarbonates and poly(L-lactic acid). J Biomed Mater Res 1996;31(1):35-41.

63. Daniels AU, Chang MK, Andriano KP. Mechanical properties of biodegradable polymers and composites proposed for internal fixation of bone. J Appl Biomater 1990;1(1):57-78.

64. Matsusue Y, Hanafusa S, Yamamuro T, Shikinami Y, Ikada Y. Tissue reaction of bioabsorbable ultra high strength poly (L-lactide) rod. A long-term study in rabbits. Clin Orthop Relat Res 1995(317):246-53.

65. Suganuma J, Alexander H. Biological response of intramedullary bone to poly-L-lactic acid. Journal of Applied Biomaterials 1993;4(1):13-27.

66. Taylor MS, Daniels AU, Andriano KP, Heller J. Six bioabsorbable polymers: in vitro acute toxicity of accumulated degradation products. J Appl Biomater 1994;5(2):151-7.

67. van Sliedregt A, van Loon JA, van der Brink J, de Groot K, van Blitterswijk CA. Evaluation of polylactide monomers in an in vitro biocompatibility assay. Biomaterials 1994;15(4):251-6.

68. Bostman OM. Absorbable implants for the fixation of fractures. J Bone Joint Surg Am 1991;73(1):148-53.

69. Bourke SL, Kohn J. Polymers derived from the amino acid L-tyrosine: polycarbonates, polyarylates and copolymers with poly(ethylene glycol). Adv Drug Deliv Rev 2003;55(4):447-66.

70. Brocchini S, James K, Tangpasuthadol V, Kohn J. A combinatorial approach to polymer design. J Am Chem Soc 1997;119:4553-4.

71. Bourke SL. A Tissue Engineering Approach to Anterior Cruciate Ligament Reconstruction. New Brunswick: Rutgers University; 2000.

72. Collins G, Yoo S, Recber A, Jaffe M. Thermal analysis of complex relaxation processes in poly(desaminotyrosyl-tyrosine arylates). Polymer 2007;48:975-88.

73. Jaffe M, Ophir Z, Collins G, Rehm O, Yoo S, Rafalko J. Process-structure-property relationships of erodable polymeric biomaterials: II-long range order in poly(desaminotyrosyl arylates). Polymer 2003;44:6033-42.

74. Jaffe M, Pai V, Ophir Z, Wu J, Kohn J. Process-structure-property relationships of erodable polymeric biomaterials, I: Poly(desaminotyrosyl Arylates). Polym Adv Technol 2002;13:926-37.

75. Ertel SI, Kohn J. Evaluation of a series of tyrosine-derived polycarbonates as degradable biomaterials. J Biomed Mater Res 1994;28(8):919-30.

76. Fiordeliso J, Bron S, Kohn J. Design, synthesis, and preliminary characterization of tyrosine-containing polyarylates: new biomaterials for medical applications. J Biomater Sci Polym Ed 1994;5(6):497-510.

77. Cooper JA, Jr., Sahota JS, Gorum WJ, 2nd, Carter J, Doty SB, Laurencin CT. Biomimetic tissue-engineered anterior cruciate ligament replacement. Proc Natl Acad Sci U S A 2007;104(9):3049-54.

78. Caruso AB, Dunn MG. Changes in mechanical properties and cellularity during long-term culture of collagen fiber ACL reconstruction scaffolds. J Biomed Mater Res A 2005;73(4):388-97.

79. Kane JB, Tompkins RG, Yarmush ML, Burke JF. Biomaterials Science. 1st ed. San Diego: Academic Press; 1996.

80. Yannas IV. Biomaterials Science. 1st ed. San Diego: Academic Press; 1996.

81. Gustavson KH. The Chemistry and Reaction of Collagen. New York: Academic Press; 1956.

82. Langer R, Vacanti JP. Tissue engineering. Science 1993;260(5110):920-6.

83. Blassingame TM. The development of synthetic and collagen hybrid scaffolds for anterior cruciate ligament reconstruction. New Brunswick: Rutgers University; 2005.

84. Dunn MG, Tria AJ, Kato YP, et al. Anterior cruciate ligament reconstruction using a composite collagenous prosthesis. A biomechanical and histologic study in rabbits. Am J Sports Med 1992;20(5):507-15.

85. Chvapil M, Speer DP, Holubec H, Chvapil TA, King DH. Collagen fibers as a temporary scaffold for replacement of ACL in goats. J Biomed Mater Res 1993;27(3):313-25.

86. Dunn MG, Bellincampi LD, Tria AJ, Zawadsky JP. Preliminary development of a collagen-PLA composite for ACL reconstruction. J Appl Polym Sci 1995;63:1423-8.

87. Jackson DW, Simon TM, Lowery W, Gendler E. Biologic remodeling after anterior cruciate ligament reconstruction using a collagen matrix derived from demineralized bone. An experimental study in the goat model. Am J Sports Med 1996;24(4):405-14.

88. Laitinen O, Pohjonen T, Tormala P, et al. Mechanical properties of biodegradable poly-L-lactide ligament augmentation device in experimental anterior cruciate ligament reconstruction. Arch Orthop Trauma Surg 1993;112(6):270-4.

89. Jaffe M, Menczel JD, Bessey WE. Thermal characterization of polymeric materials. Brooklyn: Academic Press; 1997.

90. Bellincampi LD, Closkey RF, Prasad R, Zawadsky JP, Dunn MG. Viability of fibroblast-seeded ligament analogs after autogenous implantation. J Orthop Res 1998;16(4):414-20.

91. Caruso AB, Dunn MG. Functional evaluation of collagen fiber scaffolds for ACL reconstruction: cyclic loading in proteolytic enzyme solutions. J Biomed Mater Res A 2004;69(1):164-71.

92. Weadock KS, Miller EJ, Bellincampi LD, Zawadsky JP, Dunn MG. Physical crosslinking of collagen fibers: comparison of ultraviolet irradiation and dehydrothermal treatment. J Biomed Mater Res 1995;29(11):1373-9.

93. Karaoglu S, M BF, Woo SL, Fu YC, Liang R, Abramowitch SD. Use of a bioscaffold to improve healing of a patellar tendon defect after graft harvest for ACL reconstruction: A study in rabbits. J Orthop Res 2008;26(2):255-63.

94. Li F, Jia H, Yu C. ACL reconstruction in a rabbit model using irradiated Achilles allograft seeded with mesenchymal stem cells or PDGF-B gene-transfected mesenchymal stem cells. Knee Surg Sports Traumatol Arthrosc 2007;15(10):1219-27.

95. Olson EJ, Kang JD, Fu FH, Georgescu HI, Mason GC, Evans CH. The biochemical and histological effects of artificial ligament wear particles: in vitro and in vivo studies. Am J Sports Med 1988;16(6):558-70.

96. Soon MY, Hassan A, Hui JH, Goh JC, Lee EH. An analysis of soft tissue allograft anterior cruciate ligament reconstruction in a rabbit model: a short-term study of the use of mesenchymal stem cells to enhance tendon osteointegration. Am J Sports Med 2007;35(6):962-71.

97. Woo SL, Niyibizi C, Matyas J, Kavalkovich K, Weaver-Green C, Fox RJ. Medial collateral knee ligament healing. Combined medial collateral and anterior cruciate ligament injuries studied in rabbits. Acta Orthop Scand 1997;68(2):142-8.

98. Durselen L, Hafner M, Ignatius A, et al. Biological response to a new composite polymer augmentation device used for cruciate ligament reconstruction. J Biomed Mater Res B Appl Biomater 2006;76(2):265-72.

99. Ko F. Three-dimensional fabrics for composites. New York: Elsevier; 1989.

100. Rogers GJ, Milthorpe BK, Muratore A, Schindhelm K. Measurement of the mechanical properties of the ovine anterior cruciate ligament bone-ligament-bone complex: a basis for prosthetic evaluation. Biomaterials 1990;11(2):89-96.

101. Hunt P, Rehm O, Weiler A. Soft tissue graft interference fit fixation: observations on graft insertion site healing and tunnel remodeling 2 years after ACL reconstruction in sheep. Knee Surg Sports Traumatol Arthrosc 2006.

102. Seitz H, Wielke B, Schlenz I, Pichl W, Vecsei V. Load sharing in augmented anterior cruciate ligament repair: a mathematical analysis based on in vitro measurements. Clin Biomech (Bristol, Avon) 1996;11(8):431-8.

103. Gilles MA, Hudson AQ, Borders CL, Jr. Stability of water-soluble carbodiimides in aqueous solution. Anal Biochem 1990;184(2):244-8.

104. Olde Damink LH, Dijkstra PJ, van Luyn MJ, van Wachem PB, Nieuwenhuis P, Feijen J. Cross-linking of dermal sheep collagen using a water-soluble carbodiimide. Biomaterials 1996;17(8):765-73.

105. Cheung DT, Perelman N, Tong D, Nimni ME. The effect of gamma-irradiation on collagen molecules, isolated alpha-chains, and crosslinked native fibers. J Biomed Mater Res 1990;24(5):581-9.

106. Liu BC, Harrell R, Davis RH, Dresden MH, Spira M. The effect of gamma irradiation on injectable human amnion collagen. J Biomed Mater Res 1989;23(8):833-44.

107. Fox DB, Cook JL, Kuroki K, Cockrell M. Effects of dynamic compressive load on collagen-based scaffolds seeded with fibroblast-like synoviocytes. Tissue Eng 2006;12(6):1527-37.

108. van Tienen TG, Heijkants RG, Buma P, de Groot JH, Pennings AJ, Veth RP. Tissue ingrowth and degradation of two biodegradable porous polymers with different porosities and pore sizes. Biomaterials 2002;23(8):1731-8.

109. Chi Z, Chou T, Shen G. Determination of single fibre strength distribution from fibre bundle testings. J Mater Sci 1984;19:3319-24.

110. Coleman BD. On the strength of classical fibres and fibrebundles. J Mech Phys Solids 1958;7:60-70.

111. Butler DL, Guan Y, Kay MD, Cummings JF, Feder SM, Levy MS. Location-dependent variations in the material properties of the anterior cruciate ligament. J Biomech 1992;25(5):511-8.

112. Castner D, Ratner B. Biomedical surface science: Foundations to frontiers. Surface Science 2002;500:28-60.

113. Ratner BD. Biomaterials science : an introduction to materials in medicine. San Diego: Academic Press; 1996.

114. Grimes M, Pembroke JT, McGloughlin T. The effect of choice of sterilisation method on the biocompatibility and biodegradability of SIS (small intestinal submucosa). Biomed Mater Eng 2005;15(1-2):65-71.

115. Jiang B, Wu Z, Zhao H, et al. Electron beam irradiation modification of collagen membrane. Biomaterials 2006;27(1):15-23.

116. Hurwitz DE, Sumner DR, Andriacchi TP, Sugar DA. Dynamic knee loads during gait predict proximal tibial bone distribution. J Biomech 1998;31(5):423-30.

117. Gushue DL, Houck J, Lerner AL. Rabbit knee joint biomechanics: motion analysis and modeling of forces during hopping. J Orthop Res 2005;23(4):735-42.

118. Messner K, Fahlgren A, Ross I, Andersson B. Simultaneous changes in bone mineral density and articular cartilage in a rabbit meniscectomy model of knee osteoarthrosis. Osteoarthritis Cartilage 2000;8(3):197-206.

9. CURRICULUM VITA

Nicky Tovar

August 1999 Rensselaer Polytechnic Institute, Troy, NY, Biomedical Engineering, B.S.
January 2009 Rutgers University and University of Medicine and Dentistry of New Jersey, New Brunswick, NJ, Biomedical Engineering, Ph.D.

Experience

6/99-8/01 Project Engineer, Polymer Technologies Incorporated, Clifton, NJ

- Provided research, development and manufacturing services to commercial and medical industries utilizing both engineered commodity-type plastics and metal products
- Led projects in the development and manufacture of injection molded cervical and anterior lumbar spine cages and hip stem plugs
- Used metal injection molding technology to produce femoral knees

6/02-Present Graduate Research Assistant, Principal Investigator: Michael Dunn, Ph.D., University of Medicine and Dentistry of New Jersey, Orthopaedic Surgery, New Brunswick, NJ

- Manage the research and development of a hybrid synthetic and natural polymer fiber scaffold for the reconstruction of the anterior cruciate ligament
- Test the strength retention and degradation rate of polymer fibers through mechanical and chemical analysis
- Production of collagen fibers by extrusion, EDC crosslinking and electron beam sterilization
- Assist in small and large animal surgeries and pre/post-operative care for numerous medical applications
- Present project updates and data analysis to medical doctors and laboratory directors

1/03-12/04 Teaching Assistant, Rutgers University, Piscataway, NJ

- Developed a biomechanical testing laboratory for 80 upper-class biomedical engineering students
- Instructed students on biomechanics and the safe use of various material testing and analysis systems
- Graded laboratory reports, advised students and updated academic progress to faculty

6/06-8/06 Product Development Intern, Integra LifeSciences Corporation, Product Development, Plainsboro, NJ

- Explored collagen thin film technology as an alternate manufacturing approach to collagen sheets

- Researched the effects of natural and synthetic crosslinking methods on bovine collagen
- Assessed manufacturing procedures on various collagen based products
- Trained in Good Laboratory Procedures for numerous collagen based products

Publications

Pending: Tovar NM, Bourke S, Murthy S, Gatt CJ, Kohn J, Dunn MG. A Comparison of Resorbable Synthetic Polymer Fibers for Anterior Cruciate Ligament Reconstruction, *Journal of Biomedical Materials Research Part A* (2009)